

fNIRS Measurement of Cortical Activity in Younger and Older Adults During
Gait and Dual-Task Assignment

Amanda Spilkin

A Thesis
In the Department of
Physics

Presented in Partial Fulfillment of the Requirements
For the Degree of
Master of Science, Physics

at Concordia University
Montréal, Québec, Canada

August 2021

© Amanda Spilkin, 2021

School of Graduate Studies

This is to certify that this thesis prepared

By: Amanda Spilkin

Entitled: fNIRS Measurement of Cortical Activity in Younger and Older Adults during Gait and Dual Task Assignment

And submitted in partial fulfillment of the requirements of the degree of
Master of Science (Physics)

Complies with the regulations of the University and meets the accepted standards with respect to originality and quality.

Signed by the final Examining Committee:

_____ Chair
Dr. Alexandre Champagne

_____ External Examiner
Dr. Claudine Gauthier

_____ External Examiner
Dr. Karen Li

_____ Examiner (Chair)
Dr. Pablo Bianucci

_____ Thesis Supervisor
Dr. Christophe Grova

Approved by

Dr. Alexandre Champagne, Graduate Program Director

August 2021

Dr. Pascale Sicotte, Dean of Faculty

Abstract

fNIRS Measurement of Cortical Activity In Younger and Older Adults During Gait and Dual-Task Assignment

Amanda Spilkin

Functional Near-Infrared Spectroscopy (fNIRS) is a non-invasive brain imaging technique which measures brain activity via local changes in blood hemoglobin concentration. Since brain activity decreases as a function of age, it is expected that aging adults will demonstrate less hemodynamic changes and therefore, indicate less cortical activation compared to younger adults. To test the stated relationships, this study involves using the Near Infra-Red Optimal Tomography (NIROT) workflow with Maximum Entropy on the Mean (MEM), using personalized fNIRS and local 3D reconstruction to assess the hemodynamic response elicited during simultaneous walking and arithmetic tasks in healthy young and older adults. Personalized fNIRS consisted of following the Optimal Montage algorithm, which maximizes the positions of fNIRS sensors to increase sensitivity to two targeted brain regions: the Inferior Frontal Gyrus (IFG) and Middle Frontal Gyrus (MFG) which are both involved in performing mental arithmetic and shown to demonstrate compensatory behaviors in single task (mental arithmetic only) when compared to dual task (walking while performing mental arithmetic).

Single and dual tasks were considered for five younger adults and two older adults. Subject-specific optimal montages were calculated to ensure maximum light sensitivity to the target ROI and sufficient spatial overlap between sensors, allowing local 3D reconstruction of [HbO] and [HbR] response along the underlying cortical surface. Single task consisted of a block design arithmetic task (Serial-Sevens: sequential subtraction. For dual task, the same arithmetic task was performed, while participants were walking on a treadmill. NIRSTORM software package was used for channel space analysis of fNIRS signal, motion correction, modified Beer Lambert Law and block averaging. Reconstruction in 3D using Maximum Entropy on the Mean (MEM) was calculated using the same number of trials for each subject. In addition to answering questions encompassing brain activity as a function of age and balancing a cognitive task during gait, the study provided data for investigating trends around motion artifacts and testing the effectiveness of an accelerometer during simultaneous gait and fNIRS acquisitions. Due to restrictions during the Covid-19 pandemic, this study serves as a proof of concept and methods in improving the quality of data.

Résumé

Mesures d'activité cérébrale en Spectroscopie Proche Infra-Rouge (SPIR) lors d'une tâche duale (démarche + calcul arithmétique) chez des adultes jeunes et âgés

Amanda Spilkin

La Spectroscopie fonctionnelle Proche InfraRouge (SPIR) est une technique d'imagerie cérébrale non invasive qui mesure l'activité cérébrale en observant les changements locaux de la concentration d'hémoglobine dans le sang. Comme l'activité cérébrale diminue avec l'âge, les adultes vieillissants présentent moins de changements hémodynamiques, ce qui indique une moindre activation corticale par rapport aux jeunes adultes. Pour tester les relations énoncées, cette étude consiste à utiliser la tomographie de la proche infra-rouge (NIROT) avec l'entropie maximale sur la moyenne (MEM), en utilisant la SPIR personnalisée et la reconstruction 3D locale pour évaluer la réponse hémodynamique suscitée pendant des tâches simultanées de démarche et d'arithmétique chez des adultes jeune et âgés en bonne santé. La SPIR personnalisée consistait à suivre l'algorithme de montage optimal qui optimise les positions spécifiques des capteurs SPIR pour la sensibilité de la SPIR à deux régions cérébrale ciblées: le gyrus frontal inférieur (GFI) et le gyrus frontal moyen (GFM). Ces deux régions impliquées dans l'exécution du calcul mental et qui démontrent des comportements compensatoires dans une tâche unique (calcul mental) par rapport à une double tâche (démarcher tout en faisant du calcul mental).

Des tâches simples et doubles (arithmétique + démarche) ont été envisagées pour cinq jeunes adultes et deux adultes plus âgés. Les montages optimaux spécifiques au sujet ont été calculés pour assurer une sensibilité lumineuse maximale à la région d'intérêt cible et un chevauchement spatial suffisant entre les capteurs, permettant une reconstruction 3D locale de la réponse de [HbO] et [HbR] le long de la surface corticale. La tâche simple consistait en une tâche arithmétique (Serial-Sevens: soustraction séquentielle). Pour la double tâche, la même tâche arithmétique a été réalisée pendant que les participants marchaient sur un tapis roulant. Le logiciel NIRSTORM a été utilisé pour l'analyse de l'espace des canaux du signal fNIRS, la correction du mouvement, la loi de Beer Lambert modifiée et la moyenne des blocs. La reconstruction en 3D en utilisant l'entropie maximale sur la moyenne (MEM) a été calculée en utilisant le même nombre d'essais pour chaque sujet.

En plus de répondre aux questions concernant l'activité cérébrale en fonction de l'âge et l'équilibre d'une tâche cognitive pendant la démarche, l'étude a fourni des données pour étudier

les tendances autour des artefacts de mouvement et tester l'efficacité d'un accéléromètre pendant la démarche et les acquisitions SPIR simultanées. En raison des restrictions pendant la pandémie de Covid-19, cette étude sert de preuve de concept et de méthodes pour améliorer la qualité des données.

Acknowledgements

Dear members of the MultiFunkIm Lab and the Department of Physics,

I am very thankful for the fulfilling knowledge and exciting experience I have received from my peers, faculty, and my supervisor, Dr. Christophe Grova. Thank you for your belief in me and providing mentorship throughout my academic career, internship, and Masters. I am forever grateful. I would like to thank Dr. Karen Li, in her guidance through this thesis. I have learned how to build an interdisciplinary platform and I am looking forward to resuming scans for this study in Fall 2021. I also thank Dr. Claudine Gauthier and Dr. Karen Li for their presence here in my MSc committee.

I am very thankful to Zhengchen Cai, my colleague who has guided me from the start and is a large reason why I am here today. I also thank my lab colleagues, Dr. Chifaou Abdallah, Edouard Delaire and Dr. Makoto Uji, who have taught me valuable skills and shared their knowledge with me. I appreciate the support and help from my friends and lab mates Yimeng Wang, Fatemeh Razavipor, Obai Bin Ka'B Ali, Julia Huck and Stephanie Tremblay. I would like to also recognize colleagues at the PERFORM Centre in helping me with acquisitions; Antonys Melek (Imaging Suite) and Marchiano Dong Jun Oh in helping in coordinating my study at the Posture and Movement Lab.

I thank the Department of Physics and faculty for many years of support and open-door policy for all topics of conversation. Dr. Alexandre Champagne and Dr. Bianucci – thank you for supporting the Space Health Division and opening an avenue to Physics student involvement!

Finally, I thank my parents, cousins and grandmother for their motivating words and their support across all years of university.

Sincerely,

Amanda Spilkin

Table of Contents

Chapter 1	1
Introduction: Concepts and Objectives of this Study	1
1.1 Hypotheses	6
Summary	6
Chapter 2	7
Multimodal investigation of dual motor-cognitive tasks	7
2.1. Multimodal Brain Imaging	7
2.1.1. Magnetic Resonance Imaging (MRI)	7
2.2. Functional Near-Infrared Spectroscopy (fNIRS)	8
2.3. Motion Artifacts in fNIRS Signal: Denoising fNIRS Signal using 9-axis Accelerometer	12
2.5. Electromyography (EMG)	13
2.4. Summary	14
Chapter 3	15
Study Protocol: fNIRS Measurement of Cortical Activity in Younger and Older Adults during Gait and Dual-Task Assignment	15
3.1. Preliminary Participant Evaluation and Selection	15
3.2. Materials	17
Magnetic Resonance Imaging (MRI)	17
fNIRS System	17
3.3. Design	17
3.4. Protocol: Block Design Paradigm for ST and DT in fNIRS recordings	20
3.3.1. Setup of the fNIRS & Gait Acquisition	21

Chapter 4	23
Methods: Analysis of Functional Data and Gait Measurements.....	23
4.1. Processing of functional MRI and anatomical MRI.....	24
4.3. Personalized fNIRS acquisition using optimal montage targeting bilateral IFG and MFG.....	24
4.5. Removal of physiological noise and very low oscillations in fNIRS.....	25
4.6. Assessment of motion artifacts in fNIRS signals using a 9-axis Accelerometer	26
4.7. Trial Selection in Block Averaging of Single and Dual Task Assessment	27
4.8. Electromyography (EMG) and Footswitch Data Processing: Detection of Changes in Muscle Contraction during Single anal Tasks	29
4.9. Footswitch recordings and data analysis.....	30
4.10. MEM Reconstruction along the cortical surface	36
Chapter 5	38
Results	38
5.1. Results: Single Subject Analysis of fNIRS and EMG Data	38
5.2. Additional Motion Artifact Testing using Repetitive Motion Protocol	38
<i>Correlation matrices (a) and (b) demonstrate a strong correlation across short-distance channel.....</i>	40
5.3. Results: Single Subject Analysis of fNIRS and EMG Data	41
Youth 1	41
Youth 2	45
Youth 3	47
Youth 4	51
Elderly 1	59
Elderly 2	63

Review of EMG and footswitch Data Across All Subjects.....	66
Summary	69
Chapter 6.....	70
Discussion	70
6.1. Hemodynamic Response in Single-Task and Dual-Task, MEM reconstructions and	
Gait Analysis	70
6.2. Gait Analysis: Measuring Cadence and Stride Time via EMG and footswitch Data	71
6.2. Optimization of current protocol.....	71
Chapter 7.....	73
Conclusion	73
Chapter 8.....	75
References	75
Appendix	80
Appendix 1 – Montreal Cognitive Assessment (MoCA)	80
Appendix 2 – Time Up and Go (TUG).....	81
Appendix 3: Evaluating Effectiveness of Accelerometer with Controlled Head Motion	
Test.....	83
Appendix 4: Trial Selection Across ST and DT Conditions	89

List of Figures

Figure 1. Illustration of the Prefrontal Cortex divided into Superior, Middle, Inferior and Precentral Gyrus. (Al-Hakim & Fallon, et al., 2006)	5
Figure 2. Infra-Red Absorption Spectrum.....	10
Figure 3: Source Detector Pairs demonstrating Short-Separation and Long-Separation Channels (Zhang et al., 2012).....	11
Figure 4: fNIRS Imaging; Methodology of Light Propagation Through Neuronal Tissue (Herold, et al., 2018).....	12
Figure 5: fNIRS Imaging of Human Neurophysiology (Herold, et al., 2018)	13
Figure 6: Experimental Setup of the A complete schematic demonstrating all recordings and their corresponding devices during the Single Task and Dual Task acquisitions.	22
Figure 7: Workflow Map.....	24
Figure 8: Position of Accelerometer for Motion Test.....	27
Figure 9: Condition for Trial Rejection in Raw fNIRS Signal.....	29
Figure 10: EMG Sensor Placement.....	31
Figure 11: Gait Cycle	31
Figure 12: Footswitch Sensor Setup and Cadence Extraction Pipeline	32
Figure 13: Footswitch Recordings Workflow and Analysis	33
Figure 14: Seletion of Cadence Trials.....	34
Figure 15: Data Quality Assessment via Trial Selection on Raw fNIRS Data.....	37
Figure 16: Accelerometer motion tests evaluating the sensitivity of the accelerometer to downward head knods.	41
Figure 17: Youth 1 -Block averaged hemodynamic response in single task and dual task across IFG and MFG regions of interest	42
Figure 18: MEM reconstruction in single task and dual task across right and left hemispheres in Youth 1	43
Figure 19: %MVC of Muscle Groups for Dual-Task versus walking-only condition for Youth 1	45

Figure 20: Youth 2 -Block averaged hemodynamic response in single task and dual task across IFG and MFG regions of interest.....	46
Figure 21: MEM reconstruction in single task and dual task across right and left hemispheres in Youth 2 ..	
Figure 22: Youth 2 -Block averaged hemodynamic response in single task and dual task across IFG and MFG regions of interest.....	48
Figure 23: MEM reconstruction in single task and dual task across right and left hemispheres in Youth 3 ..	49
Figure 24: %MVC of Muscle Groups for Dual-Task versus walking-only in Youth 3	51
Figure 25: Block averaged hemodynamic response in single task and dual task across IFG and MFG regions of interest	52
Figure 26: MEM reconstruction in single task and dual task across right and left hemispheres in Youth 4 ..	53
Figure 27: Youth 5 - Block averaged hemodynamic response in single task and dual task across IFG and MFG regions of interest.....	56
Figure 28: MEM reconstruction in single task and dual task across right and left hemispheres in Youth 5 ..	57
Figure 29: %MVC of Muscle Groups for Dual-Task versus walking-only in Youth 5	59
Figure 30: Elderly 1 - Block averaged hemodynamic response in single task and dual task across IFG and MFG regions of interest.....	60
Figure 31: MEM reconstruction in single task and dual task across right and left hemispheres in Elderly 1 ..	61
Figure 32: %MVC of Muscle Groups for Dual-Task versus walking-only in Elderly 1	63
Figure 33: Block averaged hemodynamic response in single task and dual task across IFG and MFG regions of interest	64
Figure 34: %MVC of Muscle Groups for Dual-Task versus walking-only in Elderly 2	66

M.Sc. Thesis in Physics

fNIRS Measurement of Cortical Activity in Younger and Older Adults during Gait and Dual-Task Assignment

Chapter 1

Introduction: Concepts and Objectives of this Study

Aging is the process by which of an individual's physical, cognitive, and social adaptative abilities diminish with increasing age. Elderly individuals often experience difficulties performing ordinary activities, such as walking, balance and concentrating on more than one activity at a given time. The study of aging is concerned with maintenance of functional health, which consist of one's quality of vision, hearing, speech, mobility, dexterity, feelings, cognition, and pain (Pechora-Fuller, et al., 2015; Statistics Canada, 2015). One theory of aging is described by the frontal lobe hypothesis of aging, which suggests that functions mediated by the Prefrontal Cortex (PFC), such as dual tasking, decline as a function of aging. This may be related to other findings which demonstrate the correlation of healthy aging with the loss of grey matter, particularly the loss of frontal lobe grey matter volume (Lucas, et al., 2019). Another theory is that of cognitive reserve theory of aging, which suggests a younger population demonstrates higher brain activity in response to increased task difficulty and attention demands compared to an older population (Holtzer et al., 2011). Though there are several modalities of brain imaging that can measure the underlying factors of cognitive aging, we are particularly interested in functional near-infrared spectroscopy (fNIRS) for its' portability and non-invasive nature during acquisitions involving both cognitive tasks and locomotion. fNIRS is an optical imaging modality with high-temporal resolution that indirectly measures brain activity via changes in vascular response (Machado et al., 2018; Yücel & Lühmann, et a., 2021).

In resting state, the brain functions by maintaining a ready supply of oxygen and glucose, two sources of energy found in the oxygenated blood. Oxygen consumption and brain activity vary in

accordance with one physical resting and active state. Upon increased physical or mental activity (or activities), increase local neuronal activity will elicit local hemodynamic response. Local blood vessels in the brain will rapidly dilate, resulting in a local increase of Cerebral Blood Flow (CBF) bringing the required amount of oxygenated blood to the region corresponding to neuronal activity. This phenomenon, known as neurovascular coupling, relates the responses in CBF and cerebral metabolic rate of oxygen (CMRO₂) to the neural activity response (Buxton, et al. 2004). During the performance of a selected cognitive task (e.g. addition/subtraction mental arithmetic), one can measure an increase in cortical activity, characterized by a local increased energy consumption. Resulting indirect hemodynamic responses associated with such a change in neuronal activity, neurovascular coupling allows studying brain regions involved during the execution of a task (e.g. region associated with language). In the context of this study, executive functions of the participants were evaluated using a cognitive task which involved the instructor giving a 3-digit number and the participant subtracts seven from each subsequent number, aloud. The dual task assignment requires the participant to walk on a treadmill and while performing the same mental arithmetic simultaneously.

Performance of a single task thus permits localization of brain regions associated to a given activity (e.g. motor cortex corresponds to walking on a treadmill). Assignment of a second task, simultaneously executed with the first one (e.g. mental arithmetic while walking on a treadmill) requires additional brain activation and recruitment of additional regions, hence a broader area over which energy is consumed to successfully execute the required dual-tasks. Brain activity decreases as a function of age; thus, the projected observation will be such that aging adults will demonstrate less cortical activation, indicating less energy consumption compared to younger adults (Beurskens et al., 2014).

To test the stated relationships, the proposed experiment involved using personalized fNIRS, a method developed by the MultifunkIm Lab and uses a subject specific setup of optodes for performing functional Near-Infrared Spectroscopy (fNIRS). The personalized fNIRS method consisted in estimating a subject specific Optimal Montage of fNIRS sources and detectors, in order to maximize a priori the sensitivity to target brain regions and reconstruct locally underlying hemodynamic activity along the cortical surface (Machado, et al, 2018; Machado 2014). In the context of this study, fNIRS was used to analyze how the brain responds to simultaneously walking and performing calculations of simple arithmetic calculations. The additional cognitive load (arithmetic calculations) to motor activity (walking) required activation across multiple regions of the cortex and required an increased consumption of energy delivered through oxygenated blood, which can be monitored with fluctuations in the fNIRS signal in our proposal. A personalized fNIRS arrangement was considered to investigate the correlation between change in brain activity in the Inferior Frontal Gyrus (IFG) and Middle Frontal Gyrus (MFG), both located within the Prefrontal Cortex (PFC). We considered to investigate those two anatomical regions since they are linked to task prioritization and compensation in single task (walking or mental arithmetic only) and dual task (walking while performing mental arithmetic) (Doi & Blumen, et al., 2017). These regions were investigated bilaterally, resulting in a total of four regions assessed via personalized fNIRS optode arrangement. We expect increased bilateral activation relative to baseline in the IFG and MFG elicited during both single tasks, and larger activation during dual-tasks for both age groups. Moreover, this study will challenge current bodies of research in determining if the hemodynamic response elicited by single and dual task conditions is larger in younger adults when compared to aging adults.

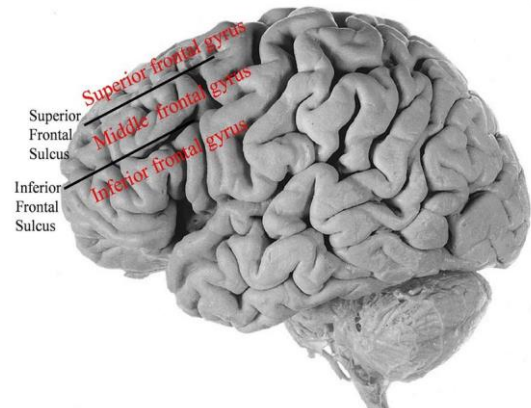


Figure 1. Illustration of the Prefrontal Cortex divided into Superior, Middle, Inferior and Precentral Gyrus. (Al-Hakim & Fallon, et al., 2006)

Though it appears that younger adults demonstrate greater activation in these regions with little compromise to their gait during dual task activity, recent studies provided results suggesting that older adults adjust their behaviours to compensate for maintaining performance of an additional task (Li, et al, 2012; Holtzer, et al., 2011). In the context of this study, compensatory behaviours could be measured via variation in gait. An individual's gait refers to his or her natural patterns in locomotive

exercises. One's gait can also change because of external influences. During dual-task assignment, or so called, multi-tasking, gait features such as swing time variability, stride-time variability and walking speed will generally decrease, while cadence, step length and stride time are more likely to increase (Beurskens et al., 2014; Mills et al., 2001; Schrager et al., 2008).

Thus, through this study, we broadened our understanding of increased cortical activation involved in task prioritization and maintenance of higher executive functions. It is suggested that the execution and maintenance of one's personal status quo motor and cognitive functions during dual-tasks assignment requires the recruitment of complementary brain regions. The additional cognitive load (arithmetic calculations) to motor activity (walking) thus requires recruitment of additional regions of the PFC and increased brain activity (Terentjeviene, A. et al., 2008).

Thus, through this study, we shall broaden our understanding of increased cortical activation involved in task prioritization and maintenance of higher executive functions. It is suggested that the execution and maintenance of one's personal status quo motor and cognitive functions during dual-tasks assignment requires the recruitment of complementary brain regions. This insists that energy is consumed throughout a larger area of the brain to carry out the desired activities. The additional cognitive load (arithmetic calculations) to motor activity (walking) requires increased activation across multiple regions, relative to individual participants' baseline brain activity.

In this study, we investigated the relationship between brain activity and dual-tasking using the Near Infra-Red Optical Tomography (NIROT) workflow with used the Maximum Entropy on the Mean (MEM) as the selected method for solving the inverse problem (Cai, et al., 2021). I used the personalized NIROT with MEM to obtain a more accurate reconstruction and estimation of [HbO]/[HbR] fluctuations within targeted ROIs. The workflow permits planning of 1) personalized fNIRS montage installation, 2) reduction of optodes position error using digitalization of sensor positions via neuro-navigation device and 3) reconstruction of hemodynamic figures using the MEM method.

1.1 Hypotheses

By applying our personalized fNIRS methodology, we are expecting to improve sensitivity of fNIRS measurements at the individual level during simultaneous, dual-task activity involving gait and

mental arithmetic. The personalized montage provides an arrangement of optodes on the scalp that can optimize the acquired signal and therefore further contrast activation patterns between younger and aging adults. The proposed personalized fNIRS investigation will also be useful in providing 3D reconstruction of [HbO] and [HbR] changes elicited by the tasks along the cortical surface. This is a more thorough representation of cortical activity and presents an additional feature to current literature, in which only fNIRS channel space analysis has been reported.

The hypotheses addressed in this study are the following:

- 1- We hypothesize that single task and dual task will result in increased bilateral activation in the PFC and IFG for both age groups.
- 2- For the single task only, we expect the increase of hemodynamic activity of [HbO] and [HbR] to be similar in both age groups .
- 3- For the dual-task only, we expect to see a larger increase of bilateral hemodynamic activity, in which [HbO] and [HbR] fluctuations will be greater in younger adults as compared to older adults, suggesting more difficulties in task prioritization and maintenance of higher executive functions in the older population.

Summary

In this thesis, we will look at how brain activity and gait characteristics are affected by dual-task exercises tasks. In elderly adults, gait characteristic such as speed and balance can become compromised with increased cognitive load during dual-task cognitive and motor activities, adjust behaviour (Korotkevich & Li, 2014). The study discussed in this thesis used various imaging and gait recording methods to provide a wholesome perspective on both brain activity originating in the regions associated to mental arithmetic and gait features such as electromuscular activity and cadence tracking. An additional aspect of my research involved investigating trends around motion artifacts and testing the effectiveness of an accelerometer during simultaneous gait and fNIRS acquisitions.

Chapter 2

Multimodal investigation of dual motor-cognitive tasks

The nature of this study involves assessing neurophysiological activity in conjunction with gait and thus requires several types of modalities for the recording of biological signals. Thus, fundamental requirements of this study involved using a portable brain imaging device, to monitor brain activity, and physical sensors that could track cadence and measure muscular bioelectrical activity. There are several methods of brain imaging that can capture the neurophysiological response to cognitive workload, each method has its' limitations, either in spatiotemporal capacities or in portability. For this reason, a multimodal approach is essential for detailed investigation using brain imaging, together with the ability of measuring features of one's gait. The following section will elaborate on the technologies and associated methodologies used to investigate brain activity and gait characteristics in single and dual task exercises.

2.1. Multimodal Brain Imaging

Multimodal brain imaging is a method combining several imaging modalities to enable the fusion of anatomical and functional data and provide quantitative and qualitative information of structural and metabolic processes. In the context of this study, we combine a participants' anatomical MRI to locate the Regions of Interest (ROI) with his or her vascular response to the Serial Sevens cognitive task in fMRI for fNIRS acquisition with personalized Optimal Montage.

2.1.1. Magnetic Resonance Imaging (MRI)

Magnetic Resonance Imaging (MRI) captures anatomical information of the brain by utilizing the magnetization properties of atomic nuclei, the spin magnetic moments of nuclei (principally hydrogen within water molecules, H_2O) and resonant excitation. Under natural circumstances, protons within an atom's nucleus oscillate freely in randomized directions. Once an external magnetic field is applied B_0 , the protons that are normally arbitrarily oriented within water nuclei are mainly forced into alignment in the same or opposite direction as the incoming magnetic field. A perpendicular magnetic field, B_1 , is applied to the static B_0 to produce a detectable RF signal (Pooley, 2005). The frequency at which the B_1 field excites unpaired protons at a specific radio frequency is known as the Larmor

frequency. By varying the sequence of RF pulses used and collected, different types of images can be obtained. Two common ways in which images can be manipulated is through Repetition Time (TR) and Time Echo (TE). TR pertains to the duration of time between successive pulse sequences applied to a single slice, while TE refers to the time between the peak of the echo and the peak of the 90° RF pulse (Pooley, 2005). TE and TR are tunable and thus, are weighted to produce the desired contrast in an image, such as T1-weighted and T2-weight MRI images. Image formation is dependent on the net magnetization. As energy is absorbed from the RF pulse, the net magnetization field rotates away from its original parallel orientation with the longitudinal field, also known as the main magnetic field. When the RF pulse ceases, the net magnetization shall begin to relax emit a signal named the spin echo (SE). The signal obtained from net magnetization are measured and converted via inverse Fourier transform into signal intensity level of each location in the imaged plane. The intensities are displayed in a matrix arrangement of pixels. The same process applies to voxels, a volume representation of pixels, observed as slice-assembled MRI in three-dimensional space (Moratal, et al. 2008). The resulting MRI scan image is thus a three-dimensional representation of voxels that are arranged in 2D slices and whose encoded signal intensities correspond to one of five tissues: skin, scalp, white matter, grey matter, and cerebrospinal fluid.

Functional Magnetic Resonance Imaging (fMRI)

fMRI is an imaging method that monitors cerebral activity and can also capture changes in activity during a task by measuring the “Blood Oxygenation Level Dependent” (BOLD) signal. The BOLD signal is detected via measurement of T2* relaxation and records fluctuations of paramagnetic deoxygenated hemoglobin, in which local decreases in HbR concentration correspond to an increased BOLD signal and therefore indicating region of increased brain activity. fMRI provides the ability to monitor blood flow changes within the whole brain with spatial resolution of millimeters (Mulert & Lemieux, et al., 2010). In this study, participants performed a cognitive task paradigm, know as Serial Sevens (S7) inside of the MRI scanner. A participants’ BOLD response to the cognitive task could then be measured and localized when projected to his or her reconstructed 3D anatomical MRI.

2.2. Functional Near-Infrared Spectroscopy (fNIRS)

fNIRS is a non-invasive, optical imaging modality that indirectly measures neural activity via changes in vascular response using infrared (IR) light. Neurovascular coupling (NVC) is a term that describes the mechanisms that link transient neural activity to the corresponding increase of localized cerebral flow (Huneau, et al., 2015). In resting state, the brain operates by maintaining a ready supply of oxygen and glucose, two sources of energy found in oxygenated blood. Upon executing some physical or mental activity, the corresponding brain region receives a surge of oxygenated blood to provide energy for the necessary task and experiences a peak at approximately five to six seconds after stimulus detection (Machado, et al., 2017). The provision of oxygenated blood to active neuronal tissue is named the hemodynamic response (HR). Brain activity thereby originates from networks of neurons that span the grey/white matter of the cortex and correspond to local fluctuations in both oxygenated hemoglobin (HbO) and deoxygenated hemoglobin (HbR) chromophores via NVC mechanisms.

fNIRS imaging of hemodynamic fluctuations are obtained by shining IR light via optodes placed directly on the scalp and measuring the amount of IR light scattered from tissues spanning the region of optodes arrangement. Optodes are designated as sources (a.k.a. emitters) or detectors, and together, form channels that emit and detect scattered IR light. The amount of reflected IR light recorded by the detector relative to the amount of light emitted from the source indirectly provides the amount of light absorbed by chromophores present in the vasculature of the cortex. The wavelengths of IR light used is normally in the range of 600-900nm. Several wavelengths along this spectrum will

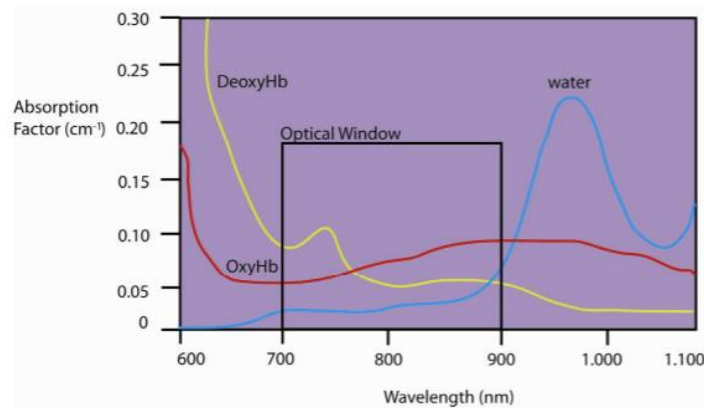


Figure 2. Infra-Red Absorption Spectrum

Figure 2 depicts the range of Infra-Red Spectrum wavelengths. Two chromophores pertinent to fNIRS are oxyHb and deoxyHb and are characterized by absorption spectra that fall within an optical window of 700-900nm. (Len-Carin, et al., 2010).

be absorbed by particular chromophores. The chromophores' light absorption spectra ($\lambda > 800$ nm for HbO (OxyHb), $\lambda < 800$ nm for HbR (deoxyHb)) is a feature that permits non-invasive quantification of local changes in cortical HbO and HbR concentration via the modified Beer–Lambert law (mBLL). The cortical concentration changes in HbO and HbR serve as indirect indications of local brain activity (Herold, F., et al., 2018). Figure 2 demonstrates the physics and methodology of fNIRS Imaging.

fNIRS imaging is based on concepts of physics, such as the modified Beer Lambert's Law (mBLL) which relates the change in optical density to the concentration of chromophores, such as oxygenated hemoglobin (HbO₂, or oxyHb) and deoxygenated hemoglobin (Hb, or deoxyHb) (Yücel & Lüthmann, et al, 2021). The OD of a tissue is a dimensionless value obtained by measuring light attenuation, as a function of wavelength, due to chromophore absorption as light travels across a given medium. The following formula is the Beer Lambert Law (BLL), where I_0 is the incident light, I the transmitted light, ϵ_λ the chromophore's extinction coefficient (in $\mu\text{M}^{-1}\text{cm}^{-1}$), c is the concentration (in μM) of the chromophore, L the distance (in cm) between light entrance and exit points and λ is the wavelength used (in nm) (Artinis Medical Systems, 2019).

$$OD_\lambda = \log\left(\frac{I_0}{I}\right) = \epsilon_\lambda c L$$

Eq 1. Optical Density with respect to wavelength

Though BLL formula well-described the behavior of optical spectroscopy via fNIRS, the model requires adjustment because we are observing light attenuation through dense and scattering biological tissues. Due to scattering of light, fNIRS cannot accurately recover $\Delta[\text{HbO}]$ and $\Delta[\text{HbR}]$, especially when targeting focal regions of the cerebral cortex. For this reason, one uses the Modified Beer Lambert Law (MBLL) which consists of an additional differential path length correction factor (DPF). The purpose of the DPF is to “improve the quantifications of $\Delta[\text{HbO}]$ and $\Delta[\text{HbR}]$ ” by

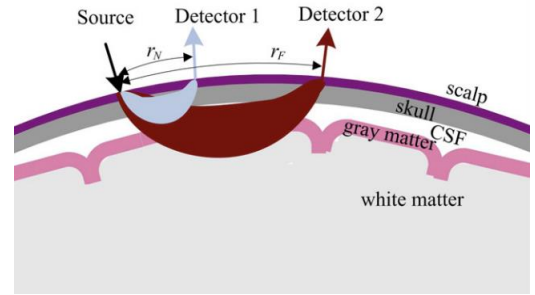


Figure 3: Source-Detector Pairs demonstrating Short-Separation and Long-Separation Channels (Zhang et al., 2012).

accounting for the increase in optical pathlength due to scattering in the tissue (Machado et al., 2017).

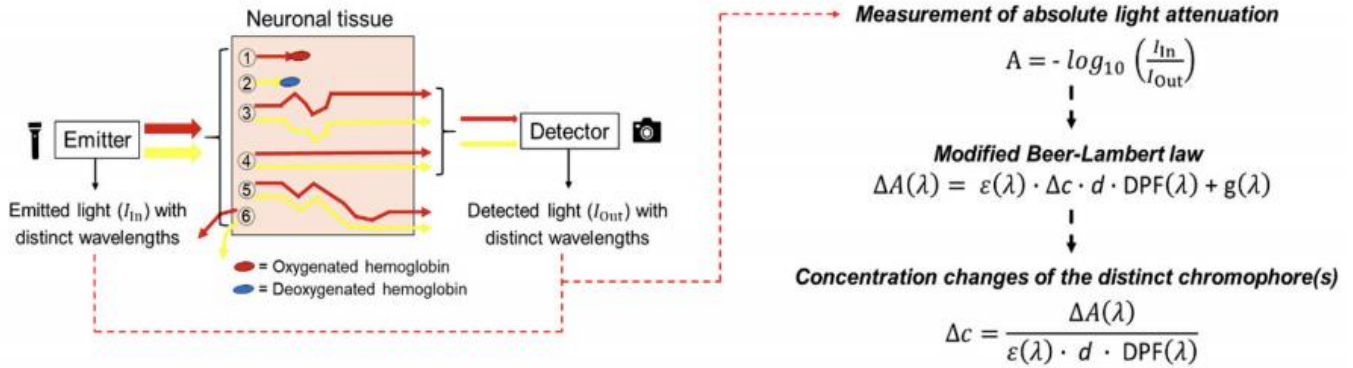


Figure 4: fNIRS Imaging; Methodology of Light Propagation Through Neuronal Tissue (Herold, et al., 2018)

The left-hand side of Figure 4 illustrates light propagation through the neuronal tissue. The photon paths depicted in red represent wavelengths of $\lambda > 800 \text{ nm}$ (mainly absorbed by oxyHb, and photon paths in yellow colors represent wavelengths of $\lambda < 800 \text{ nm}$ (mainly absorbed by deoxyHb). The photon path tagged with the number 3 represent a photon path that experiences scattering events before being recorded by a detector. The photon path tagged with the number 4 depicts a ballistic photon. The photon path tagged with the number 5 represents a photon that does not reach a detector and is lost due to scattering. Photon path tagged with the number 6 illustrates a photon that does not reach a detector due to backward scattering. On the right-hand side of the figure, the formulas to calculate concentration changes in chromophores are given, where A is the light attenuation, $\Delta A(\lambda)$ is the change in light attenuation at a specific wavelength (λ), I_{in} is the intensity of emitted light, I_{out} is the intensity of recorded light, $\varepsilon(\lambda)$ is the extinction coefficient of the chromophore at a certain wavelength (λ), Δc is the change in chromophore concentration, d is separation (distance) between source and detector and $DPF(\lambda)$ is the differential path length factor (DPF) for a specific wavelength (λ). (Herold, et al., 2018).

fNIRS measure relative concentrations of chromophores in HbO and HbR, characterized by the consumption of oxygen and glucose in a designated cortical area. The fNIRS signal is obtained when IR light of specific wavelength is absorbed by a chromophore, thus indicating metabolic consumption of energy and corresponds to the loss of light intensity across some focal region of the cerebral cortex. The change in concentration is given by

$$\Delta c = \frac{\Delta OD_{\lambda}}{\varepsilon_i L DPF}$$

Eq 2. Change in Chromophore Concentration

Where Δc is the change in concentration, ΔOD_{λ} is the change in optical density with respect to wavelength, ε_i is the extinction coefficient, L is the length and DPF stands for the differential path length correction factor.

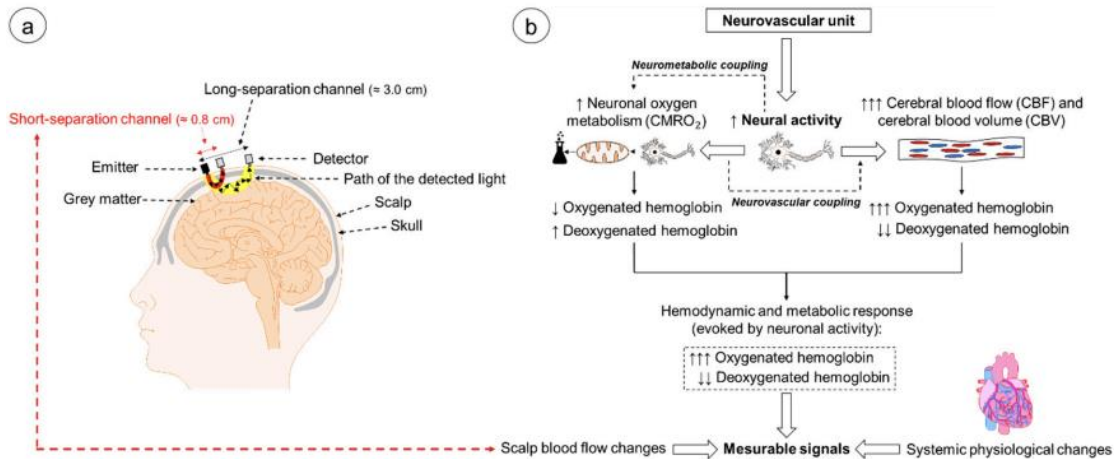


Figure 5: fNIRS Imaging of Human Neurophysiology (Herold, et al., 2018)

Figure 5(a) illustrates an emitter/source and detector pair forming one channel across the cortex. Long-distance source-detector channel pairs serve as the basis of fNIRS montages and are normally position 2.0cm to 4.5cm apart. Figure 5(b) demonstrates the neurophysiological unit's metabolism and associated changes in oxygenated and deoxygenated hemoglobin concentrations induced by neural activity. (Herold, et al., 2018).

These phenomena are recorded via optodes placed on the scalp; one optode will emit IR light (the source), and the other will receive the scattered light (the detector). The trajectory that IR light takes across the cortex will resemble somewhat the shape of a banana, as depicted in Figure 5. The typical range for source and detector (SD) pair separation is between 2.0cm and 4.5cm, as illustrated in Figure 3a. The distance between the source and detector can be tuned according to the size of the region you chose to measure, specifically in the area of grey matter. Variations in the amount of scattered light measured over a set of SD pairs on the scalp can be used to compute the associated changes in [HbO] and [HbR] with respect to a baseline. For this reason, fNIRS SD pairs are installed between 2.0 and 4.5cm separation, providing an optimal balance between penetration depth and Signal-to-Noise Ratio (SNR) (Cai, et al., 2021). Short-separation (SS) channels, typically source-detectors pair separation of 2.0cm or less, are used for detection blood monitoring hemodynamic fluctuations in superficial tissue and are used for regressing the estimated fNIRS measurements from the scalp (Santosa, et al., 2020).

2.3. Motion Artifacts in fNIRS Signal: Denoising fNIRS Signal using 9-axis Accelerometer

Though fNIRS is known for its non-invasive and portable design, quality signal is best obtained when the optodes maintain constant contact with the participant's skin. Inconsistent contact between

fiber optic light and the skin generates noise and data loss during acquisition. Motion, such as turning of the head or brisk movement, often causes optodes to lift off the skin on the scalp and decouple light traveling from source and detector, resulting in high-frequency spikes or baseline shifts. These artifacts are commonly detected and removed or corrected before further processing” (Yücel, et al., 2017). In Chapter 4 – Methods: Analysis of Functional Data and Gait Measurements, I will present the process I applied to screening motion artifacts in raw, unfiltered fNIRS data and evaluation of the sensitivity of the Witmotion WT901BLECL Bluetooth 5.0 Gyro Sensor to head motion during DT exercises.

2.5. Electromyography (EMG)

Electromyography (EMG) signal originates from electrical currents generated in muscles contractions. There are two types of EMG sensors. The first consists of a needle that is inserted into the muscle to obtain electrical activity directly from muscle fibers. The second type of EMG sensor is a non-invasive sensor usually placed on the surface of the skin and records the potential difference (or voltage) between two electrodes from active motor units that span the sensor. One of the objectives of measuring EMG signal in muscle is to obtain information of Motor Unit Action Potentials (MUAPs) that could be used in assessing muscular health or diagnosis of neuromuscular disorders activity (Raez & Hussein, et al. 2006). In this thesis, I will refer to EMG sensors of non-invasive nature.

The formula for a simple model of an EMG signal is

$$x(n) = \sum_{r=0}^{N-1} h(r)e(n-r) + w(n)$$

Eq. 3: EMG Signal Function

where, $x(n)$ is the modeled EMG signal, $e(n)$ represents the firing impulse, $h(r)$ represents the MUAP, $w(n)$ represents the zero mean additive white Gaussian noise and N is the number of motor unit firings.

EMG sensors that are glued to the skin surface often records activity of multiple motor units at a given time and can demonstrate a multitude of entangled signals. Processing of EMG signals is necessary for the filtering of unwanted signal or noise and to obtain the shapes and firing rates of desired MUAPs in EMG signals. To achieve the follow, bandpass filtering and thresholding is applied to raw EMG signal to obtain specific features of muscular activity (Raez & Hussein, et al. 2006).

2.4. Summary

In this chapter, I presented the method of brain imaging and gait recordings that were used for in this study. I provided descriptions of physics and neuroscience to better explain the functions and nature obtained in fNIRS, MRI and MEG. The motivation behind using multiple imaging modalities and fusing gait recordings was to provide a rich data set that could provide information on brain activity and changes in gait during periods of increased cognitive load. The next chapter will information on the protocol of this study and acquisition workflow.

Chapter 3

Study Protocol: fNIRS Measurement of Cortical Activity in Younger and Older Adults during Gait and Dual-Task Assignment

The following protocol has been approved by the “Comité Centrale d’éthique de la Recherche” (CCER). The study took place at the PERFORM Center at Concordia University, 7200 Sherbrooke St W, Montreal. The following section presents a detailed protocol, including subject recruitment, selection, study design, data acquisition and data analysis. Due to restriction imposed by the Covid-19 pandemic, all pilot studies, acquisitions, and participant recruitment was halted in March 2020. The project is planned to recommence in Fall 2021.

3.1. Preliminary Participant Evaluation and Selection

Subject recruitment consisted of public advertisement through professional social media networks, such as LinkedIn, and the distribution of flyers at the PERFORM Center. Study candidature was open to adults between the ages of 18-35 years of age and 65+ years of age. The conditions of recruitment for both age groups required a minimum ability to walk without support (ex. cane, wheelchair) and those who are not currently taking a Central Nervous System stimulant and/or other drugs related to Attention Deficit Disorder (ADD).

Participants selected for this study were chosen from a pool of candidates that passed both a psychological screening and met the required criteria for MRI safety. Candidates first underwent two tests assessing minimum mobility and cognitive functions required for the study protocol. The two tests provided were the *Montreal Cognitive Test* (MoCA) and second, the *Time Up & Go* (TUG) test (Fraser & Li, et al. 2007; Herman T., et al, 2011; Nasreddine, Z. S., et al., 2003).

The MoCA (Nasreddine, Z. S., et al., 2003) assesses moderate cognitive impairment and tests higher cognitive and executive functions related to attention, concentration, memory, calculation, language, conceptual thinking, orientation and visuoconstructional skills. The total score that can be obtained is 30 points; a score of 26 points indicates that an individual possesses average cognitive abilities. The TUG test ((Herman T., et al, 2011) is a clinical performance-based assessment for quantifying gait and dynamic balance ability and targeting lower extremity

function, mobility and fall risk. The general protocol of the TUG aims at evaluating if an individual can walk, turn and sit independently quantifying gait, dynamic balance abilities. The TUG instructions ask the subject to stand up from a standard chair, walk a distance of 3m (marked on the floor) at their regular pace, turn, walk back and sit down. Participants are asked to do this twice and each run is measured with a stopwatch. Better performance is determined by a shorter time to complete the task (Herman T., et al, 2011). An individual is deemed a “risk” for falls if he or she completes the TUG test in more than 12 seconds. For full description and illustration of the MoCA and TUG exam, please consult, respectively, Appendix 1 and Appendix 2 of this thesis.

Once the participant passed the MoCA and the TUG assessments, they were provided with another questionnaire, ensuring that the participant was fit for Magnetic Resonance Imaging.

The following contraindications for this MRI study were:

- Pacemaker
- Aneurysm Clip
- Heart/Vascular Clip
- Prosthetic Valve
- Transdermal Patches (Must be removed prior to scanning)
- Metal Prosthesis
- Pregnancy
- Claustrophobia
- Metal fragments in body

Finally, exclusion criteria for our proposed fNIRS and Gait Study were the following:

- Participants who did not pass the MRI scan criteria.
- Participants who got a score lower than 26/30 on the MoCA test.
- Participants who completed the TUG test in more than 12s.
- Participants who are currently taking Central Nervous System stimulant and/or other drugs related to Attention Deficit Disorder.
- Participants who have suffered from a neurological disorder.

3.2. Materials

Magnetic Resonance Imaging (MRI)

The MRI system provided by the Imaging Lab at PERFORM is a 3T General Electric (GE) scanner with eight channels coils. The MRI sequence consisted of a T1 and T2 anatomical scans, a functional MRI (fMRI) scan and Diffusive Tensor Imaging (DTI) scan. The duration of the scan lasted approximately 60 minutes and was performed under supervision of an MRI lab technician. The following protocol was used to record anatomical and functional data while the participant performed Serial Seven cognitive task.

fNIRS System

The fNIRS system used for this study is The Brainsight fNIRS system provided by Rogue Research and is installed at the PERFORM Center of Concordia University. The Brainsight fNIRS system is a continuous wave NIRS system equipped with 32 laser emitters (16 sources operating at 690 nm and 16 sources operating at 830 nm) and 32 detectors.

To ensure good quality fNIRS recordings and minimize the effects of motion during fNIRS acquisitions, optodes were glued on the scalp using a clinical adhesive, collodion . Each optode was covered by a rectangular gauze (approximately 2cm²), covered with a required amount of collodion to cover the gauze, and dried with pressurized medical air will be used to ensure firm adhesion to the scalp. The participants' hair was parted and the scalp was cleaned with an alcohol swab to obtain optimal contact between the optode position and the scalp. Collodion has been used across several fNIRS studies and the method of choice for extensive acquisitions (Pellegrino, Machado, et al., 2016; Machado et al., 2018). The use of collodion in the gluing of personal montages has been shown to minimize motion artifacts in fNIRS recordings and has been previously used in the NIROT workflow (Cai, et al., 2021).

3.3. Design

The following section provides a detailed schedule and description of the study design. There was a total of two visits to the PERFORM Center to complete the study.

Session 1

Following the TUG test and MoCA described in section 3.1. Preliminary Participant Evaluation and Selected participants underwent a series of brain imaging scans inside of the GE 3T scanner at the PERFORM Center of Concordia University, Montreal, Canada. The MRI sequence consisted of T1 and T2 anatomical MRIs, two fMRI scans consisting of block design cognitive task, and one DTI lasting approximately 25 minutes.

#	Scan	Sequence	Purpose
1	Anatomical T1-weighted scan	BRAVO, 1 mm isotropic 3D acquisition, 192 sagittal slices, 256×256 matrix, TE = 3.18 ms, TR = 8.16 ms, flip angle 12°.	Brain anatomy
2	Cube; T2-weighted scan	Cube, 1 mm isotropic 3D acquisition, 192 sagittal slices, 256×256 matrix, TE = 87.34 ms, TR = 3000 ms, flip angle 90°.	Brain anatomy
3	fMRI	EPI (Echo-Planar Imaging) sequence, 3.7 mm isotropic, TE=25 ms, TR=2 s, flip angle 70°.	Activation Mapping
4	Diffusion MRI (DTI)	2D Spin Echo sequence, 2mm axial, TE = 82 ms, TR = 8500s	Diffusion Maps; white matter pathways
Total Scan Time			
Approximately 60 minutes			

T1-weighted anatomical images were obtained using the 3D BRAVO sequence (192 axial slices, 1×1×1 mm³, 256×256 matrix). T2-weighted anatomical images were acquired using the

3D Cube T2 sequence (168 sagittal slices, $1 \times 1 \times 1 \text{ mm}^3$ voxels, 256×256 matrix). Participants also underwent two functional MRI acquisitions while conducting the Serial Sevens cognitive task; the same task as in the fNIRS acquisition. fMRI acquisition consisted of EPI gradient echo sequence (32 axial slices, $3.7 \times 3.7 \times 3.7 \text{ mm}^3$ voxels, TE = 25ms, TR = 2,000ms) which sought activation mapping while the participant . The total duration of MRI scans was approximately 60 minutes.

During T1 and T2 MRI scans, the participant laid stationary and at rest; at capturing images of the individual's anatomical brain structures. Next, during the fMRI, the participants would perform a cognitive task; a mental arithmetic activity via Serial Sevens.

Session 2

The second session is a three-hour visit, which consisted of fNIRS, Electromyography (EMG) and Switch Foot System installation, performance of dual-task activities, and fNIRS recordings. The fNIRS recordings was separated into five parts; one recording for the participants' responses in resting state, two recordings during single task and two recordings during dual task activities. There is one type of single task assignment, standing stationary during mental arithmetic, tested via Serial Sevens, and one type of dual-task activity, which consists of performing both self-paced walking on treadmill and mental arithmetic simultaneously.

Below is the description of three types of recordings:

1st - resting state recording, in which the participant in standing, stationary (5 min)

2nd - single task: participant is standing, stationary, and performs mental arithmetic (Serial Sevens) (appr. 15min)

The participant remains stationary on the treadmill for to record resting state and then begin Serial Sevens for 30 seconds (single task). Jitter was be applied to each interval of standing/mental arithmetic ($1 \text{ min} \pm 15 \text{ s}$) until the 15 minute recording is complete. This single task consists of a total of 10 blocks and is performed twice, generating a total of 20 blocks.

3rd - Dual-task: participant walks on treadmill and performs mental arithmetic (Serial Sevens) (appr. 15min)The participant walks on the treadmill for 1min to record single task. At 1min mark, participant began Serial Sevens for 30 seconds (dual task). Then the participant stopped performing mental arithmetic but continues walking on treadmill for 1min. Jitter was applied to each interval of walking/Serial Sevens+walking (1min ± 15s) until the 15 minute recording is complete. This dual task consists of a total of 10 blocks and is performed twice, generating a total of 20 blocks.

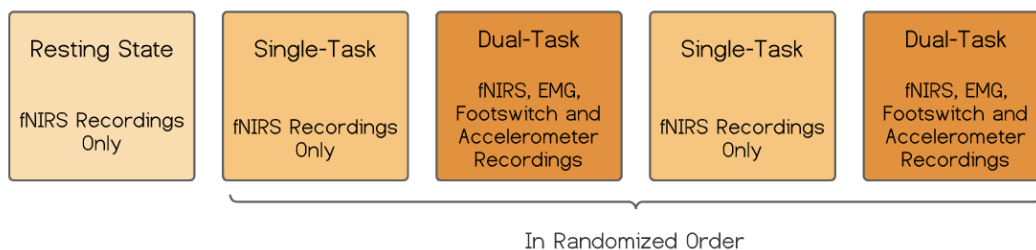
4th – single task: same as the description in the 2nd task

5th – dual task: same as the description in the 3rd task

The reason why there are two single runs and two dual task runs in the design is to ensure that there is integrity in the data in case of participant/researcher novelty and uncertainty in the procedure. Also, it will provide more data for comparison of brain region activation and physical adaptation to single versus dual task.

3.4. Protocol: Block Design Paradigm for ST and DT in fNIRS recordings

Single and dual task activities consisted of continuous fNIRS recordings. A stimulus block design was used to test the brain response while performing mental arithmetic during ST, serial-sevens subtraction only, and DT, serial seven subtraction while walking. This design was chosen to enable the extraction of the hemodynamic response during each event and conduct averaging within a condition.



ST and ST blocks were assigned to be 30s in duration; a length of time long-enough to assume a peak hemodynamic response at 5s to 6s after onset, a plateauing hemodynamic response until 30s

and return to baseline in the 10s following the block. Jitter as introduced in between each trials and ranged between $60s \pm 15s$. The objective of adding jitter to the block stimulus design is to minimize the effect of confounding physiological signals that may share rhythmic frequencies with the timing of the paradigm and sampling frequency of fNIRS data at 10Hz (i.e. Meyer waves at 0.1Hz)(Yucel & Selb, et. al., 2016). The addition of jitter would increase the likelihood of obtaining a less biased hemodynamic response during each stimulus block.

3.3.1. Setup of the fNIRS & Gait Acquisition

The setup of the protocol consists of multiple devices used for recordings brain activity, electromuscular activity and gait recordings via fNIRS (BrainSight, Rogue Research), EMG and footswitch, respectfully. EMG data is comprised of a total of eight muscles activity recordings and is monitored by the TeleMyo Direct Transmission System (Telemyo DTS). Footswitch data, also recorded using the Telemyo DTS, consists of four sensors, counting the heels and toes of the right foot and left foot, and are recorded along with EMG data via gait recordings software - Neuroaxon. An

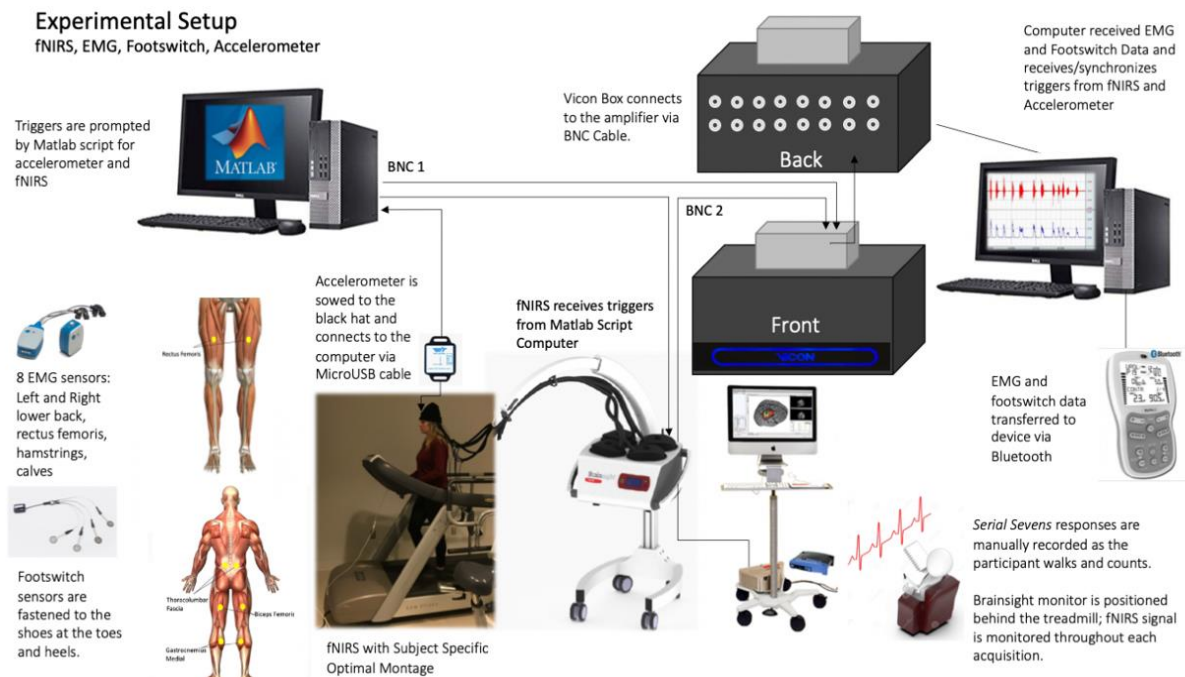


Figure 6: Experimental Setup of the A complete schematic demonstrating all recordings and their corresponding devices during the Single Task and Dual Task acquisitions.

accelerometer was also used to measure head motion of the subjects during the run testing DT condition. The following Figure 5c provides a systemic overview of the acquisition methods and workflow of the study.

A Matlab script originating from the primary PC synchronized accelerometer and fNIRS recordings, as well generated random 3-digit numbers for the Serial-Sevens stimulus-block model in Single (ST) and Dual-Task (DT) conditions.

During ST conditions, the goal was to obtain fNIRS recordings only, and therefore, we relied on the triggers generated by the governing computer workstation and communication of triggers to the Brainsight system. During DT conditions, the goal was to record fNIRS data from the Brainsight system, EMG and footswitch data from the Neuroaxon system and accelerometer. The primary workstation, consisting of a Matlab script, generated triggers which were sent to the was relayed to the Brainsight system and continued to the Vicon Box. The Vicon Box was responsible for synchronizing triggers obtained from both the Brainsight system and triggers set by the Neuroaxon system monitoring EMG and footswitch recordings. The Neuroaxon system was located on a secondary workstation and received transmitted data from EMG and footswitch sensors via Bluetooth. Because EMG, footswitch and fNIRS recordings were often started a couple of seconds apart due to separate workstations, the first trigger's time stamp from the Neuroaxon system was adjusted in time to the first trigger recorded in the primary workstation generating fNIRS triggers.

During DT condition, the protocol enforced that each participants wear a harness to minimize risk of falls and/or loss of balance. fNIRS sensors cables were fastened with tape to the harness with the intention of reducing the motion of the optode cables while a participant is walking on the treadmill. Further testing is required to test the most optimal workflow and safety considerations of the harness; these concerns are addressed in Chapter 6: Discussion.

Chapter 4

Methods: Analysis of Functional Data and Gait Measurements

This chapter addresses the methodology and analysis applied to data obtained in fNIRS and gait measurements. The first section describes the personalized montage generated by the Optimal Montage Algorithm and NIROT workflow with MEM (Machado, et al., 2018; Cai, et al., 2021). The second section provides evaluation of accelerometer-based motion artifact detection and trial selection to minimize the number of noisy, artifact trials in the analysis. Figure 7: Workflow Map, present a global perspective of each step in the workflow of this study.

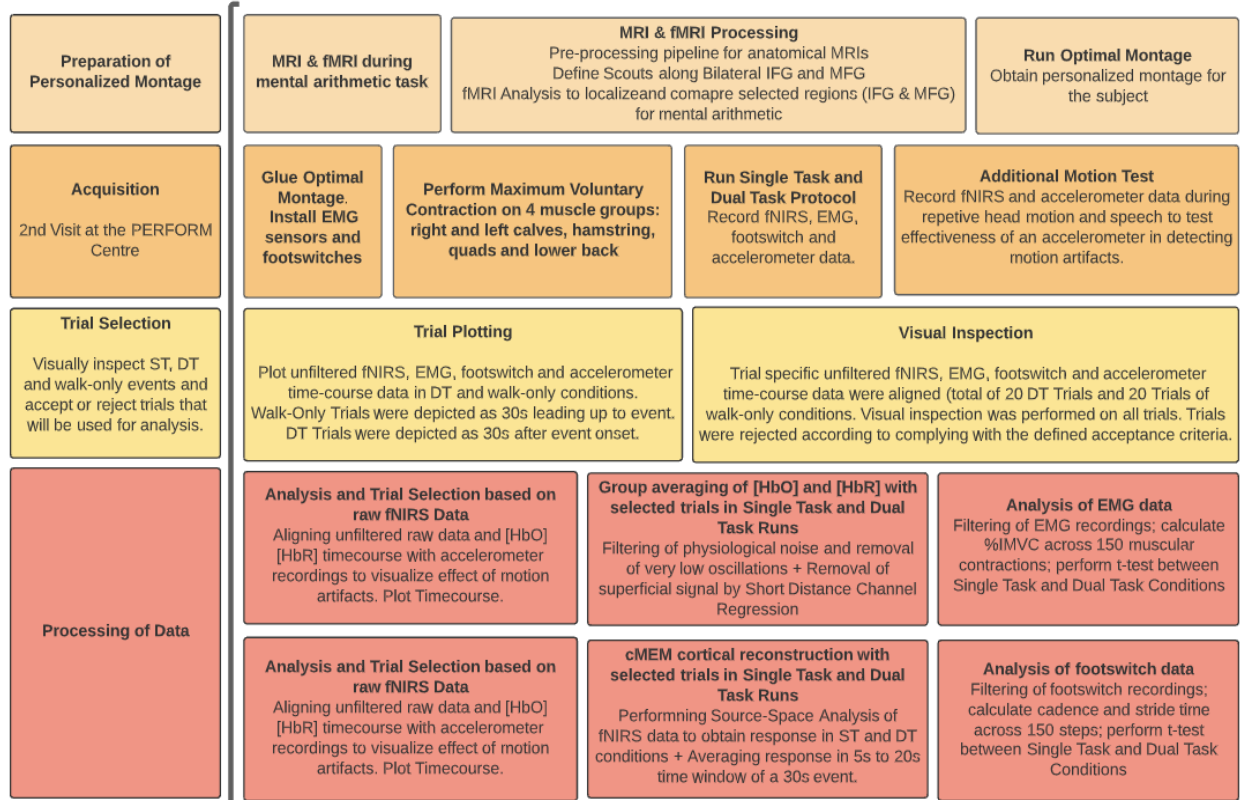


Figure 7: Workflow Map

The following workflow map presents a top level description of acquisition preparation and, data verification and data analysis required across all types of recordings.

There were three types of data analysis in this study. The first involved studying fNIRS signals using the personalized montage system generated by the MultifunkIm Lab' Optimal Montage Algorithm. The second and third sets of data involved gait measurements, which were provided via EMG and the foot switch system. This section delves into specifics of each analysis, dealing with synchronization of time course of data from different sources, the algorithms used in analysis, filtering of signal, and the removal of physiological and motion artifacts.

4.1. Processing of functional MRI and anatomical MRI

Anatomical MRI

Analysis of MRI data consisted of using Statistical Parametric Mapping (SPM12) and FreeSurfer6.0 software which served in segmentation of the subject's brain and creation of five distinct surfaces; the scalp, skull, cerebrospinal fluid (CSF), white and grey matter. Scalp and skull masks were segmented using SPM. Gray matter and white matter masks were produced from the cortical/subcortical segmentation using FreeSurfer6.0 (Cai, et al., 2021).

4.3. Personalized fNIRS acquisition using optimal montage targeting bilateral IFG and MFG

The Optimal Montage algorithm is a method that determines a priori the optimal position of fNIRS sensors that will provide maximum light sensitivity to a target brain region. The optimal positioning of optodes is characterized by the arrangement of sources and detectors that maximize the sensitivity of the montage over a specified Region of Interest (ROI). ROIs that were defined on the left and right IFG and MFG on the participant's anatomical mid-surface were projected to the fMRIs projected surface to visualize and compare if the demarcated ROIs contain levels of increased brain activity, as stated in the hypothesis. fMRI maps served solely as guides for demarcation of ROIs along the right and left hemisphere.

Personalized montages were calculated to target signal from 21 channels, composed of three sources, seven detectors, and one proximity on each hemisphere. Optodes were arranged bilaterally across the Prefrontal Cortex (PFC), specifically into regions of the. A personalized fNIRS montage,

generated via the Optimal Montage (OM) algorithm, was the method used in determining the location of each source and detector.

To generate a participant's personalized montage, a head model was generated using the anatomical MRI acquired during the first session of this study. The OM algorithm requires the calculation of optical fluences for each fNIRS optode using Monte Carlo simulation using 10^8 photons projected onto the head model using MCXLab (Cai, et al, 2020; Fang & Boas, et al., 2009). The location of the proximity was determined at the time of acquisition and was placed in the middle of the sources. The proximity sensor serves as a method of short-distance channel regression when it is close to a source (inter-optode distance, approximately 1.5cm between source and proximity) and is used as a method to regress out superficial extra-cerebral activity (Cai, et al., 2020).

Subject specific montage methodology has been proposed as an effective approach to overcome individual anatomical differences, as each participant differs in head size, shape, and most importantly, distinction and variability of brain volume and structure. Furthermore, the OM algorithm provides some technical advantages to acquiring more robust data by improving the observation of spatial overlap of signal, allowing for more accurate local 3D reconstruction in the targeted Volume of Interest (VOIs) and offers the highest Signal to Noise Ratio (SNR). The OM algorithm maximizes a priori the sensitivity to target brain regions and permits reconstruction of locally underlying hemodynamic activity along the underlying cortical surface (Machado, et al, 2018). For these reasons, we considered our proposed personalized montage method for this fNIRS study.

4.5. Removal of physiological noise and very low oscillations in fNIRS

Systemic physiological fluctuations are largely impacting raw fNIRS signals, specific preprocessing should be considered to disentangle the hemodynamic activity of interest from these fluctuations (Yücel et al., 2017).

To do so, raw fNIRS signals at 690 and 830 nm were first bandpass filtered (0.01Hz-0.5Hz) using the infinite impulse response (IIR) filter to remove very low oscillations (0.01Hz-0.1Hz) caused by changes in blood pressure and vasoreactivity. Bad channels were removed based on the presence of negative signal. Next, short-distance channel regression was applied for superficial signal correction

originating into close distance source detector pairs (Machado & Cai, et al., 2021). After the raw signal was converted to optical density measurements of [HbO], [HbR] and [HbT] via MBLL, a low pass filter with high cut-off frequency of 0.1Hz was applied to remove Meyer waves (~0.1Hz), and physiological noise originating from heartbeat (appr. 1Hz) and respiration (appr. 1.5-3Hz) (Yücel et al., 2017; Machado et al., 2018). All signal processing of fNIRS raw data was performed in Brainstorm, using the toolbox NIRSTORM developed in the MultiFunkIm Lab: (<https://github.com/Nirstorm/nirstorm/wiki>).

4.6. Assessment of motion artifacts in fNIRS signals using a 9-axis Accelerometer

Inconsistent contact between fiber optic and the skin may generate noise and data loss during acquisition. Motion, such as turning of the head or brisk movement, often causes optodes to lift off the skin on the scalp and decouple light traveling from source and detector, resulting in high-frequency spikes or baseline shifts (Virtanen, et al. 2011). As described in section 3.2. Materials used in fNIRS acquisitions, the clinical adhesive, collodion, was used in gluing of the personal montage to minimize the effects of motion on raw fNIRS signal and decoupling of fNIRS optodes and the scalp (Yücel et al., 2014). To evaluate the effectiveness of collodion in reducing sensor sensitivity to motion, a 9-axis accelerometer (Witmotion, WT901BLECL Bluetooth 5.0 Gyro Sensor) was sewed to a tight hat which each participant wore on top of the optical fibers of the fNIRS system. During the DT exercises of this study, the accelerometer continuously monitored the participant's head motion, recording x, y and z acceleration and angular data at a sampling frequency of 5Hz. fNIRS data was recorded simultaneously using the BrainSight system.

The accelerometer data was first upsampled to 10Hz to match the sampling frequency of fNIRS recordings. To ensure that fNIRS data and accelerometer data were synchronized in time, the accelerometer time-series data consisted of time-stamps that marked the onset of each event inside of the DT run. The first time-stamp in the accelerometer time-series was then aligned in time with the first event trigger recorded by

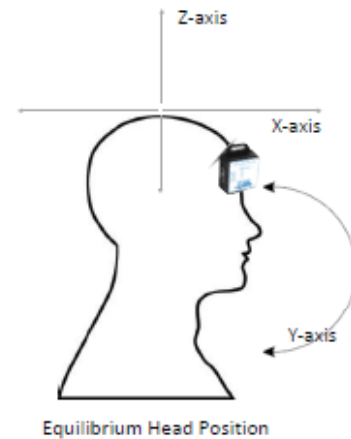


Figure 8: Position of Accelerometer for Motion Test

the BrainSight system. The two sets of recordings were aligned along their time series demonstrate synchronized fNIRS raw data and head motion recordings.

Three-axis acceleration, angle time-series data recorded by the accelerometer was aligned with 1) raw, unfiltered fNIRS time-series signal, 2) unfiltered [HbO]/[HbR] time-series, 3) EMG time-series data and 4) footswitch data that illustrated a 60s time-window around each of 20 DT trials (see Appendix C for each participant's DT and ST trial selection evaluations). Figure 6: Trial Selection Evaluation in DT Conditions demonstrates an example of how all sources of data were combined to assess the effectiveness of the accelerometer in capturing motion and visual identification of sudden changes in raw fNIRS time-series signal and unfiltered [HbO]/[HbR] time-series.

4.7. Trial Selection in Block Averaging of Single and Dual Task Assessment

Visual inspection of signal quality was performed on all 20 trials of ST and DT conditions for each participant. The raw, unfiltered time-series signal and unfiltered channel-space [HbO] and [HbR] amplitudes after mBLL computation were studied simultaneously to visualize potential motion artifacts characterized by sharp peaks in signal amplitude. By visually inspecting the raw signal, I could better identify sudden changes in signal that could suggest motion artifacts or other sources that may have contributed to noisy signal. I then applied the short-distance channel regression and the mBLL function on the raw signal to visualize if the [HbO] and [HbR] also suggested motion artifact; this was evaluated by aligning the raw signal and [HbO]/[HbR] time-series and visually discerning the quality of the signal and evaluating the criteria for acceptability in block averaging analysis, shown in *Table 1: Conditions for Trial Rejection of fNIRS ST and DT Trials via Raw Signal Inspection*. This was done on each raw-signal time series of each trial, in which the task duration was 30s. To ensure the analysis of the complete hemodynamic response within the given channels, the time window for observation for each event was set at 65 seconds, i.e. 10 seconds before the task onset and 55 seconds after the task onset.

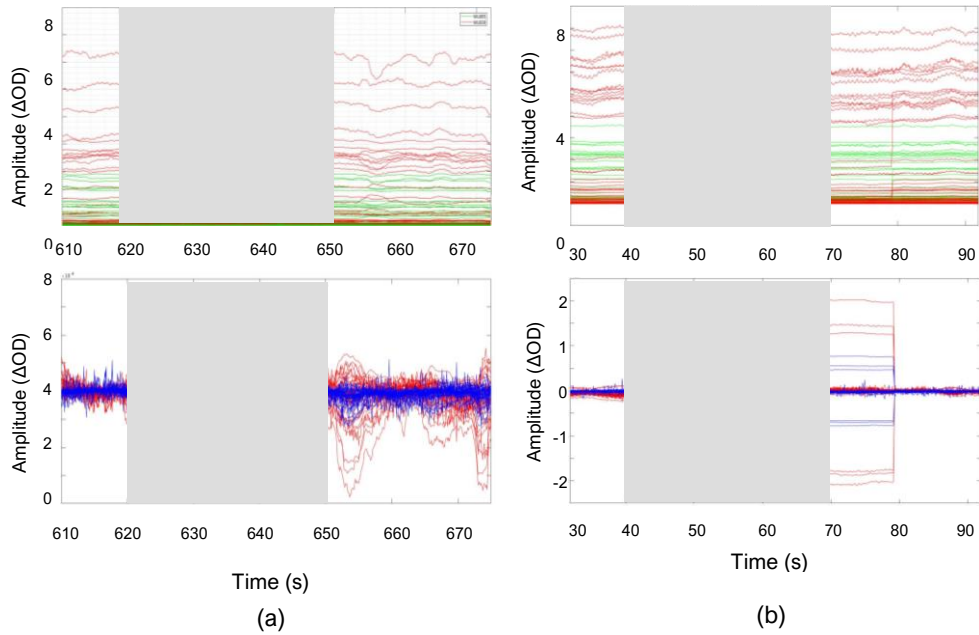


Figure 9: Condition for Trial Rejection in Raw fNIRS Signal
 Figure 9(a) demonstrates a rejected trial due to raw fNIRS data and unfiltered HbO and HbR containing apparent motion artifacts which lasts more than 8s. Figure 9(b) demonstrates a rejected trial due to raw data channels containing signal saturation.

Type of Artifact	Condition
Motion	Trial was rejected if raw data and unfiltered HbO and HbR contain one or more sharp peaks during 30s time window of the event.
Duration of Artifact	Trial was rejected if raw data and unfiltered HbO and HbR contains artifact which lasts more than 8s leading in, during, or at the leading out segment of the event.
Saturation of Channels	Trial was rejected if raw data contains channels demonstrating channel signal saturation and unfiltered HbO and HbR contains concentration changes that demonstrates sharp increases and plateaus.

Table 1. Conditions for Trial Rejection of fNIRS ST and DT Trials via Raw Signal Inspection

4.8. Electromyography (EMG) and Footswitch Data Processing: Detection of Changes in Muscle Contraction during Single anal Tasks

Prior to beginning the Single and Dual Task acquisitions, the Maximum Voluntary Contraction (MVC) was tested for all eight muscle groups and used for the normalization of the EMG signal. EMG recordings were bandpass filtered (Butterworth 50–300 Hz), fully-rectified (i.e. taking the absolute value) and studied by taking the root-mean squared (RMS) ratio between each muscle group and its Maximum Voluntary Contraction (MVP) (Li et al., 2012). This processing pipeline is termed Isometric Normalization of EMG data and demonstrates the extent of muscular contraction during walk relative to the recorded contraction when a participant exerts his or her maximal extension or contraction force on that muscle. On average, participants took 32 ± 2 steps during the dual-task assessment, in which one the duration of one event was 30 seconds. To obtain a more accurate values of variability via percentage of maximum voluntary contraction, a total of 150 peak EMG recordings were studied by taking the greatest 30 recordings with the largest amplitudes across five DT events. The same was conducted on the 30 seconds leading up to each DT event, recording the greatest 30 peak bursts during a participant's walking phase. The average, range and standard deviation of these selected EMG recordings were calculated and compared across two conditions: walking-only and dual-task (walking + Serial Sevens).

EMG Analysis Pipeline

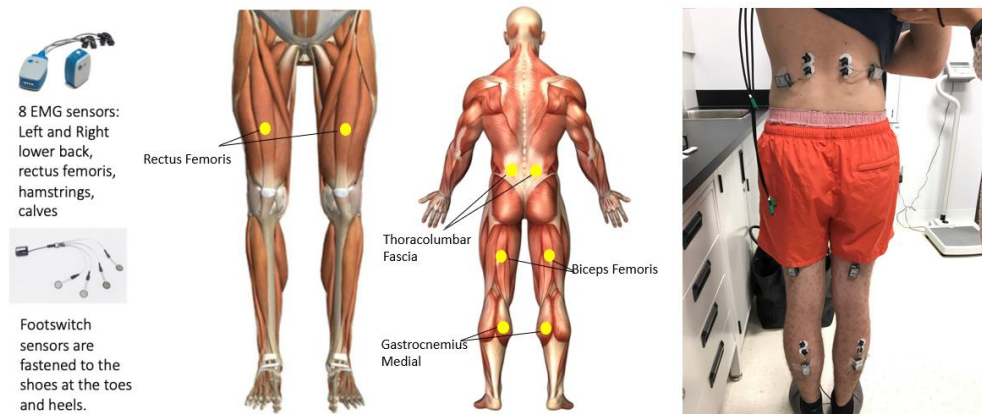
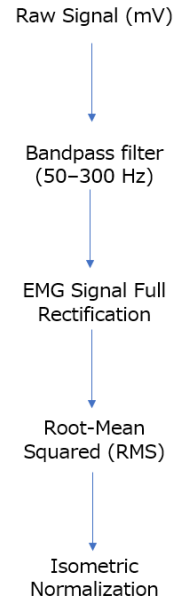


Figure 10: EMG Sensor Placement

The left-hand side of Figure 9 presents the sensors belonging to the Telemyo DTS EMG System used in this study. The three figure to the right illustrate the location of the EMG sensors. The muscle groups studied were the Gastrocnemius Medial (Calf), the Biceps Femoris (Hamstring), Rectus Femoris (Quads). EMG data from the Thoracolumbar Fascia (lower back) was recorded, though was not considered in the analysis.

4.9. Footswitch recordings and data analysis

Footswitch sensors were positioned on both the heel and toe of both feet. Data obtained from the footswitches installed on the shoes were used to identify phase of gait, such as cadence stride time (duration of time of a complete cycle, heel contact to next heel contact – for one foot), as demonstrated in Figure 7: Gait Cycle.

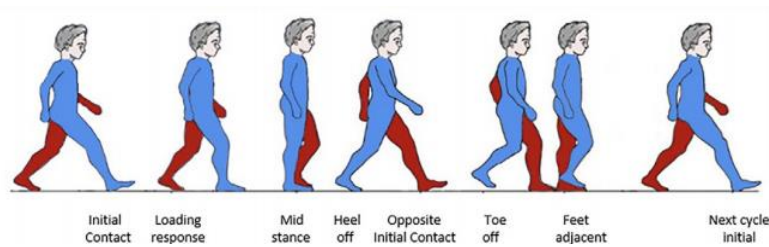


Figure 11: Gait Cycle

One full gait cycle begins at the heel strike of one foot and is complete when the same heel strikes again in preparation for the next step. (Ben-Gal, et al., 2020).

Footswitch recordings were first high-pass filtered at 50Hz and exported to Matlab to study responses obtained from left and right foot. A script was generated to calculate cadence and stride time at the single-subject level according to formulas Equation 3(a) and 3(b). Since each participant is exhibited unique features regarding gait, footswitch data, measured in millivolts, mV, were first visually inspected to discern the mV range for heel versus toe interaction. This mV range of heel versus toe recordings was then use to binarize the data in order to segment heel and toe contact with the ground from the recorded signal (heel = 1, toe = 0). This binarized signal reporting heel and toe contact was then considered as the input for calculating cadence and stride time.

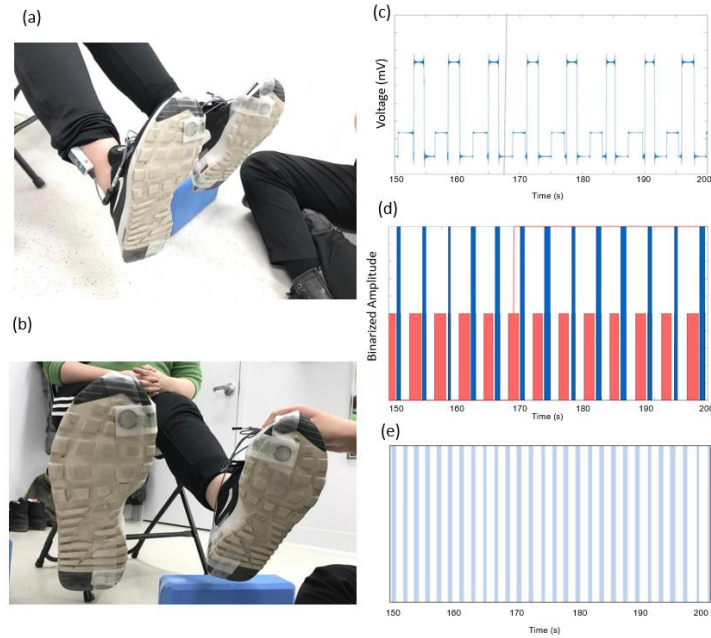


Figure 12: Footswitch Sensor Setup and Cadence Extraction Pipeline

Figure 11 (a) and (b) demonstrate the setup of the footswitch on the participants' shoes. Figure 11 (c) is the signal obtained from the footswitch sensors Highpass filtered at 50Hz. Figure 11 (d) is the plotted figure of footswitch data binarized with the time values associated to swing (value of 0), toe strike (value of 1) and heel strike (value of 2). Figure 11 (e) is the extracted heel strike data which is superimposed on the associated EMG, accelerometer and fNIRS time-course data.

$$Cadence = \left(\frac{\#steps}{30s} \right) \times 2 = \#steps/minute$$

DT condition: 30s duration of walking while calculating Serial Sevens

Equation 5: Cadence Equation

$$Stride\ Time\ (s) = Cadence / 60$$

Equation 6: Stride Time Equation

Binarized footswitch data were visually examined to ensure that the sensors consistently captured heel and toe interactions and did not have large gaps that would bias cadence and stride time calculations. Once verified, cadence and stride time were then calculated across each participants' custom selected trials for each subject across two conditions: Dual-Task (DT) or Walking-Only. A 'trial' was defined as the 30s period in which a participant performed DT condition of calculation Serial Sevens while walking.

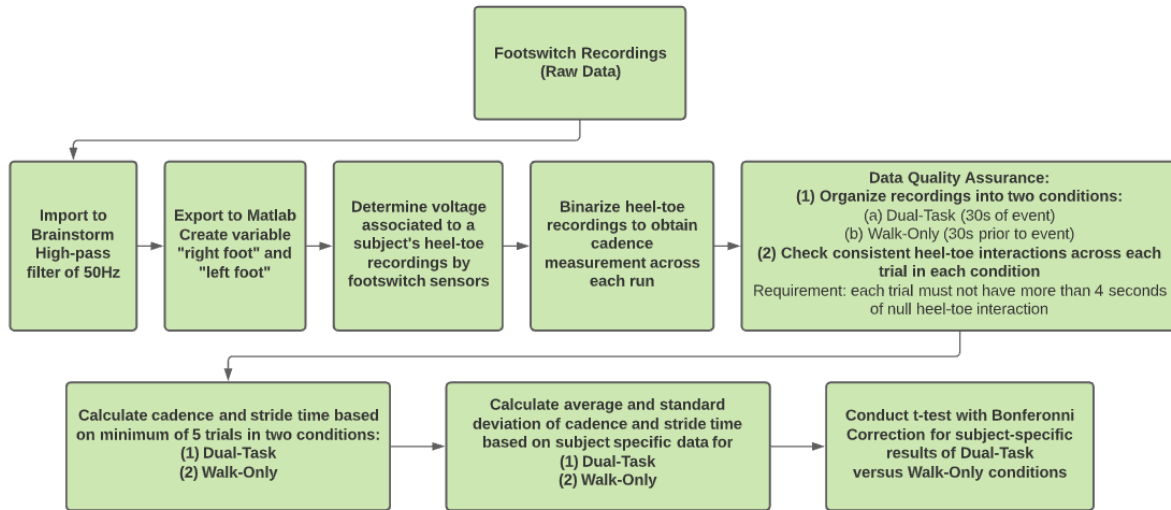


Figure 13: Footswitch Recordings Workflow and Analysis

Difference of gait performance between DT and ST conditions was finally assessed using a student's t-test on cadence and stride time. Figure 13(a) is an example of accepted footswitch-cadence trial during dual-task with consistent data used in alignment with fNIRS, accelerometer and EMG data. Figure 13(b) is an example of a discarded footswitch trial during dual-task due to inconsistent sensor contact between the heel and the treadmill carpet.

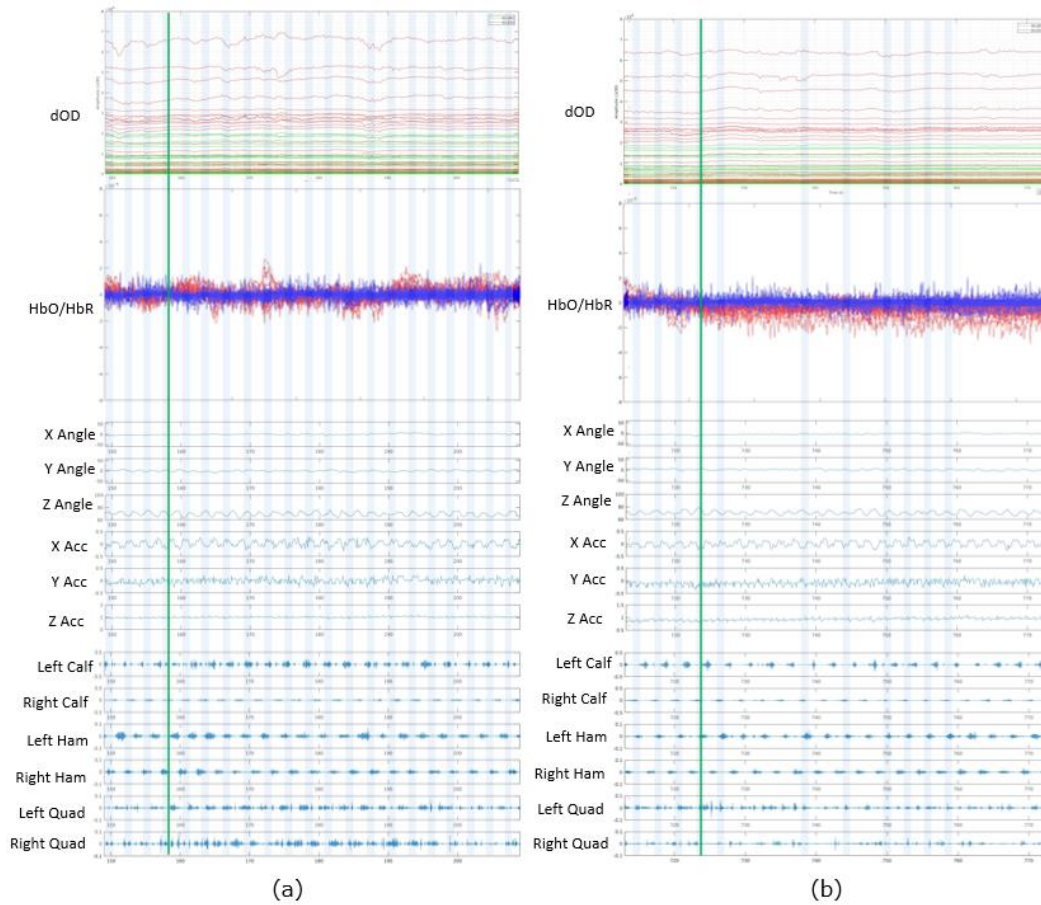


Figure 14: Selection of Cadence Trials

The following two figures illustrate case by case analysis of data acquired during dual-task trials. The onset of the dual-task event (walking + Serial Sevens) is depicted with a green vertical bar and marks the onset of the 30s dual-task. Figure 13(a) demonstrates an accepted trial for footswitch data. 13(b) is a rejected footswitch trial due to inconsistent sensor contact with the ground, depicted by inconsistent vertical bars across data.

<i>EMG and footswitch Data Measurement and Analysis Pipeline</i>	
Selection Criteria	<p>Footswitch recordings were studied under two conditions: Walking Only versus Dual-Task.</p> <p>The foot with the most consistent footswitch recordings was selected as the dominant foot for analyzing gait parameters. Consistent footswitch data must have continuous cycles of gait throughout the duration of the 30s condition.</p>
Processing	Recordings were imported into Brainstorm and high-pass filtered at 50Hz to obtain heel-toe defined voltage.
Gait Metrics	<p>Cadence (steps/min): To calculate the cadence during two conditions ('Walk Only' and 'Dual'), 30s time window before the task and 30s during the task was used to generate binary values indicating the start of each consecutive step. The number of steps were recorded over five trials of the two conditions and multiplied by two to achieve the cadence during each trial.</p> <p>Stride Time: calculated from the interval of time required between steps. The Stride Time is calculated by taking the value obtained in a participants' cadence divided by 30s, and then multiplied by two.</p>
Method	Time-series of footswitch recordings were imported from Brainstorm to MATLAB to obtain threshold voltage ranges for heel-contact and toe-contact. Measurements of toe-heel footswitch voltages were translated into binary values (1 = heel contact with the treadmill belt/beginning of step, 0 = foot is in swing). A script was written to obtain the cadence and stride time for five trials of each condition; Walking Only (30s time window before the onset of dual-task) and Dual-Task (30s of the Dual-Task: Walking and S7 simultaneously).
Analysis	<p>Single-Subject Cadence in two conditions (Walking Only versus Dual-Task).</p> <p>Single-Subject Stride Time (Walking Only versus Dual-Task).</p> <p><i>t-test</i> and <i>p-value</i> between two conditions .</p>

Table 2. EMG and footswitch Data Measurement and Analysis Pipeline

4.10. Trial Selection across Single-Task and Dual-Task Conditions

In this section, I will address the process and requirement involve in properly conducting trial selection. Trial selection brings together all pre-processing inspection methods mentioned in Chapter 4 and is the process less noisy and less artifactual data set for analysis using the NIROT workflow. Trial selection therefore combines 1) ensuring the quality of data before performing analysis, and 2) evaluate the effectiveness of the accelerometer in capturing head motion as a factor in noisy fNIRS signal. As discussed in Section 4.7. Trial Selection in Block Averaging of Single and Dual Task Assessment, trial selection was conducted according to a defined set of criteria. The step of performing trial selection prior to continuing the data analysis was essential because the protocol for this study required a lot of movement. Participants were asked to walk on a treadmill while wearing a harness, and wear a hat to hold the accelerometer flat upon their forehead while the fNIRS montage as glued to their scalp. These factors could lead to a participants' discomfort and can affect the quality of the fNIRS signal if there are brisk movement of the head.

After participants completed their 2nd session at the PERFORM Centre, fNIRS data, EMG, footswitch and accelerometer were saved imported into their respective software to perform trial selection process to 1) ensure the quality of all data before performing analysis, and 2) evaluate the effectiveness of the accelerometer in capturing head motion as a factor in noisy fNIRS signal. Trial selection was conducted on all ST and DT runs across all participants; each participant performed 20 trials of ST condition and 20 trials of DT condition. Trials were accepted or rejected based on the criteria stated in Table 3:

Type of Artifact	Condition
Motion	Trial was rejected if raw data and unfiltered HbO and HbR contain one or more sharp peaks during 30s time window of the event.
Duration of Artifact	Trial was rejected if raw data and unfiltered HbO and HbR contains artifact which lasts more than 8s leading in, during, or at the leading out segment of the event.

Table 3: Assessing Rejection Criteria of raw fNIRS Signal for Trials Selection

Saturation of Channels	Trial was rejected if raw data contains channels demonstrating channel signal saturation and unfiltered HbO and HbR contains concentration changes that demonstrates sharp increases and plateaus.
------------------------	--

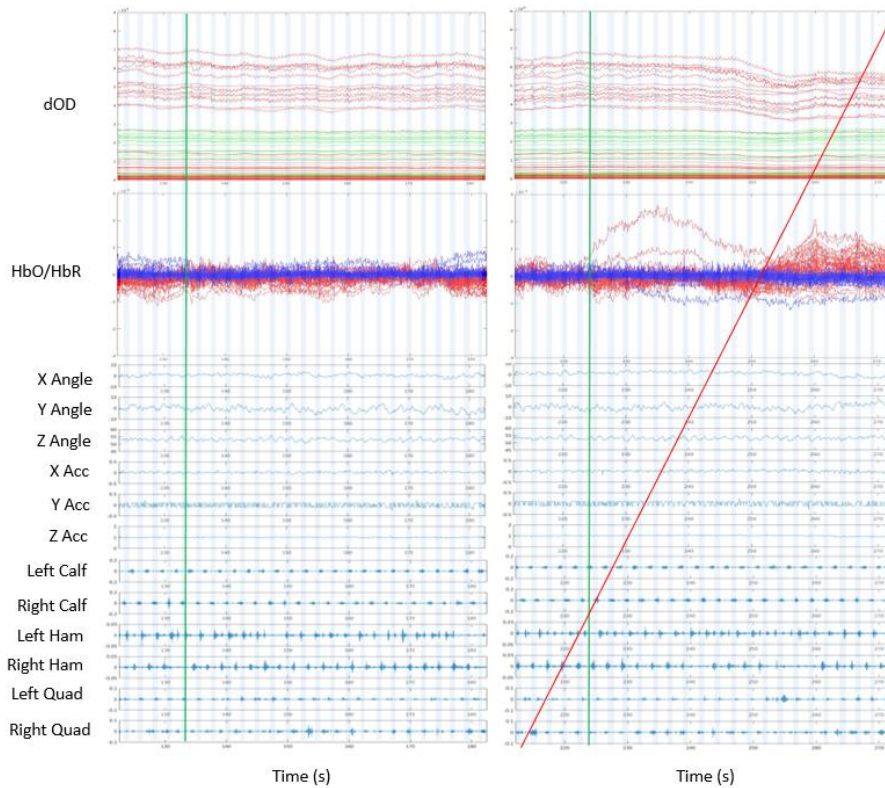


Figure 15: Data Quality Assessment via Trial Selection on Raw fNIRS Data

The data set on the left-hand side of Figure 14 depicts an accepted trial for NIROT method analysis. The unfiltered, raw fNIRS signal and $[HbO]/[HbR]$ do not exhibit motion artifacts mentioned in the rejection criteria (Table 3). The data set on the right-hand side of Figure 14 depicts a rejected trial for NIROT method analysis. The unfiltered, raw fNIRS signal and $[HbO]/[HbR]$ suggests presence of motion artifacts such as sudden peaks in amplitude and drifts lasting for more than 8s, according to the rejection criteria mentioned in Table 3.

4.10. MEM Reconstruction along the cortical surface

In this thesis, I used Maximum Entropy on the Mean (MEM) as inverse problem solution in the NIROT method reconstruct the obtained fNIRS recordings onto the cortical surface or each

participant. The MEM framework is a chosen approach in fNIRS analysis for its capacity to recover spatially extended generators and pays close attention to potential bias in reconstruction. In the context of this study, the motivation of generating MEM reconstruction of signal in the source space was to generate sensitivity maps of brain activity elicited during single and dual task assignments, suggesting a solution of the inverse problem.

Calculation of the MEM reconstruction maps of DT versus ST conditions required the following workflow. First, selected trials of ST and DT condition were converted from raw NIRS signal into Optical Density (OD) measurements, applying short-distance channel regression for removal of superficial physiological fluctuations. The OD timecourses were then band-pass filtered between 0.01Hz and 0.08Hz via 3rd order Butterworth filter. Next, ST and DT condition data were blocked averaged over a window of -10s to 55s to obtain information on the response around the event onset, occurring between 0s to 30s. This was repeated for data obtained from the left and right hemisphere, and for ST and DT conditions, resulting in a total of four blocked average timecourses (*four scenarios: ST/Right, ST/Left, DT/Right, DT/Left*); the decision for dividing the left and right sides of the montage was based on keeping a consistent analysis method for both [HbO]/[HbR] response and MEM. Head models were computed using fluences and enabled by the extraction of corresponding sensitivity maps.

Finally, MEM reconstruction was calculated using the OD input to obtain eight outputs: the [HbO] and [HbR] response in the selected ROIs on left and right hemispheres and for all four scenarios. To better extract the prominent hemodynamic response to the onset of S7 calculation, MEM reconstructions of [HbO] and [HbR] were time averaged between 5s and 20s out of the 30s event blocks. Lastly, the left and right new 5s-20s time averaged reconstructions were grouped by conditions to obtain bilateral [HbO] and [HbR] reconstructions along the cortex. The results provided a total of eight spatial maps that demonstrated the averaged reconstructed signal between 5s-20s. The benefit of calculating the reconstruction along the cortical surface using MEM provides the solution to the inverse problem, confirmation or refuting that the signal obtained falls within the left and right IFG and MFG regions of interest.

Chapter 5

Results

5.1. Results: Single Subject Analysis of fNIRS and EMG Data

The following chapter will present the results obtained from fNIRS and gait data from seven subjects at the single-subject level on our preliminary collected data consisting in five young adults, 28 ± 6 years of age, 3 females; and two older adults, 67 ± 2.5 years of age, 1 female. A total of 30 participants were anticipated for this study; however, due to restriction imposed by the Covid-19 pandemic, all acquisitions and further participant recruitment was halted. All subjects passed the MoCa Test with a grade of 26 or higher out of 30 (minimum grade required to pass the MoCA) and successfully completed the TUG test prior as a criterion of acceptance for participation in this study.

The results addressed in this chapter encompass data recordings from participants' second visit to the PERFORM Centre, which entail fNIRS, EMG and footswitch recordings. The analysis conducted includes block averaging of selected ST and DT trials, MEM reconstruction of response along the right and left hemispheres based on selected ST and DT trials, and the statistical analysis of EMG and footswitch data. Prior to performing the single and dual task analysis pipelines according to the NIROT workflow, I performed a trial selection process which will be presented in section 4.10. *Trial Selection across Single-Task and Dual-Task Conditions*

5.2. Additional Motion Artifact Testing using Repetitive Motion Protocol

A motion test protocol was designed to study the effectiveness of using an accelerometer in measuring motion of specific head movements and observed artifacts in raw fNIRS data. The design of the motion test protocol consisted of four tests of varying head movements (rotations right, left, upward and downwards) and two tests to measure jaw movement (jaw clenching and speech). The motion test sought out two outcomes. The first objective was to validate the detection and amplitudes of each movement by the hardware within the inertial sensor, the Witmotion accelerometer; the same model that was used in acquisitions throughout this study. The second was to calculate the correlation of detected motion recordings to the signal obtained across fNIRS channels worn by the participant. The correlation coefficient, R , was calculated to measure the strength of the relationship between the

relative movements of motion recordings and the signal obtained across fNIRS channels. The sensor was attached in the same position worn by participants during acquisitions as presented on the right in Figure 8 and fastened tightly to the forehead to reduce faulty motion.

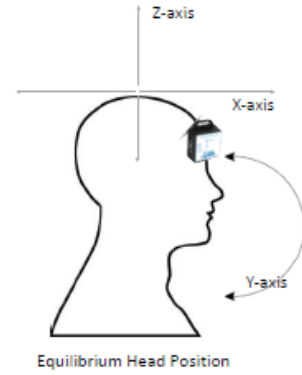


Figure 8: Position of Accelerometer during Motion Test

The motion test protocol consisted of four runs of varying head movements, and two runs involving jaw movements and speech. The head motion tests comprised of head rotations in right, left, upward and downward orientation. Head movement tests consisted of 10 runs with movements repeated over 5 to 10 seconds. Jaw movement tests consisted of 10 runs with movements repeated over 10 to 15 seconds. A MATLAB script was generated to initiate triggers for starting head motions and jaw movements and the recording of associated accelerometer measurements. Measurements of the inertial sensor were recorded at a sampling rate of 150Hz. fNIRS

	Head Movement Motion Test	Correlation Coefficient (R)
Run 01	Rotations left. Number of trials: 10, inter-trial duration 5-10 seconds. Total duration of the run: 1-2 minutes	0.237
Run 02	Rotations right. Number of trials: 10, inter-trial duration 5-10 seconds. Total duration of the run: 1-2 minutes	0.144
Run 03	Rotations upward. Number of trials: 10, inter-trial duration 5-10 seconds. Total duration of the run: 1-2 minutes	0.122
Run 04	Rotations downward. Number of trials: 10, inter-trial duration 5-10 seconds. Total duration of the run: 1-2 minutes	0.095
Run 05	Jaw contraction. Number of trials: 10, inter-trial duration 10 to 15 seconds.	0.523
Run06	Speech "A – B – C". Number of trials: 10, inter-trial duration 10 to 15 seconds.	0.011

Table 4: Head movement testing accelerometer data for correlated measurements of fNIRS motion artifact detection

Table 4 presents the correlation coefficients between acceleration (X,Y and Z-axes), angular velocity (X,Y and Z-axes) and angular position (X,Y and Z-axes) and all channels of the optimal montage, ranging from SID1 to S7D21. The correlation coefficient across Run 01 to Run 06 demonstrate weaker correlations when considering both short-distance and long distance channels and thus require correlation coefficients calculated for short versus long distance channels to take into account superficial activity from the scalp obtained across short-distance channels.

signal was recorded with 10Hz sampling rate via the Brainsight Machine by Rogue Research,

consistent with the study. The difference in sampling rates between the inertial sensor and fNIRS raw signal recordings was resolved by down sampling the rate of the inertial sensor to 10Hz to match that of fNIRS data . The placement of fNIRS optodes was defined via subject specific optimal montage and consisted of 21 long distance channels and six short-distance channels.

Figure 33 to Figure 38 (in Appendix 3) present the correlation coefficients and coefficients of determination between acceleration (X,Y and Z-axes), angular velocity (X,Y and Z-axes) and angular position (X,Y and Z-axes) and each channel of the optimal montage, ranging from S1D1 to S7D21. Correlation coefficient matrices were produced for two fNIRS emitter wavelengths; 685nm and 830nm. In the context of this thesis, I am only interested in the correlation coefficient (R). In this section, I will present the motion test result of one of six motion tests evaluating the sensitivity of the accelerometer to downward head nods. In the correlation matrices presented in Figure 15 (a) and (b), the vertical axis lists all short-distance channels (six channels, from S1D17 to S7D21), followed by the accelerometer channels for acceleration, angular position and gyrosopic position in x, y and z axes. The horizontal axis presents all the channels used in the optimal montage inside of this study. Correlation matrices in (a) and (b) indicate some stronger correlation in x, y and z-direction acceleration with channels S2D2 S2D5 and SD12 (correlation tends towards 1). A strong correlation in short-distance channels, such as S1D17 and S3D17 (correlation tends towards 1), which can suggest that superficial activity may be producing potential bias in the data.

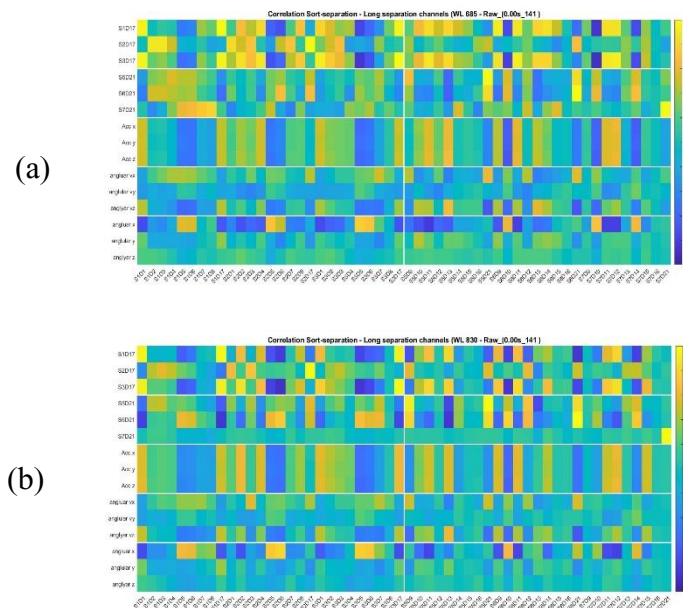


Figure 16: Accelerometer motion tests evaluating the sensitivity of the accelerometer to downward head knods.

Correlation matrices (a) and (b) demonstrate a strong correlation across short-distance channel

5.3. Results: Single Subject Analysis of fNIRS and EMG Data

Youth 1

Youth 1 suggests a positive [HbO] response relative to baseline in both ST and DT conditions along the right ROI, and a negative [HbO] response in both ST and DT conditions along the left ROI (ST: 12 trial block average; DT: 9 trial block average), as presented in Figure 16. The ST and DT conditions across the right and IFG and MFG present a positive[HbO] response and a positive [HbR]. A similar,

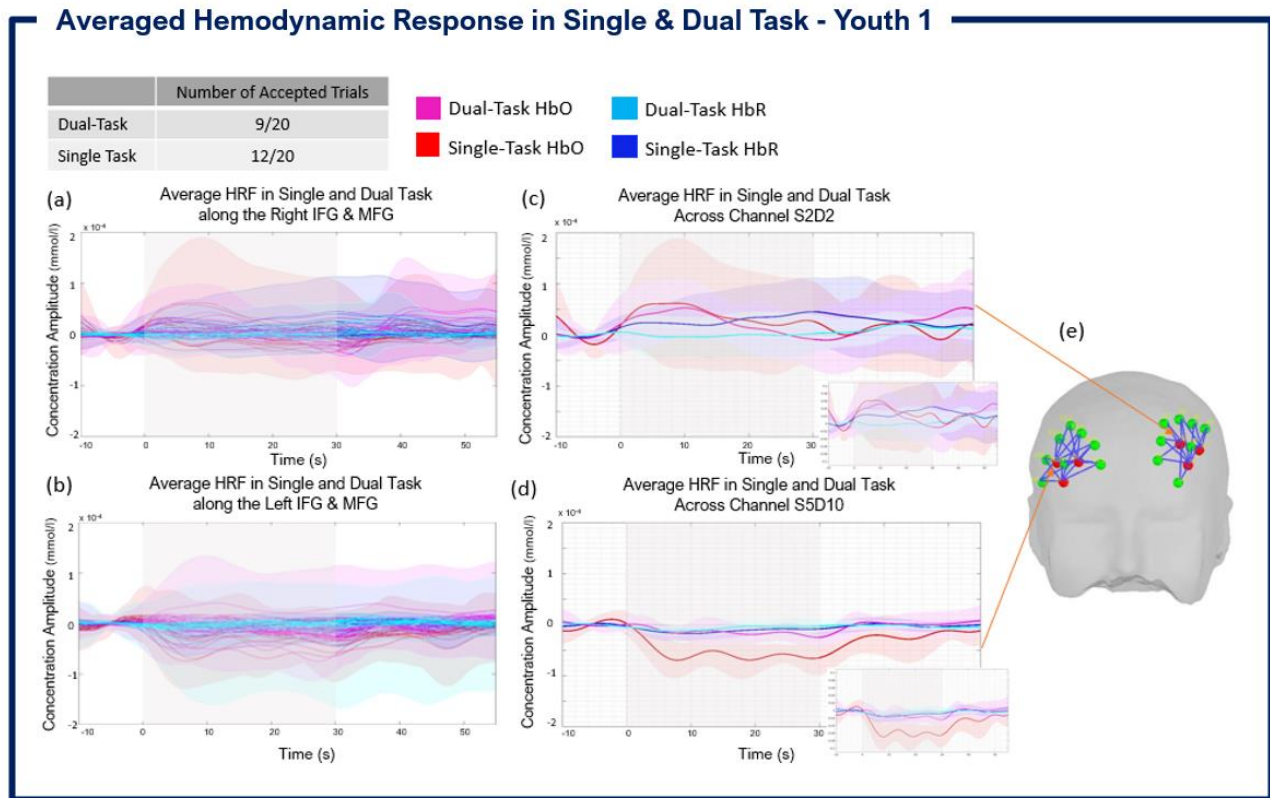


Figure 17: Youth 1 -Block averaged hemodynamic response in single task and dual task across IFG and MFG regions of interest

Figure 16(a) and (b) depict the single task (block averaged across 9/20 accepted trials) and dual task conditions (block averaged across 12/20 accepted trials) across the right and left IFG and MFG. Figure 16(c) portrays the hemodynamic response from one channel, S2D2, within the right optimal montage. Figure 16(d) portrays the hemodynamic response from one channel, S5D10, within the left optimal montage. Figure 16(e) depicts the personalized optimal montage of Youth 1; arrows point to the channels S2D2 and S5D10 and represent the region which experiences the largest hemodynamic response across the right and left IFG and MFG, respectively.

but opposite phenomenon is observed across the left IFG and MFG, in which both ST and DT conditions present a negative [HbO] response and a positive [HbR]. This can suggest in a change in HbT (i.e. in cerebral blood volume) (Pham, et al., 2019). Figure 17 (a) and (b) presents the averaged MEM reconstruction along the cortical surface, contrasting ST versus DT response. The MEM response presents a negative [HbO] response in both ST and DT, with DT eliciting a greater response relative to ST (i.e. more negative) during the 30s event window across both left and right hemispheres, demarcated in grey shaded area on time courses of Figure 17. This result coincides with the of the average hemodynamic response along the left and right ROIs. Figure 17(c) and 17(d) demonstrate the associated MEM HbO and HbR reconstructions with responses averaged in the 5-20s time window in ST and DT events. Each figure was set to scale and represent the range of signal amplitude,

demonstrating negative and positive responses of HbO and HbR concentrations along the cortex in response to ST and DT. Based on the current results of MEM cortical reconstruction, Youth 1 results indicate more activity along the left hemisphere. Youth 1's response to ST and DT indicate that activity falls within the demarcated scout along the left IFG and MFG, and less so along the right IFG and MFG.

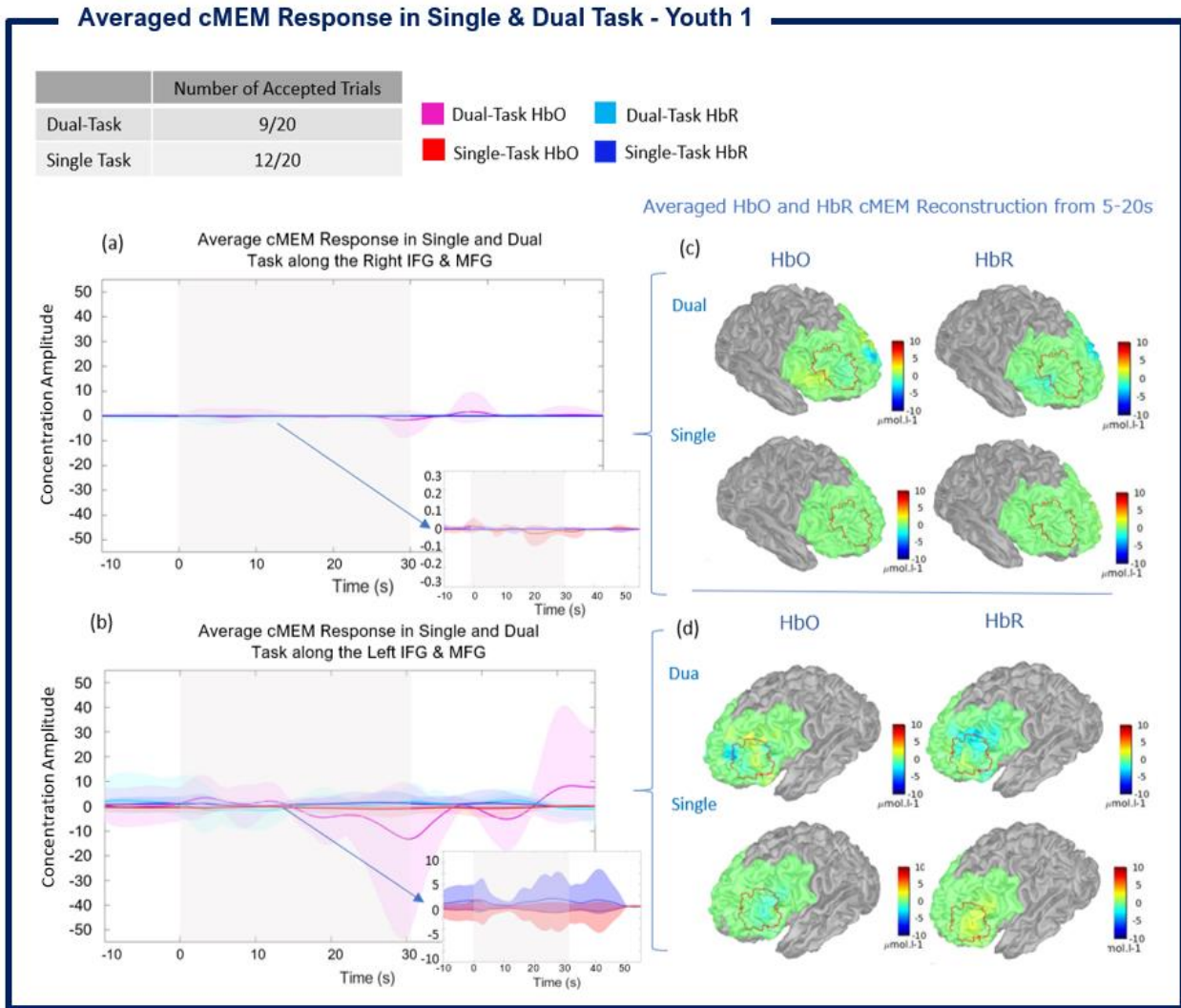


Figure 18: MEM reconstruction in single task and dual task across right and left hemispheres in Youth 1

Figure 17 (a) and (b) presents the averaged MEM reconstruction along the cortical surface, contrasting ST versus DT response. The MEM response presents a negative [HbO] response in both ST and DT, with DT eliciting a greater response relative to ST (i.e. more negative) during the 30s event window across both left and right hemispheres, demarcated in grey shaded area on time courses Figure 17(c) and 17(d) demonstrate the associated MEM HbO and HbR reconstructions with responses averaged in the 5-20s time window in ST and DT events.

Youth 1 demonstrates greatest amount of statistically significant variability in EMG recordings within the right hamstring, showing increased %MVC in dual-task relative to walking only (DT: 1.827% ± 0.010% versus Walk-Only: 1.734% ± 0.180%, p<0.001). Though results also showed that there is significant variability and decreased muscular activity in DT relative to walk-only condition in the right quad (4.811% ± 1.008% vs 5.122 ± 0.745%; 0.155% increase, p<0.001) and the right calf (1.211% ± 0.188% vs 1.366 ± 0.190%; 0.311% increase, p=0.003), respectively, as reported in Table 4. Gait recordings indicated minor variability in cadence and stride time across conditions. Cadence remained near-constant in DT and walk-only conditions and did not reach statistical significance (112 steps/min ± 3.265 versus 110 steps/min ± 5.291, p>0.001). Stride time also remained near-constant and did not demonstrate statistically significant results (1.072s ± 0.030 versus 1.086 ± 0.047; p<0.001),

Youth 1 - Average %MVC Across Dual-Task and Walk-Only Recordings

Muscle Group	Dual Task (Walking + S7) Average %MVC ± Std	Walking Only Average %MVC ± Std	p-value	t-test
Left Calf	1.666 ± 0.311	1.701 ± 0.360	p = 0.371	-0.895
Right Calf	1.211 ± 0.188	1.366 ± 0.190	p < 0.001	-8.829
Left Hamstring	0.431 ± 0.058	0.446 ± 0.063	p = 0.037	-2.078
Right Hamstring	1.827 ± 0.010	1.734 ± 0.180	p < 0.001	4.204
Left Quad	2.971 ± 0.406	3.102 ± 0.550	p = 0.020	-2.340
Right Quad	4.811 ± 1.008	5.122 ± 0.745	p = 0.003	-3.038

Table 5: Youth 1 - Average %MVC Across Dual-Task and Walk-Only Recordings

Average Cadence and Stride Time Recordings for Dual Task Vs. Walking Only Conditions

	Cadence (steps/min)				Stride Time (s)			
	Dual Task (Walking + S7) Average ± Std	Walking Only Average ± Std	p-value	t-test	Dual Task (Walking + S7) Average ± Std	Walking Only Average ± Std	p-value	t-test
Youth 1	112.0 ± 3.265	110.0 ± 5.291	p = 0.512	0.668	1.072 ± 0.030	1.086 ± 0.047	p = 0.445	-0.780
Youth 3	113.0 ± 3.098	113.0 ± 1.330	p = 0.969	0.040	1.056 ± 0.014	1.056 ± 0.006	p = 0.980	0.015
Youth 4	96.0 ± 14.624	107.0 ± 6.408	p = 0.133	-1.636	1.266 ± 0.095	1.122 ± 0.034	p = 0.019	3.430
Youth 5	88.0 ± 4.899	90.0 ± 2.906	p = 0.259	-1.170	1.368 ± 0.038	1.332 ± 0.022	p = 0.239	1.222
Elderly 1	36.0 ± 2.666	37.0 ± 2.000	p = 0.694	-0.400	3.268 ± 0.242	3.222 ± 0.166	p = 0.642	0.472

Table 11: Average Cadence and Stride Time Recordings for Dual Task versus Walking-Only Conditions

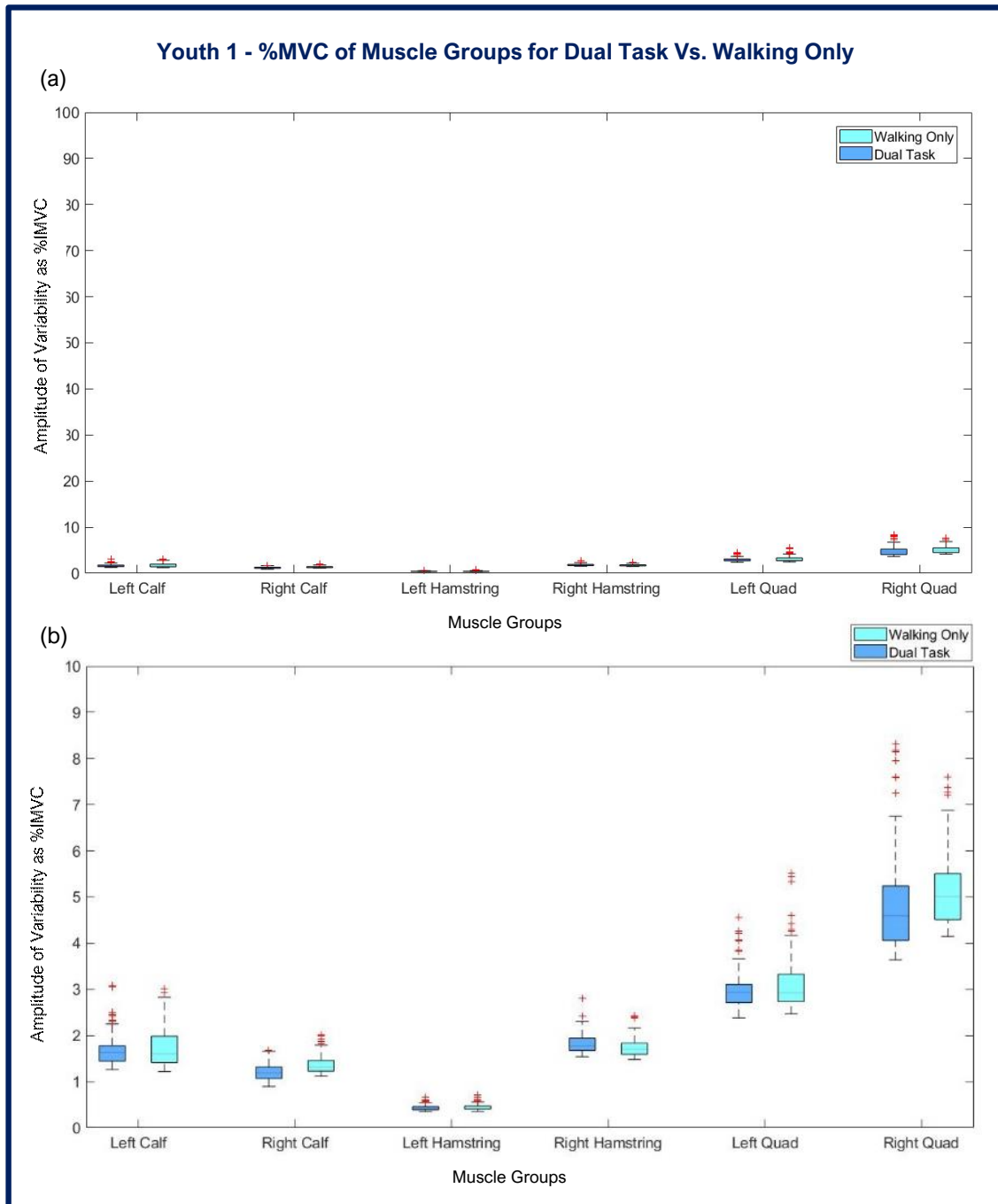


Figure 19: %MVC of Muscle Groups for Dual-Task versus walking-only condition for Youth 1

Figure 18(a) depicts changes in muscular activity in six muscle groups during in DT conditions in terms of percent of Maximum Voluntary Contraction (%MVC), based on 100%. Amplitude of Variability as %MVC in Walk-Only periods is demonstrated using cyan boxplot. Amplitude of Variability as %MVC in Dual-Task periods is demonstrated using dark blue boxplot. Figure 18(b) represents the same data, scaled and zoomed in on the %MVC axis to demonstrate the mean value of each muscle group and in both Walk-Only and Dual-Task activity during Dual-Task block design paradigm.

Youth 2

Youth 2 demonstrates an opposite hemodynamic response between left and right defined prefrontal ROIs. Youth 2 presents a negative [HbO] response relative to baseline in ST while demonstrating a positive [HbO] response in DT condition along the right ROI, both responses being shifted in time, the positive DT HbO response occurring later during the task. On the contrary, Youth 2 presents a negative [HbO] response in ST condition and positive [HbO] response in DT along the left ROI (ST: 9 trial block average; DT: 8 trial block average), as presented in Figure 19. In ST conditions across the right IFG and MFG, [HbO] and [HbR] demonstrate a positive response. This phenomenon suggests that there is a change in HbT (i.e. in cerebral blood volume) (Pham, et al., 2019). Figure 20(a) & 20(b)

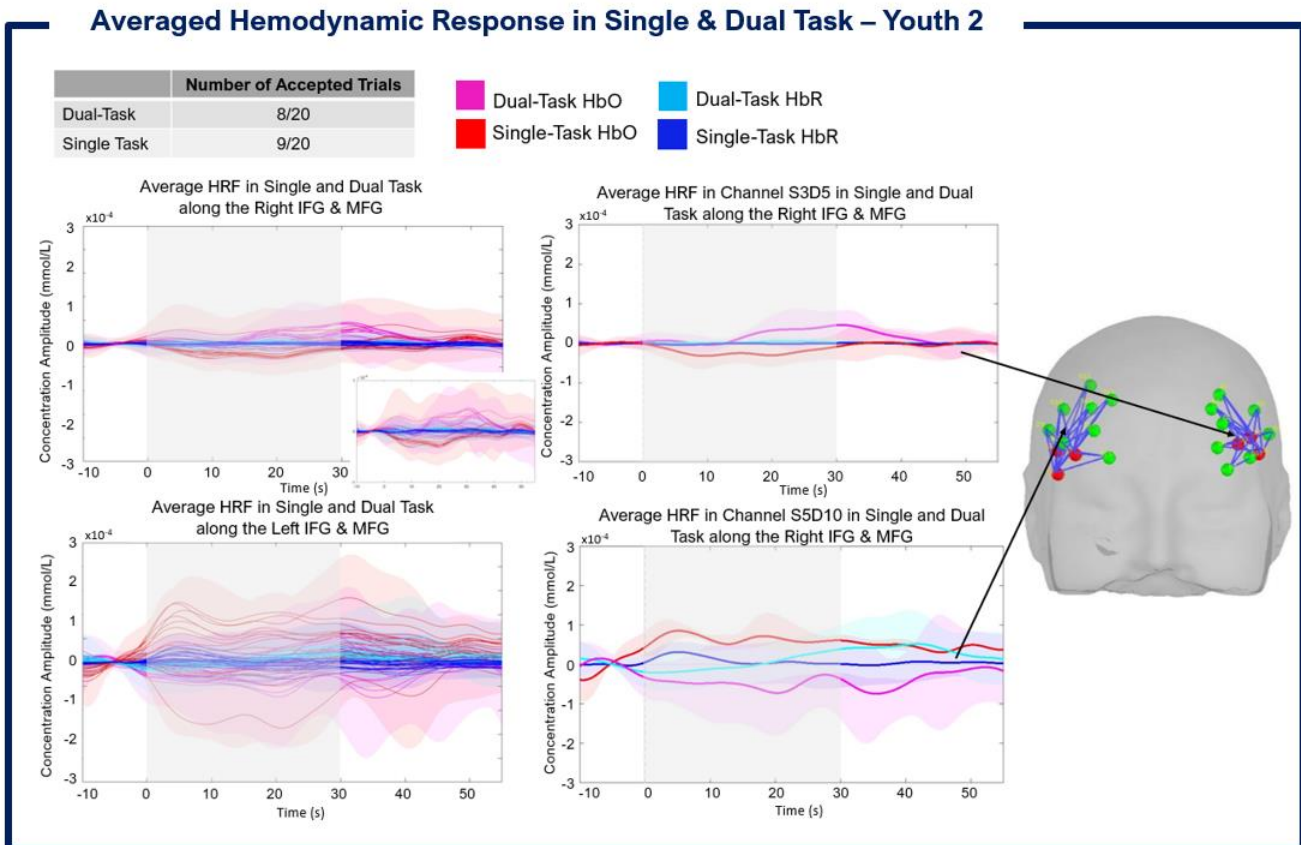


Figure 20: Youth 2 -Block averaged hemodynamic response in single task and dual task across IFG and MFG regions of interest

Figure 19(a) and (b) depict the single task (block averaged across 9/20 accepted trials) and dual task conditions (block averaged across 8/20 accepted trials) across the right and left IFG and MFG. Figure 19(c) portrays the hemodynamic response from one channel, S3D5, across within the right optimal montage. Figure 19(d) portrays the hemodynamic response from one channel, S5D10, across within the left optimal montage. Figure 19(e) depicts the personalized optimal montage of Youth 2; arrows point to the channels S3D5 and S5D10 and represent the region which experiences a greater hemodynamic response across the right and left IFG and MFG, respectively.

demonstrate the averaged MEM reconstruction along the cortical surface, contrasting ST versus DT response. In both the left and right IFG and MFG, The MEM response presents a negative [HbO] response in ST and DT conditions, with DT eliciting a greater response relative to ST during the 30s event window across both left and right hemispheres, demarcated in grey. The shaded regions around the averaged signals demonstrate a large standard deviation, suggesting that results may be affected by artifacts. Figure 20(e) & 20(f) demonstrate the associated MEM HbO and HbR reconstructions with responses averaged in the 5-20s time window ST and DT events. Each figure was set to scale and

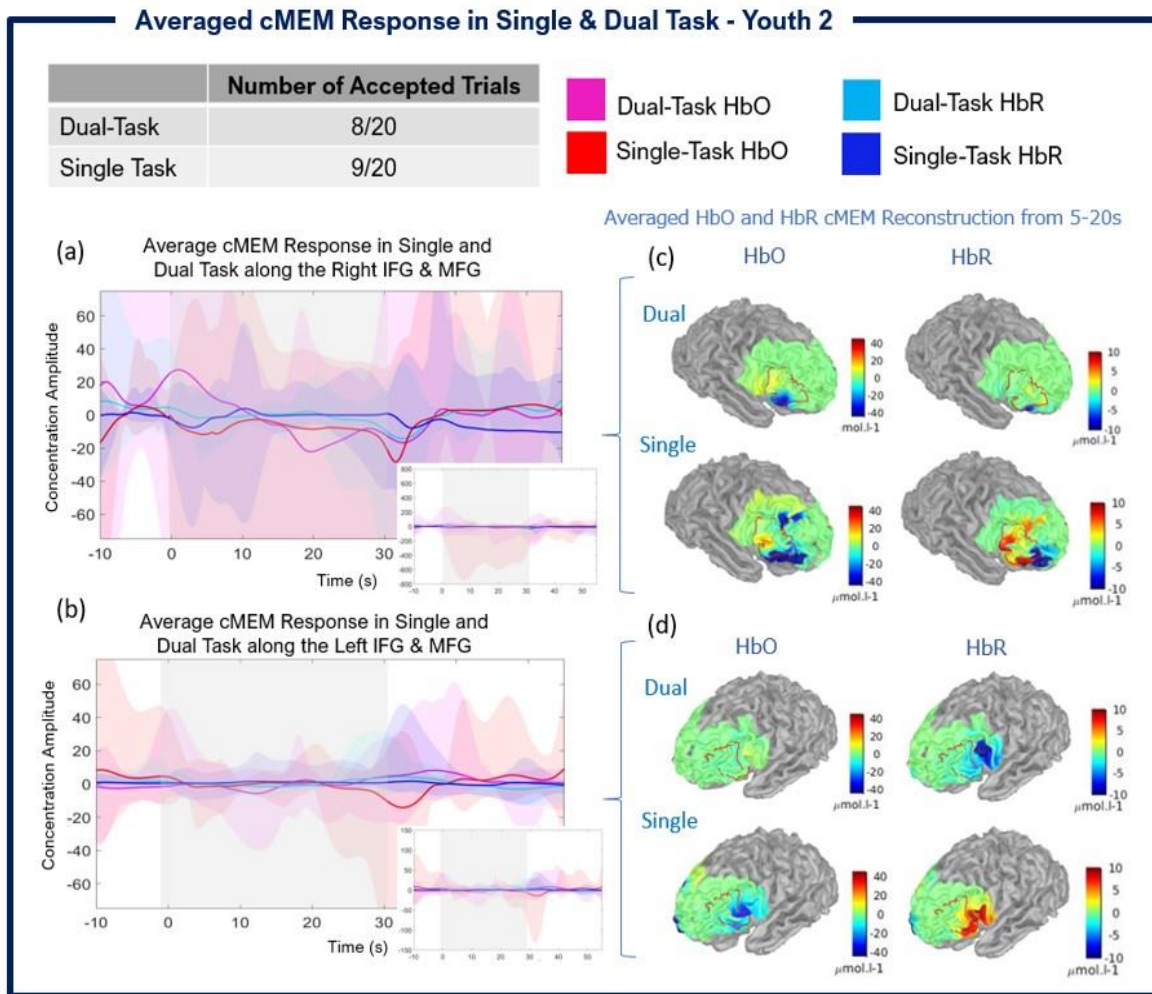


Figure 21: MEM reconstruction in single task and dual task across right and left hemispheres in Youth 2

Figure 20(a) and (b) depict the single task (averaged across 9/20 accepted trials) and dual task conditions (averaged across 8/20 accepted trials) across the demarcated ROIs (right and left hemispheres). The plots on the lower right in (a) and (b) demonstrate a zoomed-out view of concentration amplitude axis of the hemodynamic response of ST and DT conditions. Figure 20(c) and (d) portrays the reconstructed HbO and HbR responses in source space across the right and left hemisphere, time averaged between 5s and 20s. The smaller graphs located on each figure in the bottom right corners are enlarged plot of the same MEM responses, setting the concentration amplitude scale to better represent the amplitude of the response.

represent the range of signal amplitude, demonstrating negative and positive responses of HbO and HbR concentrations along the cortex in response to ST and DT. Based on the current results of MEM cortical reconstruction, Youth 2 results indicate more activity along the left hemisphere. Youth 2's response to ST and DT indicate that activity falls outside of the demarcated ROIs along the left IFG and MFG, and more within the demarcated ROIs the right IFG and MFG. Youth 2 completed the study with unsuccessful EMG and footswitch recordings; EMG sensors were installed but were not configured properly to transmit EMG data to the Telemetry DTS device.

Youth 3

Youth 3 demonstrates an [HbO] increase relative to baseline in both ST and DT conditions based on 10 and 11 block averaged trials, respectively. Figure 21 depicts the ST and DT conditions across the right and left IFG and MFG exhibiting a positive [HbO] response for both ST and DT, with DT eliciting

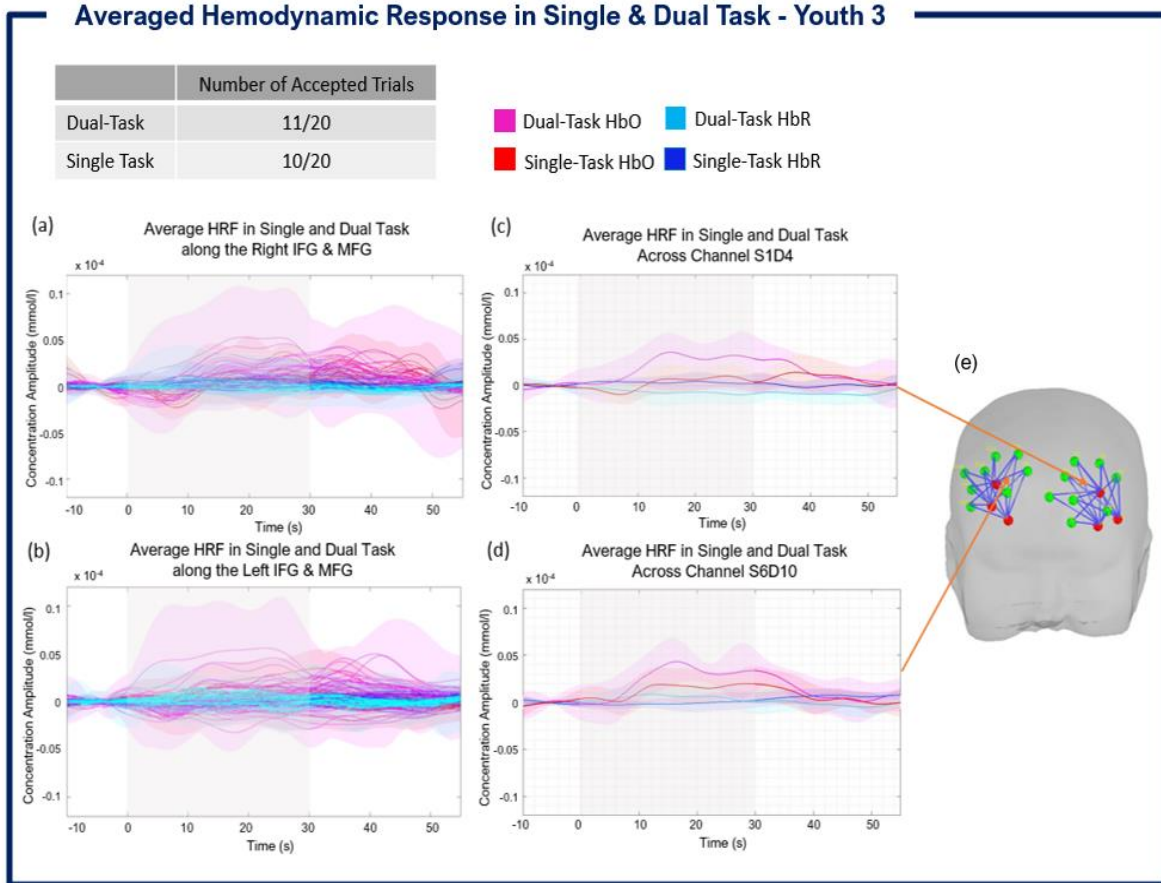


Figure 22: Youth 2 -Block averaged hemodynamic response in single task and dual task across IFG and MFG regions of interest

Figure 21(a) and (b) depict the single task (block averaged across 10/20 accepted trials) and dual task conditions (block averaged across 11/20 accepted trials) across the right and left IFG and MFG. Figure 21(c) portrays the hemodynamic response from one channel, S1D4, across within the right optimal montage. Figure 21(d) portrays the hemodynamic response from one channel, S6D10, across within the left optimal montage. Figure 21(e) depicts the personalized optimal montage of Youth 3; arrows point to the channels S1D4 and S6D10 and represent the region which experiences a greater hemodynamic response across the right and left IFG and MFG, respectively.

Averaged cMEM Response in Single & Dual Task - Youth 3

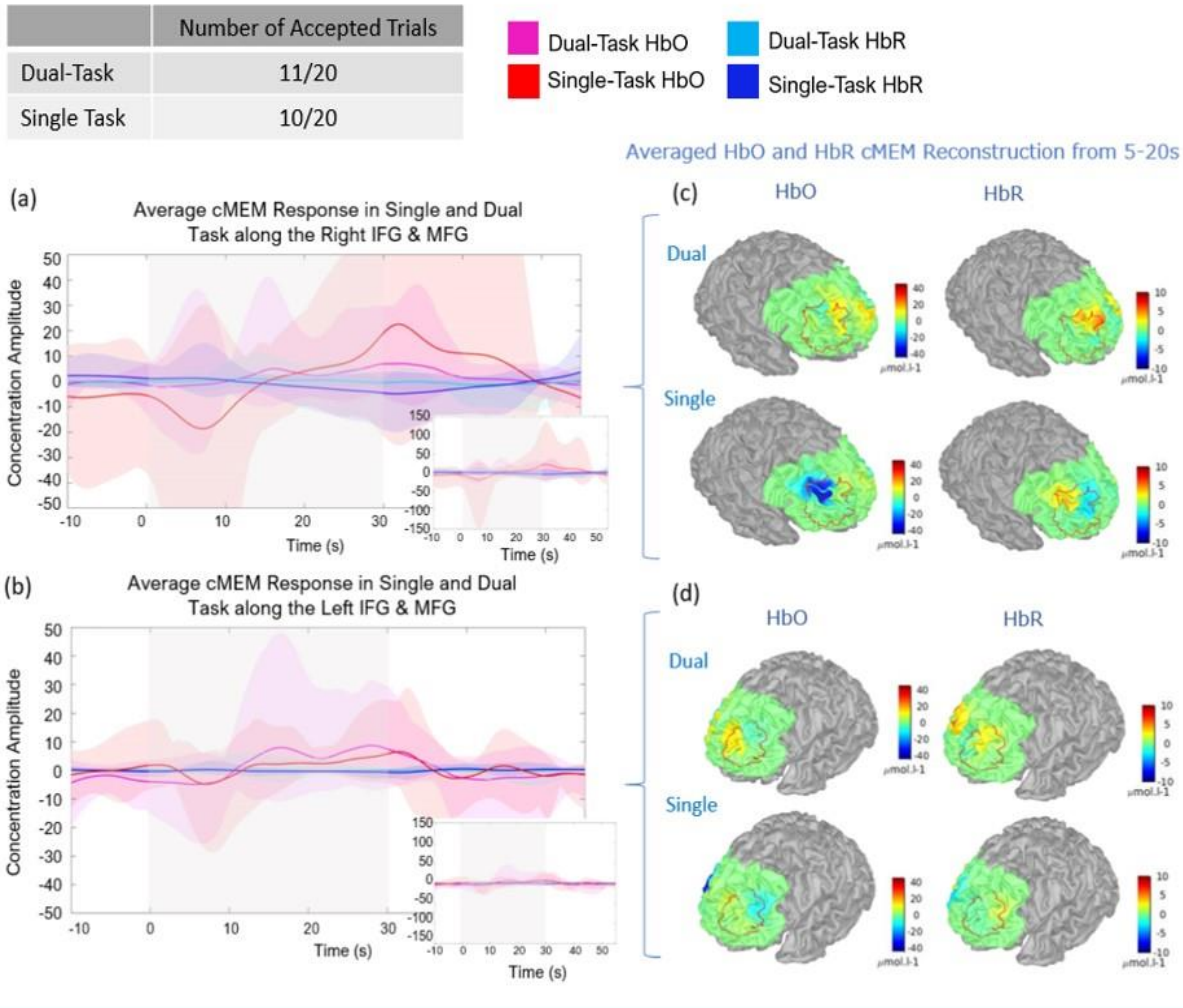


Figure 23: MEM reconstruction in single task and dual task across right and left hemispheres in Youth 3

Figure 22(a) and (b) depict the single task (averaged across 10/20 accepted trials) and dual task conditions (averaged across 11/20 accepted trials) across the demarcated ROIs (right and left hemispheres). Figure 22(c) and (d) portrays the reconstructed HbO and HbR responses in source space across the right and left hemisphere, time averaged between 5s and 20s. The smaller graphs located on each figure in the bottom right corners are enlarged plot of the same MEM response, setting the concentration amplitude scale to better represent the amplitude of the response.

a larger response relative to ST during the 30s event window along the left and right ROIs, as demarcated in grey. Figure 22 demonstrates the averaged MEM reconstruction along the cortical surface, contrasting ST versus DT response. The response obtained via MEM presents a negative undershoot and then positive response to both ST and DT, with DT eliciting a greater response relative to ST during the 30s event window across both left and right hemispheres, again demarcated in grey.

Momentary undershoots, from t=0s to 6s, are observed in figure 21(a) & (b), and figure 22(a) & (b). Figure 22 demonstrates the associated MEM [HbO] and [HbR] reconstructions with responses averaged in the 5-20s time window ST and DT events. Each figure was set to represent the range of signal amplitude, demonstrating negative and positive responses of HbO and HbR concentrations along the cortex in response to ST and DT. Based on the current results, Youth 3 results indicate more activity along the right hemisphere. Youth 3's response to ST and DT indicate that activity lies majority on inside the demarcated ROI along the right and left IFG, further validating that our proposed subject specific optimal montage covered a desired ROI for the purpose of mental arithmetic.

Youth 3 demonstrated greatest amount of variability in EMG recordings within the left hamstring, showing an increase in %MVC in DT when compared to walking only (DT: 5.149% ± 1.100% versus 0.470% ± 0.080%; 4.679% increase, p<0.001), followed by the right quad (DT: 6.887% ± 1.631% vs 5.291 ± 1.830%; 1.596% increase, p<0.001), as presented in Table 6. Also, EMG recordings within the left calf decreased in %MVC in DT relative to walking only (DT: 2.026% ± 0.260% versus 2.387% ± 0.820%; 0.361% decrease, p<0.001), followed by the left quad (2.707% ± 0.880% vs 3.453 ± 1.190%; 0.746% decrease, p<0.001). Gait recordings indicated no significant increase or decrease in cadence and stride time across conditions. Cadence remained near-constant in DT and walk-only conditions and did not exhibit any statistically significant difference (DT: 113 steps/min ± 3.098 versus Walk-Only 113 steps/min ± 1.330, p=0.969). Stride time also remained near-constant and did not demonstrate any statistically significant difference (DT: 1.056s ± 0.014 versus Walk-Only 1.056 ± 0.006, p=0.980), as described in Table 11.

Youth 3 - Average %MVC Across Dual-Task and Walk-Only Recordings

Muscle Group	Dual Task (Walking + S7) Average %MVC ± Std	Walking Only Average %MVC ± Std	p-value	t-test
Left Calf	2.026 ± 0.260	2.387 ± 0.820	p < 0.001	-5.136
Right Calf	3.245 ± 1.000	3.257 ± 0.780	p = 0.908	-0.115
Left Hamstring	5.149 ± 1.100	0.470 ± 0.080	p < 0.001	4.141
Right Hamstring	1.746 ± 0.310	1.673 ± 0.680	p = 0.234	1.192
Left Quad	2.707 ± 0.880	3.453 ± 1.190	p < 0.001	-6.144
Right Quad	6.887 ± 1.631	5.291 ± 1.830	p < 0.001	7.972

Average Cadence and Stride Time Recordings for Dual Task Vs. Walking Only Conditions

	Cadence (steps/min)				Stride Time (s)			
	Dual Task (Walking + S7) Average ± Std	Walking Only Average ± Std	p-value	t-test	Dual Task (Walking + S7) Average ± Std	Walking Only Average ± Std	p-value	t-test
Youth 1	112.0 ± 3.265	110.0 ± 5.291	p = 0.512	0.668	1.072 ± 0.030	1.086 ± 0.047	p = 0.445	-0.780
Youth 3	113.0 ± 3.098	113.0 ± 1.330	p = 0.969	0.040	1.056 ± 0.014	1.056 ± 0.006	p = 0.980	0.015
Youth 4	96.0 ± 14.624	107.0 ± 6.408	p = 0.133	-1.636	1.266 ± 0.095	1.122 ± 0.034	p = 0.019	3.430
Youth 5	88.0 ± 4.899	90.0 ± 2.906	p = 0.259	-1.170	1.368 ± 0.038	1.332 ± 0.022	p = 0.239	1.222
Elderly 1	36.0 ± 2.666	37.0 ± 2.000	p = 0.694	-0.400	3.268 ± 0.242	3.222 ± 0.166	p = 0.642	0.472

Table 11: Average Cadence and Stride Time Recordings for Dual Task

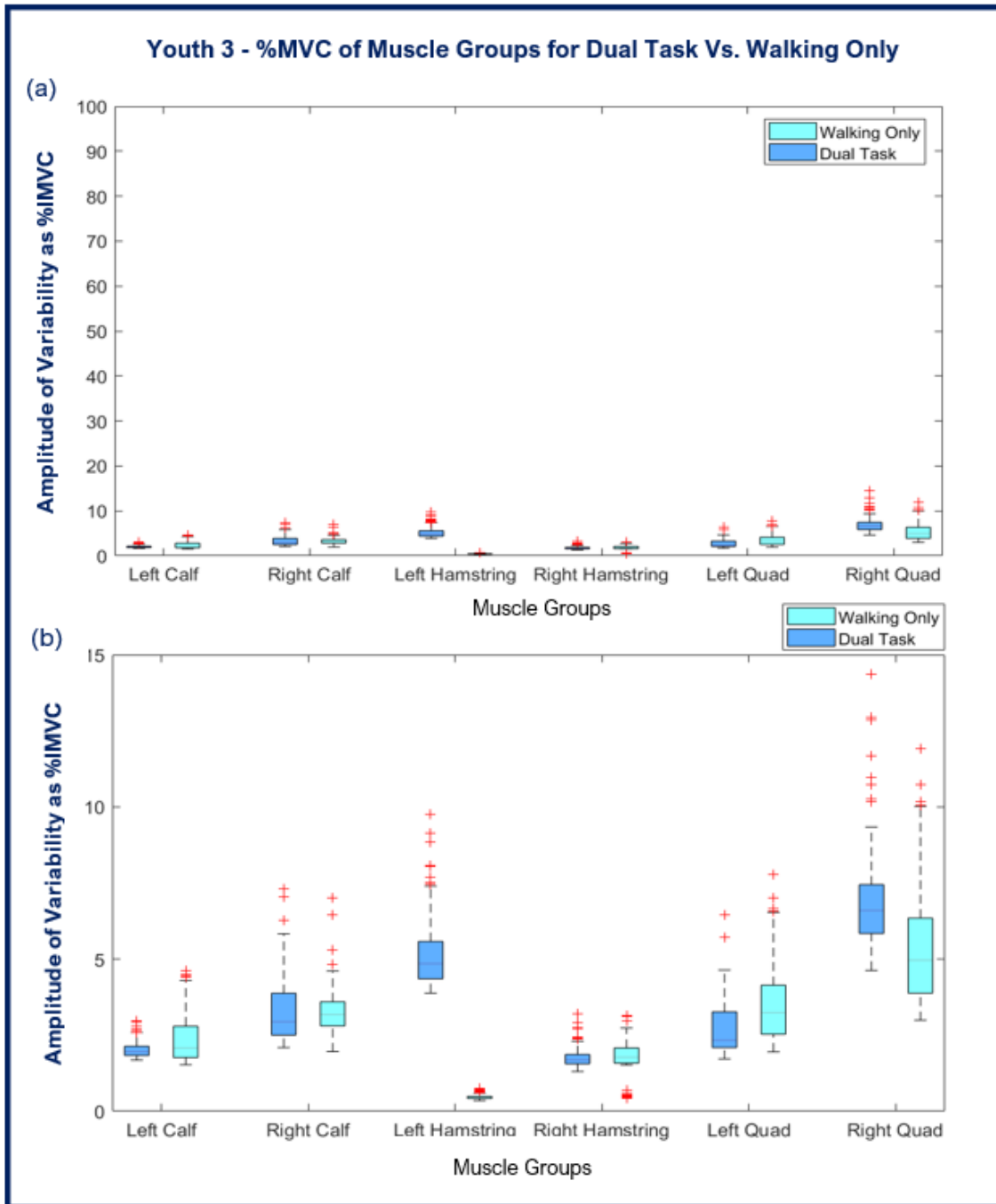


Figure 24: %MVC of Muscle Groups for Dual-Task versus walking-only in Youth 3

Figure 23(a) depicts changes in muscular activity in six muscle groups during in DT conditions in terms of percent of Maximum Voluntary Contraction (%MVC), based on 100%. Amplitude of Variability as %MVC in Walk-Only periods is demonstrated using cyan boxplot. Amplitude of Variability as %MVC in Dual-Task periods is demonstrated using dark blue boxplot. Figure 23(b) represents the same data, scaled and zoomed in on the %MVC axis to demonstrate the mean value of each muscle group and in both Walk-Only and Dual-Task activity during Dual-Task block design paradigm. The muscle groups that demonstrated statistically significant increase were the left hamstring in DT vs. walking only (DT: $5.149\% \pm 1.100\%$ versus $0.470\% \pm 0.080\%$; 4.679% increase, $p < 0.001$), followed by the right quad (DT: $6.887\% \pm 1.631\%$ vs $5.291 \pm 1.830\%$; 1.596% increase, $p < 0.001$), and a statistically significant decrease in left calf in DT relative vs. walking only (DT: $2.026\% \pm 0.260\%$ versus $2.387\% \pm 0.820\%$; 0.361% decrease, $p < 0.001$), followed by the left quad ($2.707\% \pm 0.880\%$ vs $3.453 \pm 1.190\%$; 0.746% decrease, $p < 0.001$).

Youth 4

Youth 4 demonstrates an [HbO] decrease relative to baseline in both ST and DT conditions based on 3 and 9 block averaged trials, respectively. Figure 24 depicts the ST and DT conditions across the right and left IFG and MFG and presents a positive [HbR] response and negative [HbO] response for both ST and DT, with ST eliciting a slightly larger negative response when compared to DT during the 30s event window along the left and right ROIs, as demarcated in grey.

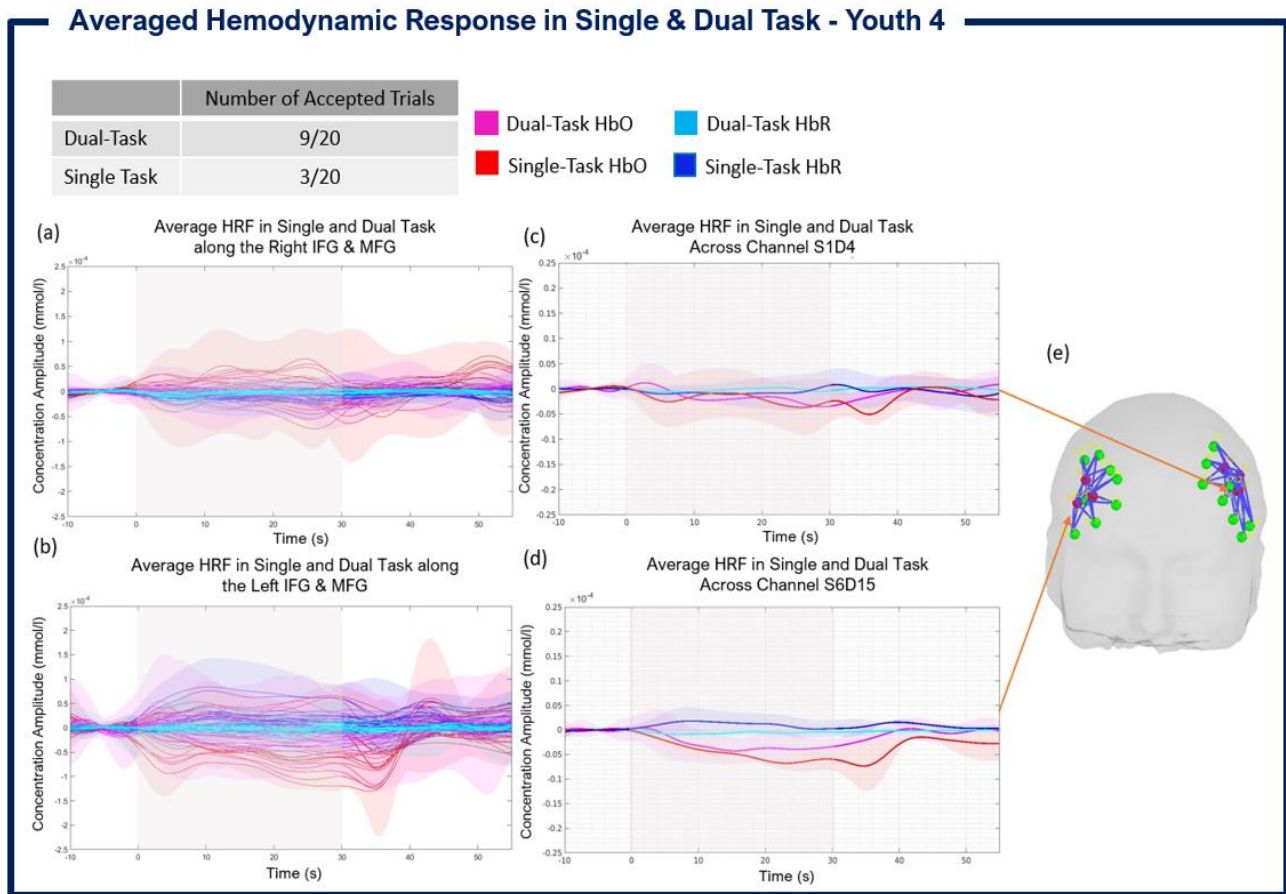


Figure 25: Block averaged hemodynamic response in single task and dual task across IFG and MFG regions of interest

Figure 24(a) and (b) depict the single task (block averaged across 3/20 accepted trials) and dual task conditions (block averaged across 9/20 accepted trials) across the right and left IFG and MFG. Figure (c) portrays the hemodynamic response from one channel, S1D4, across within the right optimal montage. Figure (d) portrays the hemodynamic response from one channel, S6D10, across within the left optimal montage. Figure (e) depicts the personalized optimal montage of Youth 4; arrows point to the channels S1D4 and S6D10 and represent the region which experiences a greater hemodynamic response across the right and left IFG and MFG, respectively.

Averaged cMEM Response in Single & Dual Task - Youth 4

	Number of Accepted Trials
Dual-Task	9/20
Single Task	3/20

■ Dual-Task HbO ■ Dual-Task HbR
■ Single-Task HbO ■ Single-Task HbR

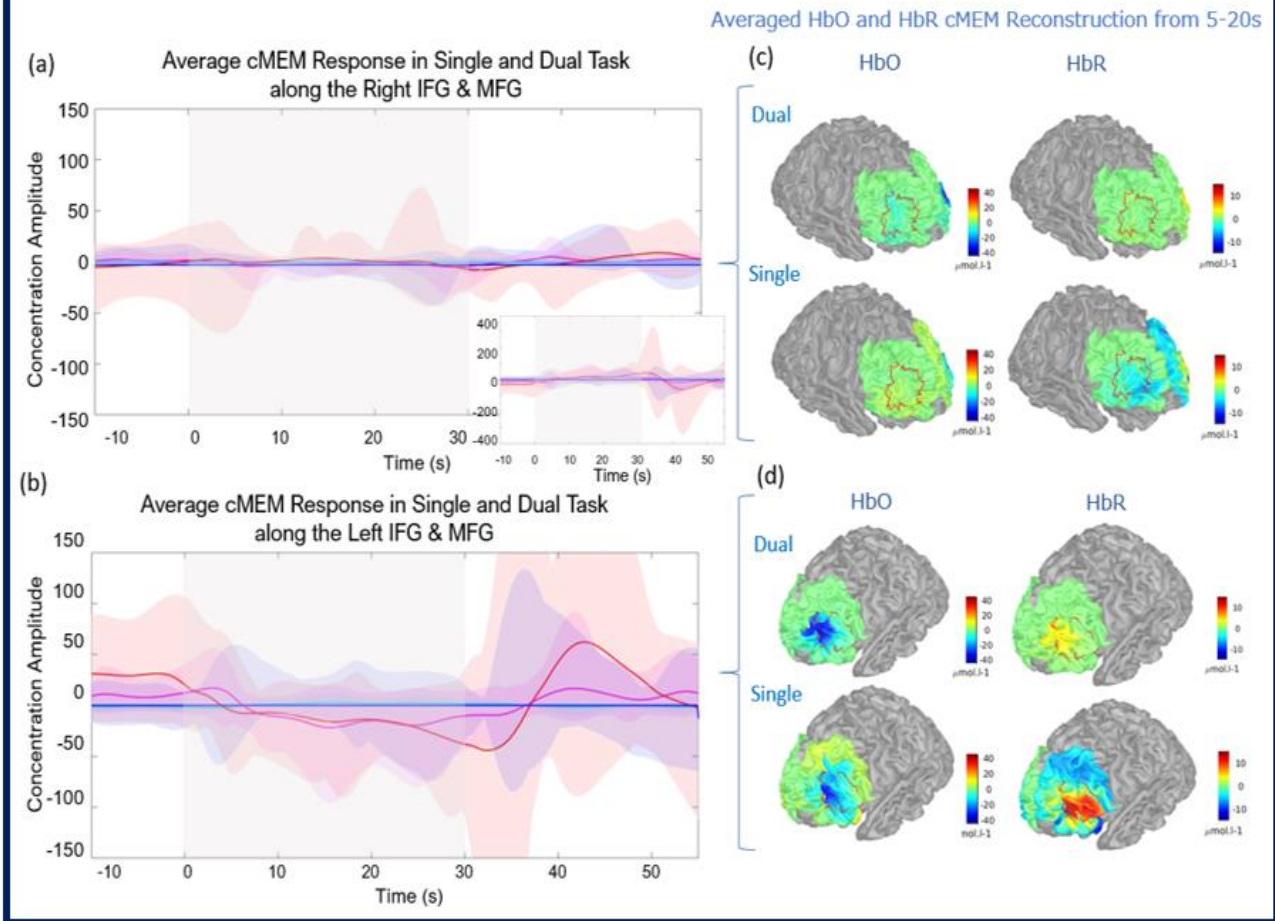


Figure 26: MEM reconstruction in single task and dual task across right and left hemispheres in Youth 4

Figure 25(a) and (b) depict the single task (averaged across 3/20 accepted trials) and dual task conditions (averaged across 9/20 accepted trials) across the demarcated ROIs (right and left hemispheres). Figure 25(c) and (d) portrays the reconstructed HbO and HbR responses in source space across the right and left hemisphere, time averaged between 5s and 20s. Youth 4's response to ST and DT indicate that activity lies within the demarcated ROIs along the right and left IFG, further confirming that our subject specific optimal montage covered the desired ROI for the purpose of mental arithmetic

Figure 25(a) and (b) demonstrates the averaged MEM reconstruction along the cortical surface, contrasting ST versus DT response. The MEM response across the left hemisphere presents a nearly equivalent negative response in both ST and DT during the 30s event window, again demarcated in grey. The response map across the left hemisphere ROIs suggests a larger increase in [HbR] during the ST condition. Nonetheless, the hemodynamic response and MEM results along the right hemisphere

are not visibly indicative of coinciding responses. Figure 25(c) and (d) demonstrate the associated MEM [HbO] and [HbR] reconstructions with responses averaged in the 5-20s time window ST and DT events. Each figure was set to represent the range of signal amplitude, demonstrating negative and positive responses of HbO and HbR concentrations along the cortex in response to ST and DT. Based on these results, Youth 4 results indicate more activity along the left hemisphere when compared to the right side. Youth 4's response to ST and DT indicate that activity lies within the demarcated ROIs along the right and left IFG, further confirming that our subject specific optimal montage covered the desired ROI for the purpose of mental arithmetic.

Youth 4 demonstrates greatest amount of variability in EMG recordings within the left calf, showing an increase in %MVC in DT to walking only (DT: 4.585% ± 1.812% versus Walk-Only: 3.567% ± 1.384%; 1.018% increase, $p < 0.001$), followed by the right hamstring (DT: 0.370% ± 0.010% vs 0.341 ± 0.061%; 0.029% increase, $p < 0.001$), as presented in Table 7. Gait recordings suggested minor variability in cadence and stride time across conditions. Cadence remained near-constant in DT and walk-only conditions and did not attain statistically significant results (DT: 96 steps/min ± 14.624 versus Walk-Only 107 steps/min ± 6.408; $p = 1.33$). Stride time also remained near-constant and did not demonstrate statistically significant results (1.266s ± 0.095 versus 1.122 ± 0.034; $p = 0.019$), as per Table 11.

Youth 4 - Average %MVC Across Dual-Task and Walk-Only Recordings

Muscle Group	Dual Task (Walking + S7) Average %MVC ± Std	Walking Only Average %MVC ± Std	p-value	t-test
Left Calf	4.585 ± 1.812	3.567 ± 1.384	$p < 0.001$	5.471
Right Calf	1.315 ± 0.147	1.284 ± 0.217	$p = 0.142$	1.474
Left Hamstring	0.930 ± 0.189	0.945 ± 0.180	$p = 0.487$	-0.695
Right Hamstring	0.370 ± 0.010	0.341 ± 0.061	$p < 0.001$	4.246
Left Quad	6.924 ± 1.678	7.031 ± 2.531	$p = 0.666$	-0.432
Right Quad	0.693 ± 0.253	0.749 ± 0.301	$p = 0.077$	-1.775

Table 7: Average %MVC Across Dual-Task and Walk-Only Recordings for Youth 4

Average Cadence and Stride Time Recordings for Dual Task Vs. Walking Only Conditions

	Cadence (steps/min)				Stride Time (s)			
	Dual Task (Walking + S7) Average ± Std	Walking Only Average ± Std	p-value	t-test	Dual Task (Walking + S7) Average ± Std	Walking Only Average ± Std	p-value	t-test
Youth 1	112.0 ± 3.265	110.0 ± 5.291	$p = 0.512$	0.668	1.072 ± 0.030	1.086 ± 0.047	$p = 0.445$	-0.780
Youth 3	113.0 ± 3.098	113.0 ± 1.330	$p = 0.969$	0.040	1.056 ± 0.014	1.056 ± 0.006	$p = 0.980$	0.015
Youth 4	96.0 ± 14.624	107.0 ± 6.408	$p = 0.133$	-1.636	1.266 ± 0.095	1.122 ± 0.034	$p = 0.019$	3.430
Youth 5	88.0 ± 4.899	90.0 ± 2.906	$p = 0.259$	-1.170	1.368 ± 0.038	1.332 ± 0.022	$p = 0.239$	1.222
Elderly 1	36.0 ± 2.666	37.0 ± 2.000	$p = 0.694$	-0.400	3.268 ± 0.242	3.222 ± 0.166	$p = 0.642$	0.472

Table 11: Average Cadence and Stride Time Recordings for Dual Task versus Walking-Only

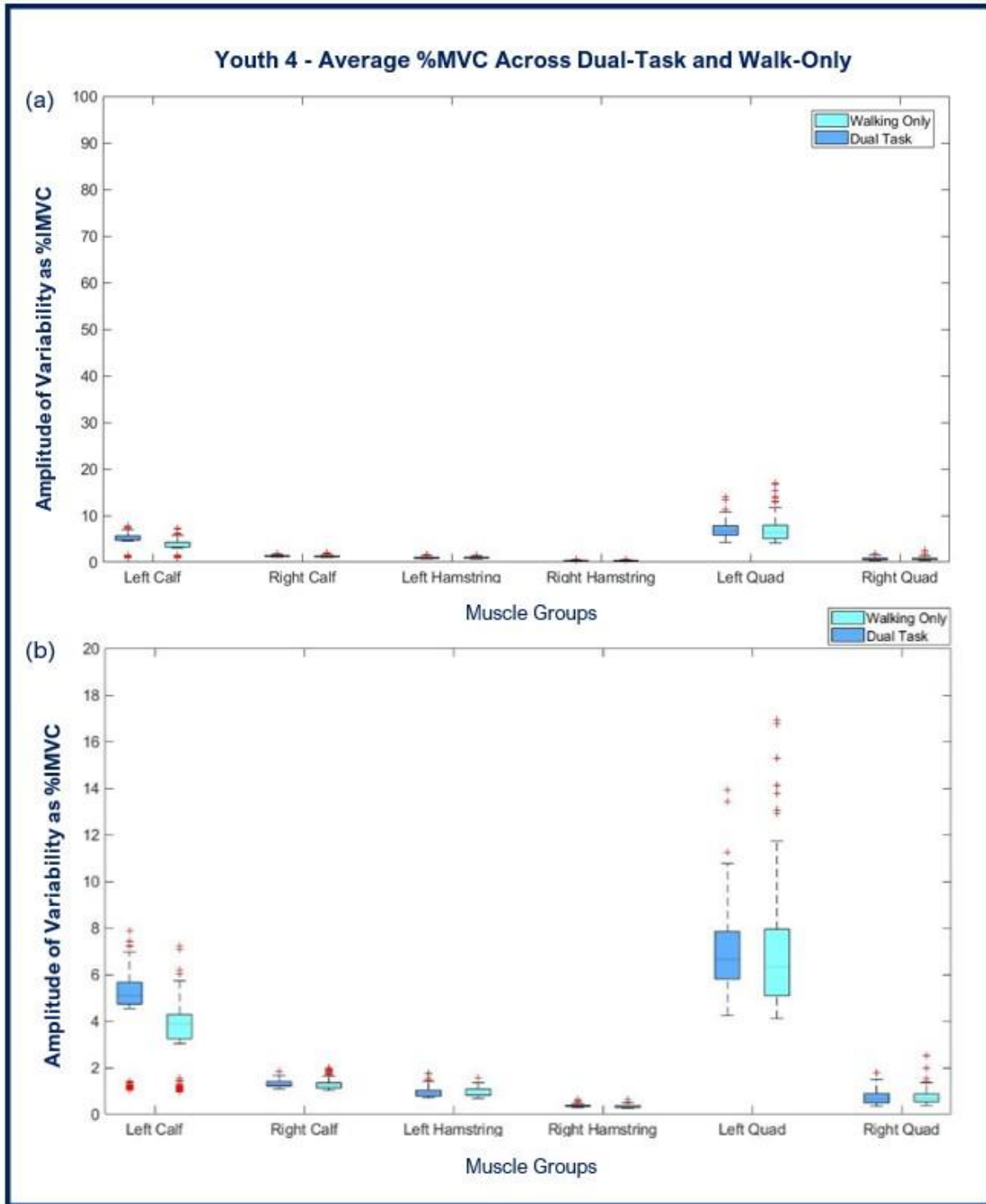


Figure 22: %MVC of Muscle Groups for Dual-Task versus walking-only in Youth 4

Figure 22(a) depicts changes in muscular activity in six muscle groups during in DT conditions in terms of percent of Maximum Voluntary Contraction (%MVC), based on 100%. Amplitude of Variability as %MVC in Walk-Only periods is demonstrated using cyan boxplot. Amplitude of Variability as %MVC in Dual-Task periods is demonstrated using dark blue boxplot. Figure 22(b) represents the same data, scaled and zoomed in on the %MVC axis to demonstrate the mean value of each muscle group and in both Walk-Only and Dual-Task activity during Dual-Task block design paradigm. The muscle groups that demonstrate the largest variability and showed a statistically significant increase in the left calf (DT: $4.585\% \pm 1.812\%$ versus Walk-Only: $3.567\% \pm 1.384\%$; 1.018% increase, $p < 0.001$), followed by the right hamstring (DT: $0.370\% \pm 0.010\%$ vs $0.341 \pm 0.061\%$; 0.029% increase, $p < 0.001$).

Youth 5

Youth 5 demonstrates a negative [HbO] response in both ST and DT conditions and along both left and right hemispheres, based on 9 and 7 block averaged trials, respectively. Figure 26 depicts DT eliciting a greater response relative to ST during the 30s event window along the left and right ROIs, as demarcated in grey. The [HbR] response is negative in both ST and DT conditions and along both left and right hemispheres. Figure 27 demonstrates the averaged MEM reconstruction along the cortical surface, contrasting ST versus DT response. Figure 27 (c) and (d) demonstrates the associated MEM [HbO] and [HbR] reconstructions with responses averaged in

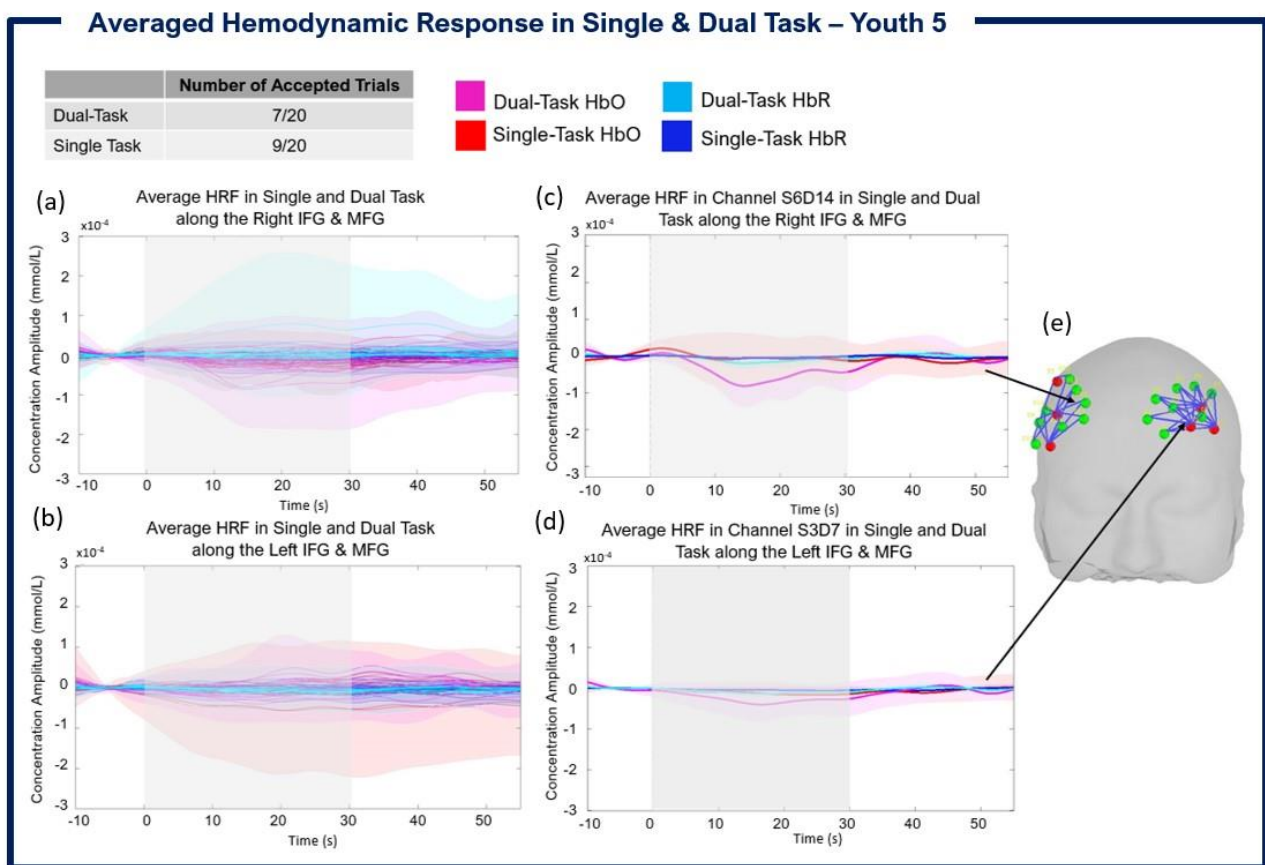


Figure 27: Youth 5 - Block averaged hemodynamic response in single task and dual task across IFG and MFG regions of interest.

Figure 26(a) and (b) depict the single task (block averaged across 7/20 accepted trials) and dual task conditions (block averaged across 9/20 accepted trials) across the right and left IFG and MFG. Figure 26(c) portrays the hemodynamic response from one channel, S6D14, across within the right optimal montage. Figure 26(d) portrays the hemodynamic response from one channel, S3D7, across within the left optimal montage. Figure 26(e) depicts the personalized optimal montage of Youth 5; arrows point to the channels S6D14 and S3D7 and represent the region which experiences a greater hemodynamic response across the right and left IFG and MFG, respectively.

the 5-20s time window ST and DT events. Each figure was set to represent the range of signal amplitude, demonstrating negative and positive responses of HbO and HbR concentrations along the cortex in response to ST and DT. Youth 5 results indicate more activity along the right hemisphere. Youth 5's response to ST and DT indicate that activity falls outside of the demarcated ROI on the right hemisphere, and both ST and DT responses lie inside the ROI left hemisphere,

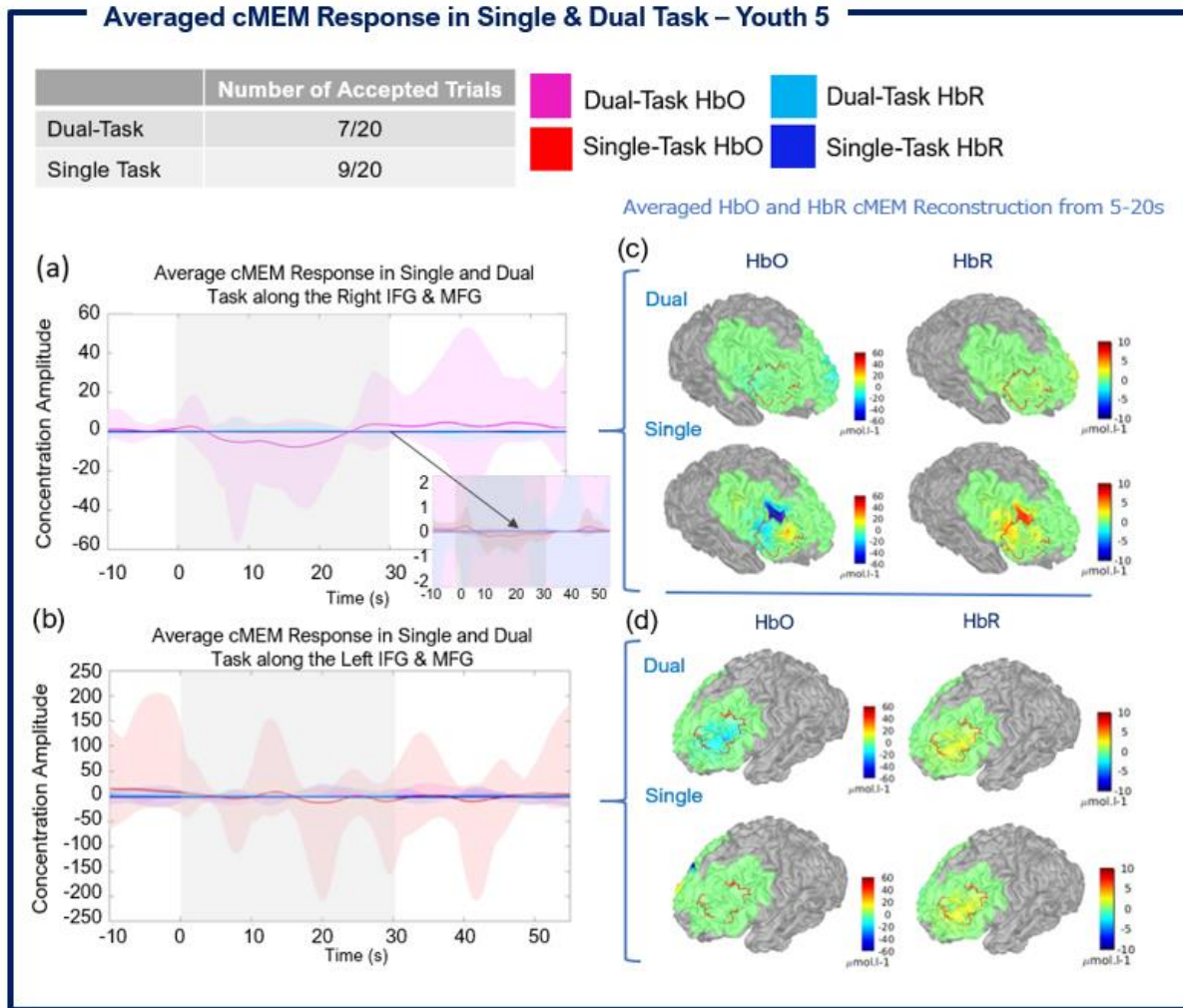


Figure 28: MEM reconstruction in single task and dual task across right and left hemispheres in Youth 5

Figure 27(a) and (b) depict the single task (averaged across 7/20 accepted trials) and dual task conditions (averaged across 9/20 accepted trials) across the demarcated ROIs (right and left hemispheres). Figure 27(c) and (d) portrays the reconstructed HbO and HbR responses in source space across the right and left hemisphere, time averaged between 5s and 20s.

despite demonstrating lower activity compared to the right side.

Youth 5 demonstrates greatest amount of variability in EMG recordings within the left quad, showing increased %MVC in DT relative to walking-only (DT: 19.527% ± 3.292% versus Walk-Only: 18.268% ± 3.163%; 1.259% increase, p<0.001). The left hamstring also showed a statistically significant decrease as %MVC in DT relative to Walk-Only (3.321% ± 0.847% vs 4.181 ± 1.83%; 0.860% increase, p<0.001), as presented in Table 8. Gait recordings indicated minor variability in cadence and stride time across conditions. Cadence remained near-constant in dual-task and walk-only conditions and did not attain statistically significant results (88 steps/min ± 4.899 versus 90 steps/min ± 2.906, p>0.001). Stride time also remained near-constant and did not demonstrate statistically significant results (1.368s ± 0.242 versus 1.332 ± 0.022; p>0.001), as per Table 11.

Youth 5 - Average %MVC Across Dual-Task and Walk-Only Recordings

Muscle Group	Dual Task (Walking + S7) Average %MVC ± Std	Walking Only Average %MVC ± Std	p-value	t-test
Left Calf	3.081 ± 0.556	2.917 ± 0.773	p = 0.036	2.108
Right Calf	1.471 ± 0.267	1.486 ± 0.245	p = 0.599	-0.526
Left Hamstring	3.321 ± 0.847	4.181 ± 1.455	p < 0.001	-6.258
Right Hamstring	1.864 ± 0.006	1.902 ± 0.618	p > 0.512	-0.657
Left Quad	19.527 ± 3.292	18.268 ± 3.163	p < 0.001	3.377
Right Quad	30.487 ± 5.448	30.878 ± 5.676	p < 0.543	-0.610

Table 8: Average %MVC Across Dual-Task and Walk-Only Recordings for Youth 4

Average Cadence and Stride Time Recordings for Dual Task Vs. Walking Only Conditions

	Cadence (steps/min)				Stride Time (s)			
	Dual Task (Walking + S7) Average ± Std	Walking Only Average ± Std	p-value	t-test	Dual Task (Walking + S7) Average ± Std	Walking Only Average ± Std	p-value	t-test
Youth 1	112.0 ± 3.265	110.0 ± 5.291	p = 0.512	0.668	1.072 ± 0.030	1.086 ± 0.047	p = 0.445	-0.780
Youth 3	113.0 ± 3.098	113.0 ± 1.330	p = 0.969	0.040	1.056 ± 0.014	1.056 ± 0.006	p = 0.980	0.015
Youth 4	96.0 ± 14.624	107.0 ± 6.408	p = 0.133	-1.636	1.266 ± 0.095	1.122 ± 0.034	p = 0.019	3.430
Youth 5	88.0 ± 4.899	90.0 ± 2.906	p = 0.259	-1.170	1.368 ± 0.038	1.332 ± 0.022	p = 0.239	1.222
Elderly 1	36.0 ± 2.666	37.0 ± 2.000	p = 0.694	-0.400	3.268 ± 0.242	3.222 ± 0.166	p = 0.642	0.472

Table 11: Average Cadence and Stride Time Recordings for Dual Task versus Walking-Only Conditions

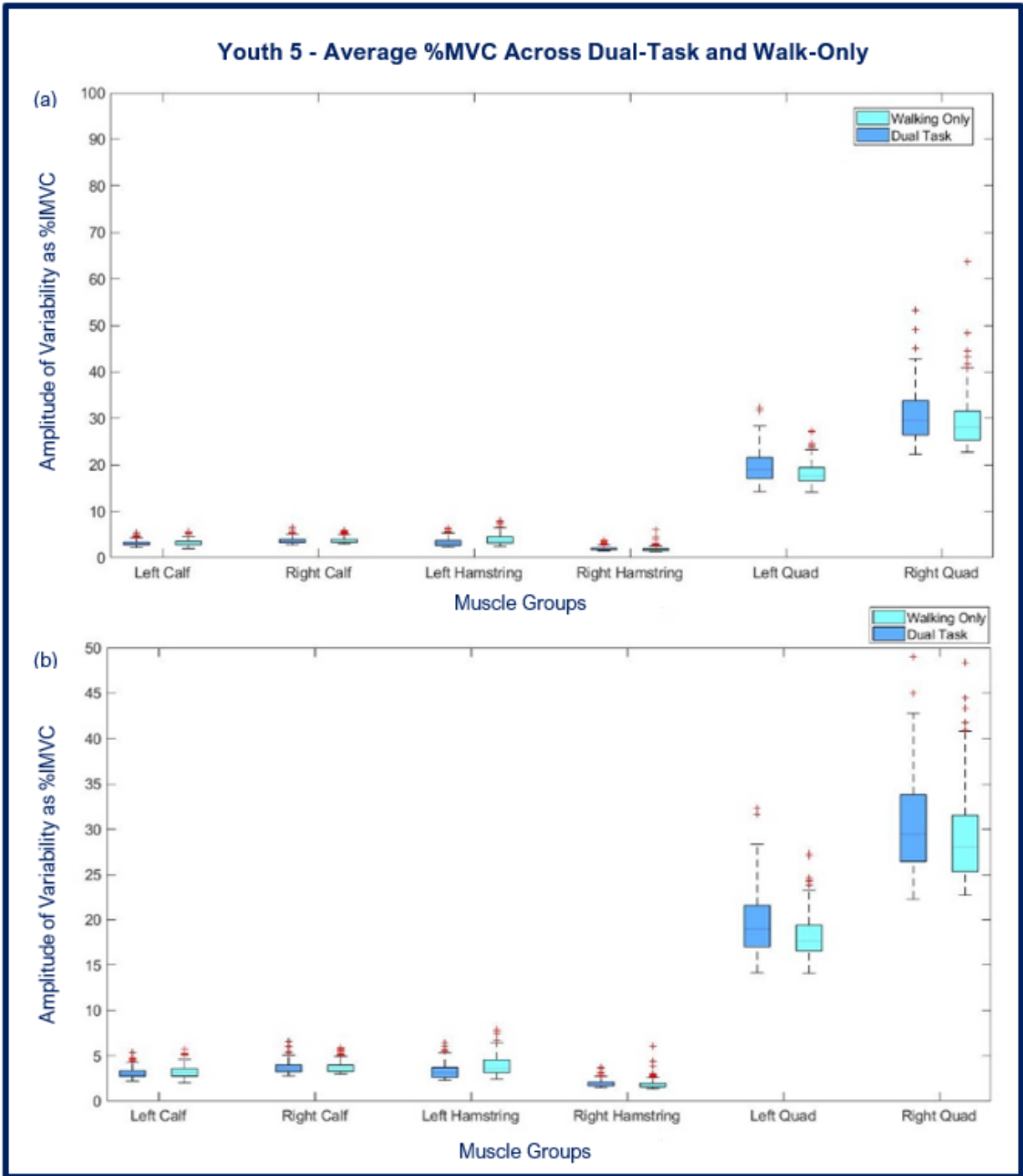


Figure 29: %MVC of Muscle Groups for Dual-Task versus walking-only in Youth 5

Figure 28(a) depicts changes in muscular activity in six muscle groups during in DT conditions in terms of percent of Maximum Voluntary Contraction (%MVC), based on 100%. Amplitude of Variability as %IMVC in Walk-Only periods is demonstrated using cyan boxplot. Amplitude of Variability as %IMVC in Dual-Task periods is demonstrated using dark blue boxplot. Figure 28(b) represents the same data, scaled and zoomed in on the %MVC axis to demonstrate the mean value of each muscle group and in both Walk-Only and Dual-Task activity during Dual-Task block design paradigm. The muscle groups that demonstrate the largest variability and showed a statistically significant increase during the DT was the left quad (DT: $19.527\% \pm 3.292\%$ versus Walk-Only: $18.268\% \pm 3.163\%$; 1.259% increase, $p < 0.001$).

Elderly 1

Elderly 1 suggests a positive [HbO] increase relative to baseline in both ST and DT conditions based on 11 and 10 block averaged trials, respectively. Figure 29(a) and (b) depicts the ST and DT conditions across the right and left IFG and MFG and present a positive [HbO] response for both ST and DT, with DT eliciting a greater response relative to ST along the right ROI, as demarcated during the 30s event window in grey. Figure 30(a) & (b) demonstrates the averaged MEM reconstruction along the cortical surface, contrasting ST versus DT response. The MEM response presents a positive response to both ST and DT, with DT eliciting a greater response relative to ST during the 30s event window across both left and right hemispheres, again demarcated in grey. Figure 30(c) & (d) demonstrates the

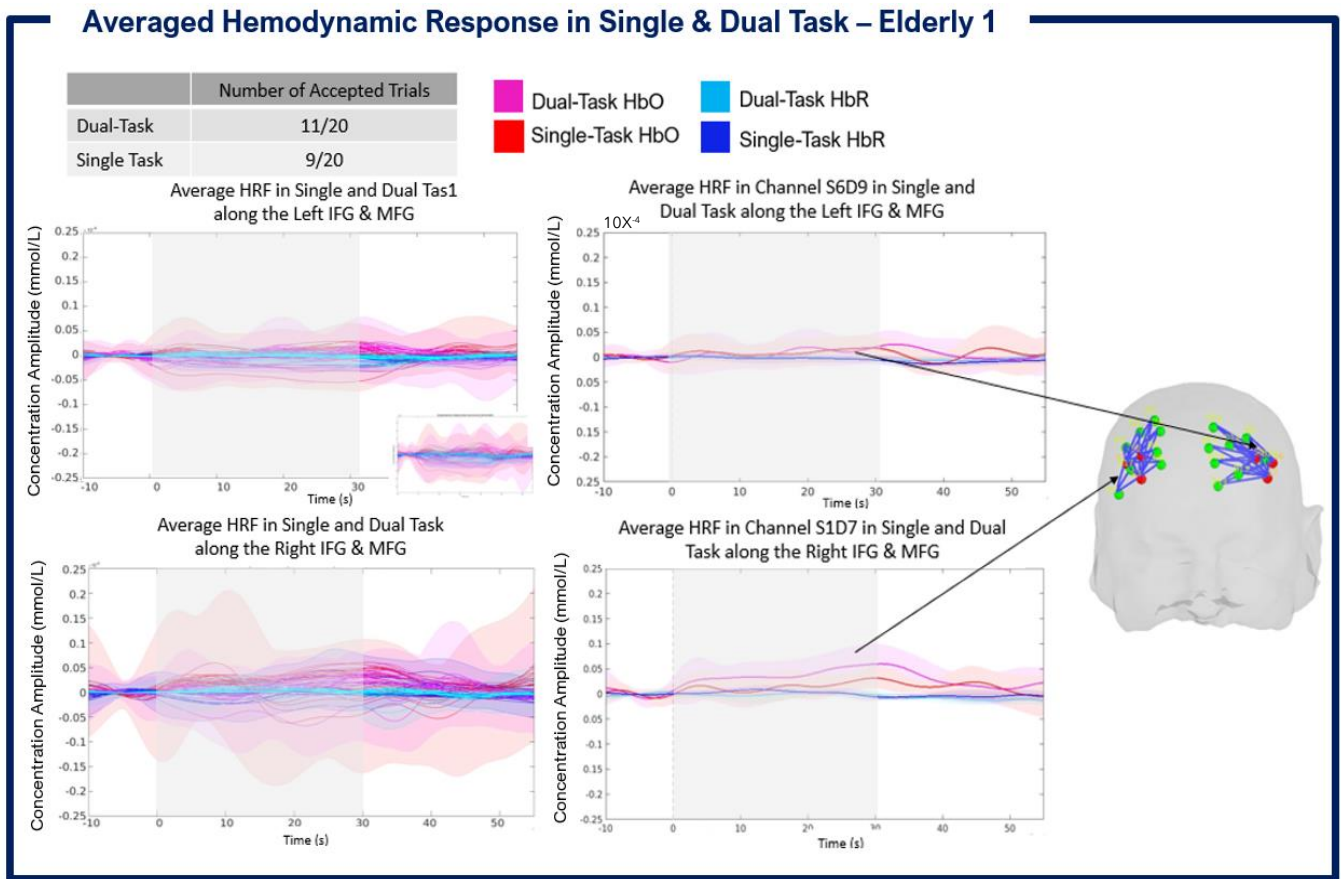


Figure 30: Elderly 1 - Block averaged hemodynamic response in single task and dual task across IFG and MFG regions of interest.

Figure 29(a) and (b) depict the single task (block averaged across 10/20 accepted trials) and dual task conditions (block averaged across 7/20 accepted trials) across the right and left IFG and MFG. Figure 29(c) portrays the hemodynamic response from one channel, S7D15, across within the right optimal montage. Figure 29(d) portrays the hemodynamic response from one channel, S2D5 across within the left optimal montage. Figure 29(e) depicts the personalized optimal montage of Elderly 2; arrows point to the channels S7D15 and S2D5 and represent the region which experiences a greater hemodynamic response across the right and left IFG and MFG, respectively.

associated MEM [HbO] and [HbR] reconstructions with responses averaged in the 5-20s time window ST and DT events. Each figure was set to represent the range of signal amplitude, demonstrating negative and positive responses of HbO and HbR concentrations along the cortex in response to ST and DT. Based on the current results, Elderly 1 results indicate more activity along the right hemisphere. Elderly 1's response to ST and DT indicate that activity falls outside of the demarcated scout along the right and left IFG and MFG and is rather posterior relative to the demarcated ROIs. On the left side, a slight negative [HbO] response appears with the target ROI during DT condition.

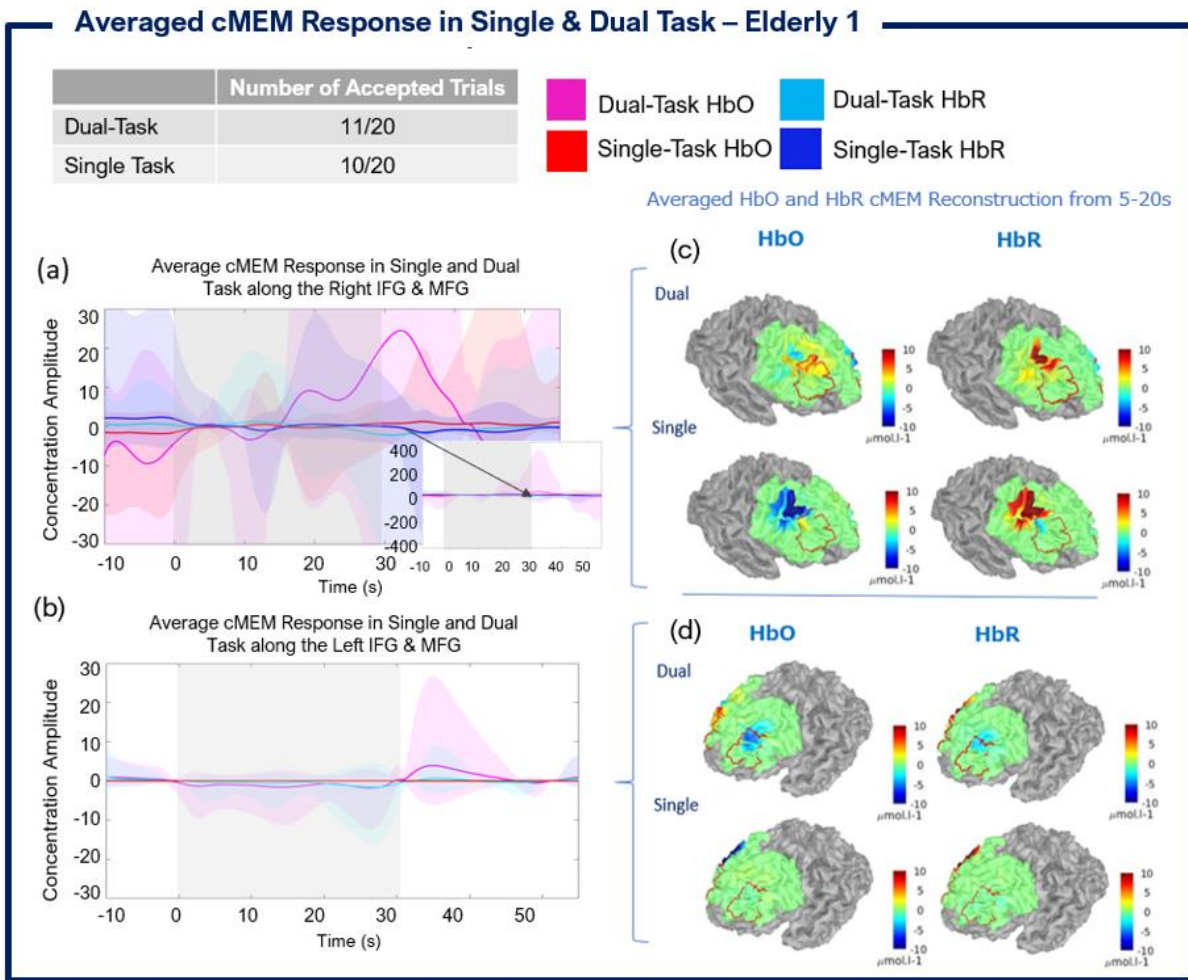


Figure 31: MEM reconstruction in single task and dual task across right and left hemispheres in Elderly 1

Figure 30(a) and (b) depict the single task (averaged across 7/20 accepted trials) and dual task conditions (averaged across 9/20 accepted trials) across the demarcated ROIs (right and left hemispheres). Figure 30(c) and (d) portrays the reconstructed HbO and HbR responses in source space across the right and left hemisphere, time averaged between 5s and 20s.

Elderly 1 demonstrates greatest amount of variability in EMG recordings within the right calf, showing increased %MVC in dual-task relative to walking only (DT: 1.024% ± 0.160% versus Walk-Only: 0.937% ± 0.173 %; 0.087% increase, p<0.001), followed by the right calf (DT: 0.826% ± 0.336% vs 0.698 ± 0.189%; 1.28% increase, p<0.001), as presented in Table 9. Gait recordings indicated minor variability in cadence and stride time across conditions. Cadence remained near-constant in dual-task and walk-only conditions and did not attain statistically significant results (113 steps/min ± 0.72 versus 114 steps/min ± 0.72, p>0.001). Stride time also remained near-constant and did not demonstrate statistically significant results (1.05s ± 0.02 versus 1.03 ± 0.02; p<0.001), as per Table 11.

Elderly 1 - Average %MVC Across Dual-Task and Walk-Only Recordings

Muscle Group	Dual Task (Walking + S7) Average %MVC ± Std	Walking Only Average %MVC ± Std	p-value	t-test
Left Calf	0.826 ± 0.336	0.698 ± 0.189	p < 0.001	4.053
Right Calf	1.024 ± 0.160	0.937 ± 0.173	p < 0.001	4.508
Left Hamstring	1.988 ± 0.961	1.962 ± 0.856	p = 0.810	0.241
Right Hamstring	1.619 ± 0.032	1.568 ± 0.544	p = 0.447	0.761
Left Quad	0.887 ± 0.247	0.831 ± 0.176	p = 0.023	2.288
Right Quad	1.226 ± 0.372	1.218 ± 0.258	p = 0.829	0.216

Table 9: Average %MVC Across Dual-Task and Walk-Only Recordings for Elderly 1

Average Cadence and Stride Time Recordings for Dual Task Vs. Walking Only Conditions

	Cadence (steps/min)				Stride Time (s)			
	Dual Task (Walking + S7) Average ± Std	Walking Only Average ± Std	p-value	t-test	Dual Task (Walking + S7) Average ± Std	Walking Only Average ± Std	p-value	t-test
Youth 1	112.0 ± 3.265	110.0 ± 5.291	p = 0.512	0.668	1.072 ± 0.030	1.086 ± 0.047	p = 0.445	-0.780
Youth 3	113.0 ± 3.098	113.0 ± 1.330	p = 0.969	0.040	1.056 ± 0.014	1.056 ± 0.006	p = 0.980	0.015
Youth 4	96.0 ± 14.624	107.0 ± 6.408	p = 0.133	-1.636	1.266 ± 0.095	1.122 ± 0.034	p = 0.019	3.430
Youth 5	88.0 ± 4.899	90.0 ± 2.906	p = 0.259	-1.170	1.368 ± 0.038	1.332 ± 0.022	p = 0.239	1.222
Elderly 1	36.0 ± 2.666	37.0 ± 2.000	p = 0.694	-0.400	3.268 ± 0.242	3.222 ± 0.166	p = 0.642	0.472

Table 11: Average Cadence and Stride Time Recordings for Dual Task versus Walking-Only Conditions

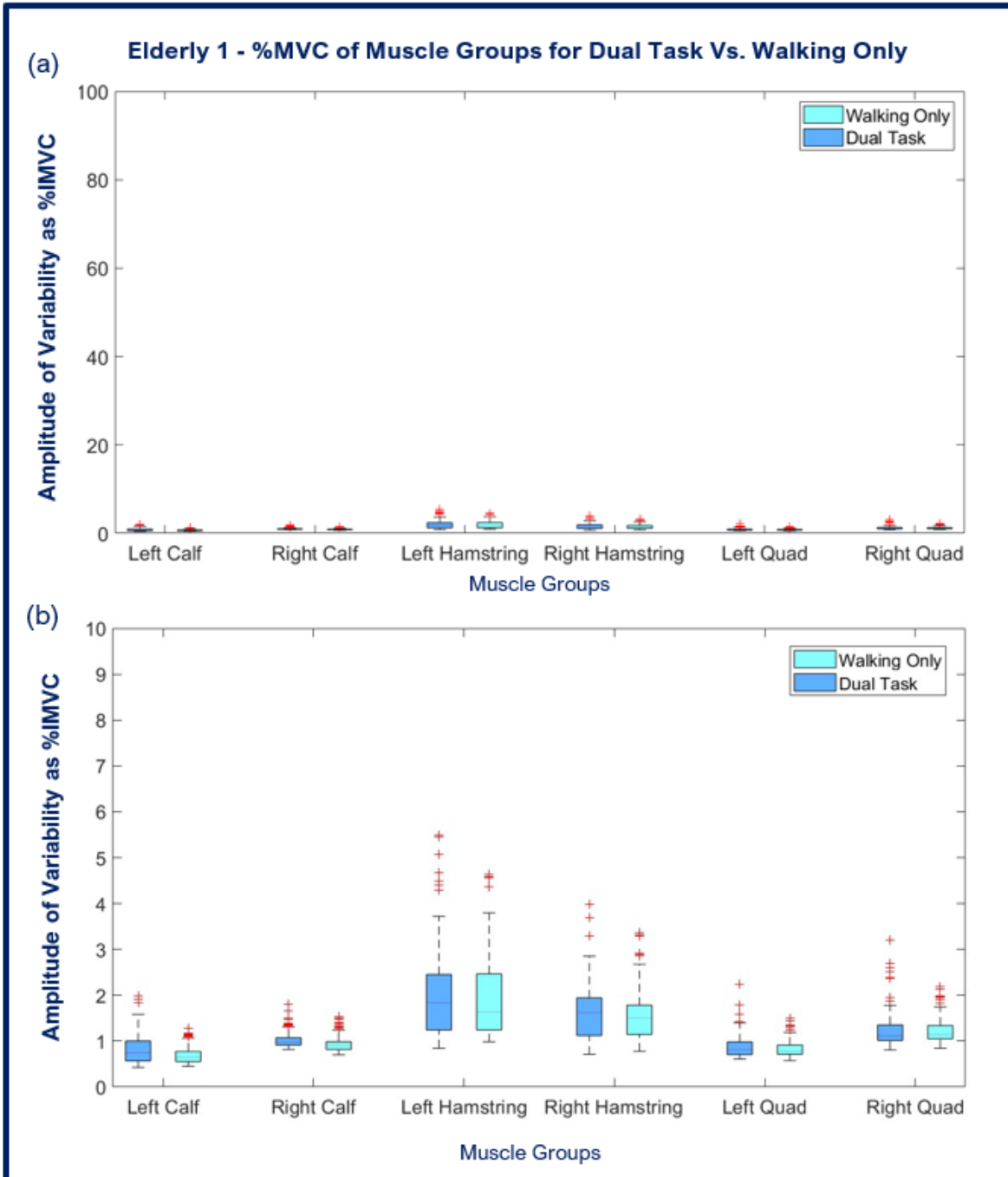


Figure 32: %MVC of Muscle Groups for Dual-Task versus walking-only in Elderly 1

Figure 31(a) depicts changes in muscular activity in six muscle groups during in DT conditions in terms of percent of Maximum Voluntary Contraction (%MVC), based on 100%. Amplitude of Variability as %MVC in Walk-Only periods is demonstrated using cyan boxplot. Amplitude of Variability as %MVC in Dual-Task periods is demonstrated using dark blue boxplot. Figure 31(b) represents the same data, scaled and zoomed in on the %MVC axis to demonstrate the mean value of each muscle group and in both Walk-Only and Dual-Task activity during Dual-Task block design paradigm. The muscle groups that demonstrate the largest variability and showed a statistically significant increase during the DT was the right calf (DT: $1.024\% \pm 0.160\%$ versus Walk-Only: $0.937\% \pm 0.173\%$; 0.087% increase, $p < 0.001$), followed by the right calf (DT: $0.826\% \pm 0.336\%$ vs $0.698\% \pm 0.189\%$; 1.28% increase, $p < 0.001$)

Elderly 2

Elderly 2 demonstrates an [HbO] increase relative to baseline in both ST and DT conditions based on 7 and 10 block averaged trials, respectively. Figure 32(a) and (b) depict a positive [HbO] response with in both ST and DT; DT appears to elicit a greater response relative to ST during the 30s event window along the left and right ROIs, as demarcated in grey. Similarly, [HbR] response in ST and DT also appear to produce a slightly positive response. MEM results could not be generated at this moment due to Brainstorm version error. The result will be produced before August 25th, 2021.

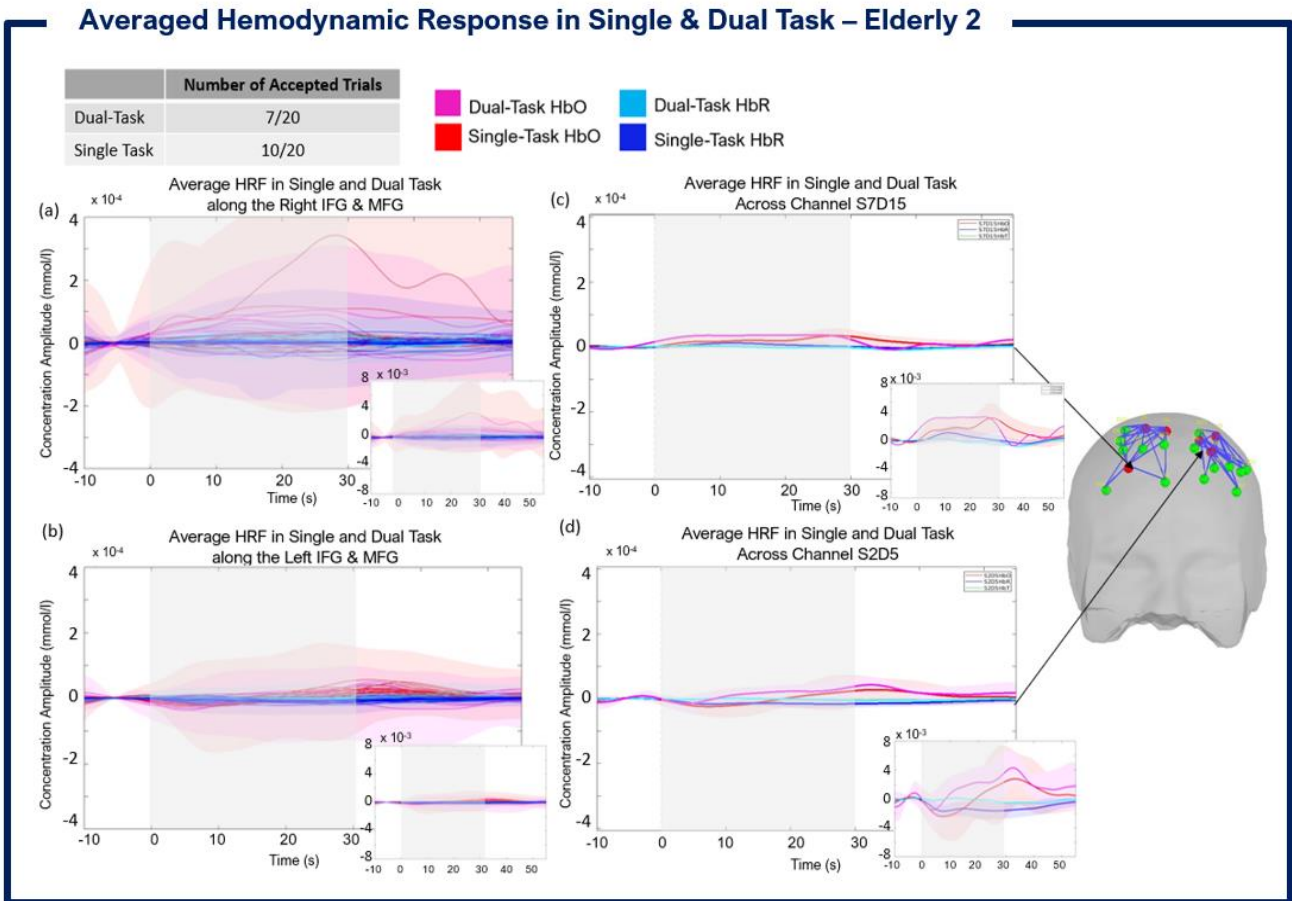


Figure 33: Block averaged hemodynamic response in single task and dual task across IFG and MFG regions of interest

Figure 32(a) and (b) depict the single task (block averaged across 10/20 accepted trials) and dual task conditions (block averaged across 7/20 accepted trials) across the right and left IFG and MFG. Figure 32(c) portrays the hemodynamic response from one channel, S7D15, across within the right optimal montage. Figure 32(d) portrays the hemodynamic response from one channel, S2D5 across within the left optimal montage. Figure 32(e) depicts the personalized optimal montage of Elderly 2; arrows point to the channels S7D15 and S2D5 and represent the region which experiences a greater hemodynamic response across the right and left IFG and MFG, respectively. The smaller graphs located on each figure in the bottom right corners are enlarged plot, setting the concentration amplitude scale to better represent the amplitude of the response.

Elderly 2 demonstrates greatest amount of variability in EMG recordings within the right hamstring, showing increased %MVC in dual-task relative to walking only (DT: 39.662% ± 18.025% versus Walk-Only: 31.867% ± 9.153%; 7.795% increase, p<0.001), followed by the left quad (DT: 20.541% ± 12.077% vs 16.346 ± 6.485%; 4.195% increase, p<0.001), and lastly, the left calf (DT: 1.030 ± 0.143% versus 0.940% ± 0.193%; 0.090% increase, p<0.001), as presented in Table 10. Elderly 2 demonstrated decreased %MVC in dual-task relative to walking only in the left hamstring (DT: 27.299% ± 7.527% versus 31.867% ± 9.153%; 7.795% increase, p<0.001), followed by the right calf (DT: 1.142% ± 0.216% vs 1.306 ± 0.666%; 4.195% increase, p<0.001). Cadence remained near-constant in dual-task and walk-only conditions and did not attain statistically significant results (113 steps/min ± 0.72 versus 114 steps/min ± 0.72, p>0.001). Stride time also remained near-constant and did not demonstrate statistically significant results (1.05s ± 0.02 versus 1.03 ± 0.02; p<0.001), as per Table 11.

Elderly 2 completed this study with unsuccessful footswitch recordings and therefore, cadence and stride time data is not available.

Elderly 2 - Average %MVC Across Dual-Task and Walk-Only Recordings

Muscle Group	Dual Task (Walking + S7) Average %MVC ± Std	Walking Only Average %MVC ± Std	p-value	t-test
Left Calf	1.030 ± 0.143	0.940 ± 0.193	p < 0.001	4.569
Right Calf	1.142 ± 0.216	1.306 ± 0.666	p = 0.004	-2.876
Left Hamstring	27.299 ± 7.527	32.572 ± 12.551	p < 0.001	-4.413
Right Hamstring	39.662 ± 18.025	31.867 ± 9.153	p < 0.001	4.723
Left Quad	20.541 ± 12.077	16.346 ± 6.485	p < 0.001	3.748
Right Quad	6.646 ± 2.846	6.288 ± 2.577	p = 0.254	1.142

Table 10: Average %MVC Across Dual-Task and Walk-Only Recordings for Elderly 2

Average Cadence and Stride Time Recordings for Dual Task Vs. Walking Only Conditions

Cadence (steps/min)					Stride Time (s)			
	Dual Task (Walking + S7) Average \pm Std	Walking Only Average \pm Std	p-value	t-test	Dual Task (Walking + S7) Average \pm Std	Walking Only Average \pm Std	p-value	t-test
Youth 1	112.0 \pm 3.265	110.0 \pm 5.291	p = 0.512	0.668	1.072 \pm 0.030	1.086 \pm 0.047	p = 0.445	-0.780
Youth 3	113.0 \pm 3.098	113.0 \pm 1.330	p = 0.969	0.040	1.056 \pm 0.014	1.056 \pm 0.006	p = 0.980	0.015
Youth 4	96.0 \pm 14.624	107.0 \pm 6.408	p = 0.133	-1.636	1.266 \pm 0.095	1.122 \pm 0.034	p = 0.019	3.430
Youth 5	88.0 \pm 4.899	90.0 \pm 2.906	p = 0.259	-1.170	1.368 \pm 0.038	1.332 \pm 0.022	p = 0.239	1.222
Elderly 1	36.0 \pm 2.666	37.0 \pm 2.000	p = 0.694	-0.400	3.268 \pm 0.242	3.222 \pm 0.166	p = 0.642	0.472

Table 11: Average Cadence and Stride Time Recordings for Dual Task versus Walking-Only Conditions

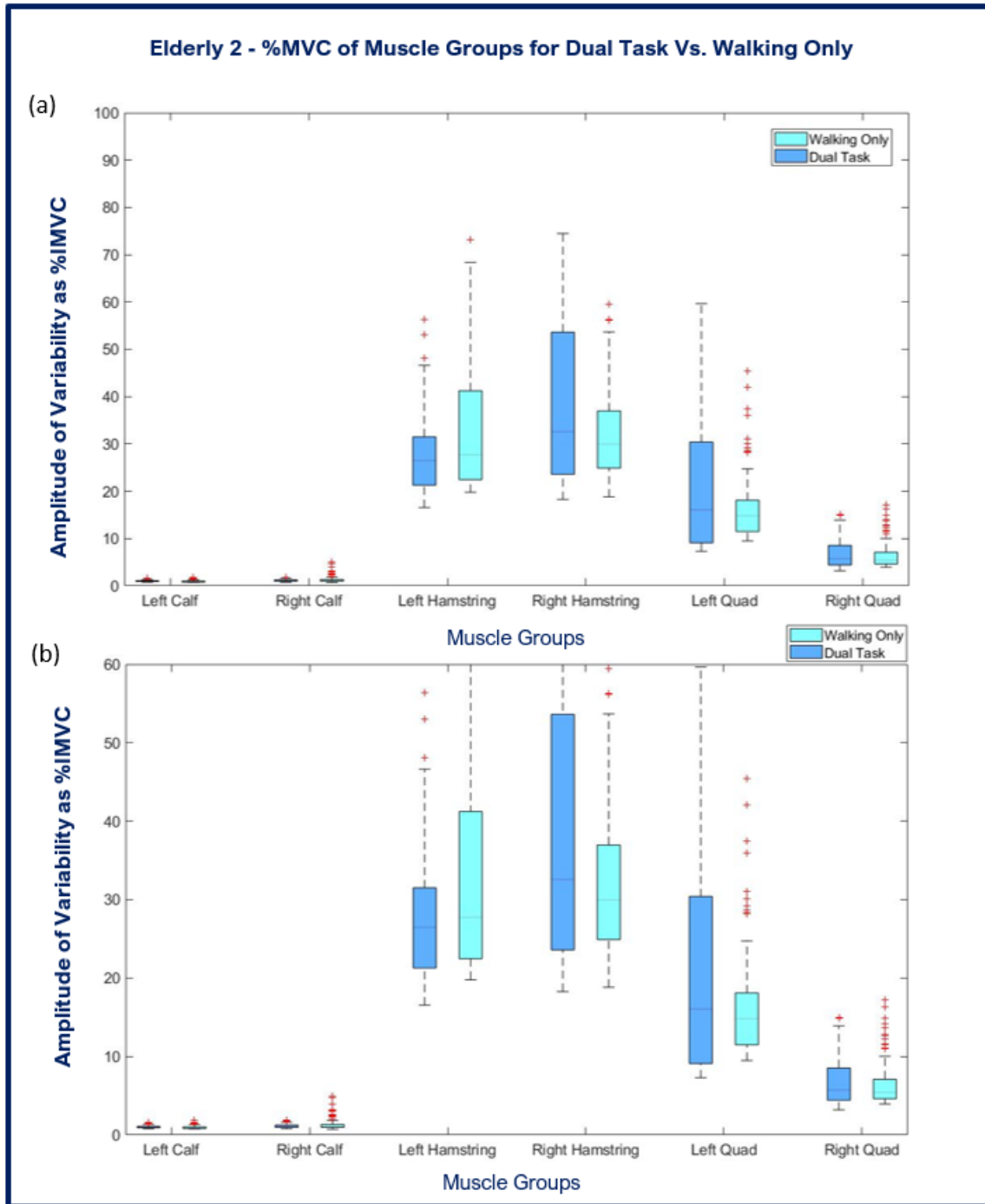


Figure 34: %MVC of Muscle Groups for Dual-Task versus walking-only in Elderly 2

Figure 33(a) depicts changes in muscular activity in six muscle groups during in DT conditions in terms of percent of Maximum Voluntary Contraction (%MVC), based on 100%. Amplitude of Variability as %MVC in Walk-Only periods is demonstrated using cyan boxplot. Amplitude of Variability as %MVC in Dual-Task periods is demonstrated using dark blue boxplot. Figure 33(b) represents the same data, scaled and zoomed in on the %MVC axis to demonstrate the mean value of each muscle group and in both Walk-Only and Dual-Task activity during Dual-Task block design paradigm. The muscle groups that demonstrate the largest variability and showed a statistically significant increase during the DT was the right hamstring (DT: $39.662\% \pm 18.025\%$ versus Walk-Only: $31.867\% \pm 9.153\%$; 7.795% increase, $p < 0.001$), followed by the left quad (DT: $20.541\% \pm 12.077\%$ vs $16.346 \pm 6.485\%$; 4.195% increase, $p < 0.001$), and lastly, the left calf (DT: $1.030 \pm 0.143\%$ versus $0.940\% \pm 0.193\%$; 0.090% increase, $p < 0.001$).

Review of EMG and footswitch Data Across All Subjects

A total of six participants (four youth, two elderly) had successfully completed the 2nd session with EMG and footswitch data. In this section, I have included all participants' EMG data and footswitch data to visualize the trend observed in particular muscle groups and discuss the study of cadence and stride time in the DT condition. Table 5 to Table 10 provide all results of five participants and their muscular activities during DT (S7 + walking) and Walking-Only conditions. We care to look at each muscle groups' behavior to evaluate if there are 1) recurring trends across conditions, 2) if increased cognitive load on has an effect on one's gait, and 3) comparing our results with the results reported in literature.

Three out of six participants showed a statistically significant increase in muscular activity in the right hamstring (Youth 1, Youth 4 and Elderly 2) in DT (S7 + Walking) versus Walking-Only condition; there is no statistically significant results showing decrease in right hamstring muscle activity. Next, three out of six participants showed a statistically significant increase in muscular activity in the left calf in DT (S7 + Walking) compared to Walking-Only condition (Youth 4, Elderly 1 and Elderly 2); only one participant demonstrated a statistically significant decrease in the left calf (Youth 3).

One out of six participants exhibited a statistically significant increase in muscular activity in the left hamstring (Youth 3), though two out of six participants shower a statistically significant decrease in the left hamstring in DT (S7 + Walking) versus Walking-Only condition. One out of six participants exhibited a statistically significant increase in muscular activity in the left hamstring (Youth 3), though two out of six participants shower a statistically significant decrease in the left hamstring in DT (S7 + Walking) versus Walking-Only condition.

The muscle group that appears to be least affected by changes in cognitive load during the DT exercise was the right quad. Only one out of six participants showed a statistically significant increase in muscular activity DT (S7 + Walking) compared Walking-Only condition, one out six participants showed a statistically significant decrease in muscular activity in DT (S7 + Walking) compared Walking-Only condition; four out of six participants showed no statistically significant increase or decrease in muscle activity in the right quad.

Youth 1 - Average %MVC Across Dual-Task and Walk-Only Recordings

Muscle Group	Dual Task (Walking + S7) Average %MVC ± Std	Walking Only Average %MVC ± Std	p-value	t-test
Left Calf	1.666 ± 0.311	1.701 ± 0.360	p = 0.371	-0.895
Right Calf	1.211 ± 0.188	1.366 ± 0.190	p < 0.001	-8.829
Left Hamstring	0.431 ± 0.058	0.446 ± 0.063	p = 0.037	-2.078
Right Hamstring	1.827 ± 0.010	1.734 ± 0.180	p < 0.001	4.204
Left Quad	2.971 ± 0.406	3.102 ± 0.550	p = 0.020	-2.340
Right Quad	4.811 ± 1.008	5.122 ± 0.745	p = 0.003	-3.038

Table 5: Youth 1 - Average %MVC Across Dual-Task and Walk-Only Recordings

Youth 3 - Average %MVC Across Dual-Task and Walk-Only Recordings

Muscle Group	Dual Task (Walking + S7) Average %MVC ± Std	Walking Only Average %MVC ± Std	p-value	t-test
Left Calf	2.026 ± 0.260	2.387 ± 0.820	p < 0.001	-5.136
Right Calf	3.245 ± 1.000	3.257 ± 0.780	p = 0.908	-0.115
Left Hamstring	5.149 ± 1.100	0.470 ± 0.080	p < 0.001	4.141
Right Hamstring	1.746 ± 0.310	1.673 ± 0.680	p = 0.234	1.192
Left Quad	2.707 ± 0.880	3.453 ± 1.190	p < 0.001	-6.144
Right Quad	6.887 ± 1.631	5.291 ± 1.830	p < 0.001	7.972

Table 6: Youth 3 - Average %MVC Across Dual-Task and Walk-Only Recordings

Youth 4 - Average %MVC Across Dual-Task and Walk-Only Recordings

Muscle Group	Dual Task (Walking + S7) Average %MVC ± Std	Walking Only Average %MVC ± Std	p-value	t-test
Left Calf	4.585 ± 1.812	3.567 ± 1.384	p < 0.001	5.471
Right Calf	1.315 ± 0.147	1.284 ± 0.217	p = 0.142	1.474
Left Hamstring	0.930 ± 0.189	0.945 ± 0.180	p = 0.487	-0.695
Right Hamstring	0.370 ± 0.010	0.341 ± 0.061	p < 0.001	4.246
Left Quad	6.924 ± 1.678	7.031 ± 2.531	p = 0.666	-0.432
Right Quad	0.693 ± 0.253	0.749 ± 0.301	p = 0.077	-1.775

Table 7: Youth 4 - Average %MVC Across Dual-Task and Walk-Only Recordings

Youth 5 - Average %MVC Across Dual-Task and Walk-Only Recordings

Muscle Group	Dual Task (Walking + S7) Average %MVC ± Std	Walking Only Average %MVC ± Std	p-value	t-test
Left Calf	3.081 ± 0.556	2.917 ± 0.773	p = 0.036	2.108
Right Calf	1.471 ± 0.267	1.486 ± 0.245	p = 0.599	-0.526
Left Hamstring	3.321 ± 0.847	4.181 ± 1.455	p < 0.001	-6.258
Right Hamstring	1.864 ± 0.006	1.902 ± 0.618	p > 0.512	-0.657
Left Quad	19.527 ± 3.292	18.268 ± 3.163	p < 0.001	3.377
Right Quad	30.487 ± 5.448	30.878 ± 5.676	p < 0.543	-0.610

Table 8: Youth 5 - Average %MVC Across Dual-Task and Walk-Only Recordings

Elderly 1 - Average %MVC Across Dual-Task and Walk-Only Recordings

Muscle Group	Dual Task (Walking + S7) Average %MVC ± Std	Walking Only Average %MVC ± Std	p-value	t-test
Left Calf	0.826 ± 0.336	0.698 ± 0.189	p < 0.001	4.053
Right Calf	1.024 ± 0.160	0.937 ± 0.173	p < 0.001	4.508
Left Hamstring	1.988 ± 0.961	1.962 ± 0.856	p = 0.810	0.241
Right Hamstring	1.619 ± 0.032	1.568 ± 0.544	p = 0.447	0.761
Left Quad	0.887 ± 0.247	0.831 ± 0.176	p = 0.023	2.288
Right Quad	1.226 ± 0.372	1.218 ± 0.258	p = 0.829	0.216

Table 9: Elderly 1 - Average %MVC Across Dual-Task and Walk-Only Recordings

Elderly 2 - Average %MVC Across Dual-Task and Walk-Only Recordings

Muscle Group	Dual Task (Walking + S7) Average %MVC ± Std	Walking Only Average %MVC ± Std	p-value	t-test
Left Calf	1.030 ± 0.143	0.940 ± 0.193	p < 0.001	4.569
Right Calf	1.142 ± 0.216	1.306 ± 0.666	p = 0.004	-2.876
Left Hamstring	27.299 ± 7.527	32.572 ± 12.551	p < 0.001	-4.413
Right Hamstring	39.662 ± 18.025	31.867 ± 9.153	p < 0.001	4.723
Left Quad	20.541 ± 12.077	16.346 ± 6.485	p < 0.001	3.748
Right Quad	6.646 ± 2.846	6.288 ± 2.577	p = 0.254	1.142

Table 10: Elderly 2 - Average %MVC Across Dual-Task and Walk-Only Recordings

Average Cadence and Stride Time Recordings for Dual Task Vs. Walking Only Conditions

	Cadence (steps/min)				Stride Time (s)			
	Dual Task (Walking + S7) Average ± Std	Walking Only Average ± Std	p-value	t-test	Dual Task (Walking + S7) Average ± Std	Walking Only Average ± Std	p-value	t-test
Youth 1	112.0 ± 3.265	110.0 ± 5.291	p = 0.512	0.668	1.072 ± 0.030	1.086 ± 0.047	p = 0.445	-0.780
Youth 3	113.0 ± 3.098	113.0 ± 1.330	p = 0.969	0.040	1.056 ± 0.014	1.056 ± 0.006	p = 0.980	0.015
Youth 4	96.0 ± 14.624	107.0 ± 6.408	p = 0.133	-1.636	1.266 ± 0.095	1.122 ± 0.034	p = 0.019	3.430
Youth 5	88.0 ± 4.899	90.0 ± 2.906	p = 0.259	-1.170	1.368 ± 0.038	1.332 ± 0.022	p = 0.239	1.222
Elderly 1	36.0 ± 2.666	37.0 ± 2.000	p = 0.694	-0.400	3.268 ± 0.242	3.222 ± 0.166	p = 0.642	0.472

Table 11: Average Cadence and Stride Time Recordings for Dual Task versus Walking-Only Conditions

Summary

In this chapter, we presented the results obtained from fNIRS, EMG, footswitch and evaluation of the accelerometer selected in this study. Trial selection reduced the number of number of averaged trials affected by motion and other artifacts that could bias fNIRS signal in analysis. I used the NIROT workflow with MEM to perform analysis at the single-subject level, which permitted me to perform a thorough analysis of [HbO]/[HbR] and MEM response bilaterally, separating the time-courses of channels across the left and right IFG and MFG. EMG and footswitch data was also analyzed in DT and Walk-Only conditions, addressing cognitive load as a factor in changes in muscle activity. Muscle groups that were recognizably affected across half of participants were the right hamstring and the left calf. The leas affected muscle group in the DT exercise was the right quad, where four out of six participants showed no statistically significant increase or decrease in muscle activity.

This study will recommence acquisitions in Fall 2021 with a more refined protocol to minimize the amount of motion artifacts in fNIRS data and a more optimized workflow for the acquisition setup. I would like to achieve the original goal of 30 participants in this study so that we continue to use the NIROT workflow with MEM and perform group-level analysis.

Chapter 6

Discussion

The multimodal approach taken to study brain and muscular activity in dual gait exercises presents promising trends towards our hypotheses and has served as a proof of concept for new methods. The quality of our fNIRS data was contaminated with too many artifacts originating from head and jaw motions due to the nature of the protocol. The dataset is also composed of only seven out of thirty participants (15 younger / 15 older), a smaller dataset because we had to stop in data acquisitions at the PERFORM Centre, first because Covid-19 pandemic lockdown and then because limited availability of the equipment during slow ramp up of research projects involving human participants at PERFORM . Nonetheless, this event did permit for thorough analysis of all data sets obtained throughout the study and suggested modifications have been made to the protocol to enhance the quality of the future data to be acquired. This chapter will present a discussion of the results obtain in this study, as well as present methods suggested to optimize the study's protocol.

6.1. Hemodynamic Response in Single-Task and Dual-Task, MEM reconstructions and Gait Analysis

Given the limited data sample we were able to acquire, results in fNIRS, EMG and footswitch data were studied at the single-subject level due an unequal number of young versus older participants; five younger adults versus two older adults. Four out of seven participants demonstrated the tendency for positive [HbO] response and two participants demonstrated negative [HbO] in both ST and DT conditions across the right and left IFG and MFG. One out of seven participants demonstrated a positive [HbO] response in ST together with a negative [HbO] response across the right IFG & MFG. Three out of seven (Youth 3, Elderly 1 and Elderly 2) presented an initial negative dip in [HbO] before restoring a greater positive hemodynamic response. MEM reconstructions were performed using a consistent number trials as that of hemodynamic response analysis. The purpose for this decision is to measure the consistency between hemodynamic response and MEM reconstruction of the response at the single-subject level.

6.2. Gait Analysis: Measuring Cadence and Stride Time via EMG and footswitch Data

Gait analysis was performed at the single subject level due to an unequal number of young adult and older adult participants. EMG results obtained across four young adult participants and two older adult participants demonstrated more statistically significant increases or decreases in electromuscular activity during DT activities. A common trend was observed in the hamstring and calves muscle groups across five out of six participants. Amongst the six studied muscle groups, the most affected muscle group was the left hamstrings in which four out of six participants showed statistically significant increase in %MVC in the left hamstring, the greatest statistically significant change in %MVC demonstrated by Elderly 2 with 7.8% increase in DT condition relative to Walk-Only (DT: $39.662\% \pm 18.025\%$ versus Walk-Only $31.867\% \pm 9.153\%$; 7.795% increase, $p < 0.001$). Half of the subjects also demonstrated greater variability as %MVC in the left calf, two out of three subjects were older adults. These results coincide with those obtained in similar gait studies involving aging population (Li, et al., 2012).

Based on current literature, the elderly population tends to respond to the increased cognitive load with increased stride length, thus reducing their cadence of walking and consequently reducing the number of gait cycles. The relationships between one's gait and dual tasking is believed that the decrease in one's cadence enables mental resources in performing the challenging mental arithmetic task (Li, et al., 2012). In similar studies, it has been found that older adults exhibit more spatial and temporal movement variability, and thus appear to be less consistent actions as compared to young adults (Seidler, et al. 2010). One cause for greater variability can be associated with peripheral changes in the neuromuscular system or may arise from increased neural noise at the central nervous system level (Faulkner, et al., 2007; Seidler, et al., 2010).

Cadence and stride time results did not reach significance when comparing DT and walking only conditions, despite showing a trend for a slight increase in cadence and stride time in three out of five subject recordings.

6.2. Optimization of current protocol

Thorough analysis of our data set has indicated that is required optimization of the current protocol. Additional requests have also been made to adjust the workflow of the study to adhere to

hygiene measures imposed by the Covid-19 pandemic. The following section will outline the suggested modifications to ensure cleaner data quality and safety throughout a participants' acquisition.

Serial Sevens (S7s) Cognitive Task

The first modification shall be made to the cognitive task performed during DT and ST runs. Throughout the study, participants calculated S7s out loud and their responses were recorded by the researcher. The intention of this paradigm was to use the number of correct/incorrect answers as a regressor in fNIRS signal analysis. When studying the data obtained in seven participants, it was found that fNIRS recordings were noisy and contained a significant amount of motion artifacts. A motion test was performed using an accelerometer and glued fNIRS montage. In both Run 05 and Run 06 (*Figure 37 and 38 in Appendix 3*), correlation values tended toward 1 in long-distance separation channels as well as short-distance channel, however, a weak correlation with accelerometer data. In Run 05 (*Figure 37*) the correlation metric $R=0.523$ across all channels of subject's montage suggests that jaw clenching does produce some motion-induced variability in fNIRS recordings even across long-distance channels. All motion test correlation matrices are demonstrated in *Figure 33 to 38 (in Appendix 3)*.

The conclusion drawn from these results suggests modifying the S7s protocol and ask the participant to perform mental calculation instead. It appears that motion caused by speech, both in ST and DT conditions, is a contributing factor to sudden changes in signal amplitude, peaks and drifts in signal. These artifacts lead to more rejected trials, and consequently decrease the Signal-to-Noise Ratio (SNR) across our averaged data. Considering trial selection can have such an impact, it would be optimal to increase the number of trials to increase the signal to noise ratio, despite having to reject some trials across runs.

Movement between PML and Physiology Lab

In response to hygiene measures imposed by Covid-19, we intend to minimize the amount of researchers and traffic between the PML and Physiology Lab. For this reason, we shall only have two

researchers present for the marking and gluing of the personalized montage and the MVC tests prior to ST and DT activities (approximately 2 out of 4 hours duration of the acquisition). The remainder of the acquisition will be performed by the primary researcher on the study.

The setup of the study will also require additional measures. The first is the disinfection of accessories and chairs used during the study, prior to the arrival of the participant. The second is to transport the Brainsight machine to the PML prior to the arrival of the participant to minimize traffic in hallways and between the two labs.

Chapter 7

Conclusion

The fNIRS and gait analysis study is the first of its' kind at the MultiFunkIm Lab and paved a new platform for brain imaging and biomechanics at the PERFORM Centre. This study served as a proof of concept for new methods and acquisitions, such as running a dual-tasking protocol, testing the effectiveness of an accelerometer for motion detection, and synchronization of different data sets involving gait, fNIRS and data provided by an inertial sensor. It is the first time that the MultifunkIm Lab runs a study with the NIROT workflow simultaneously with EMG and footswitch recordings. Though I have learned a realm of new acquisition and analysis methods, there is much to consider in the future design of this study's protocol.

The dual-task cognition-walking paradigm increased the complexity of this study, in which motion artifacts caused by mobile fNIRS and gait analysis became fundamental in assessing data quality and optimizing the protocol. One path worth investigating is that of purchasing a more accurate accelerometer and performing motion sensitivity tests prior to restarting acquisitions. A second path could benefit from the accelerometer test data by performing short-distance regression on the fNIRS source detector pairs to analyze the difference in correlation between sensors and accelerometer data, compared to the current data, which has not regressed the signal for short-distance channels. A third path for improvement is that of increasing the number of trials across ST and DT conditions. Considering trial selection reduces the total number of averaged trials across [HbO]/[HbR] and MEM responses, it would be optimal to maintain a higher number of trials to increase the signal to noise ratio.

Despite some challenging factors in the completion of the dataset, several tools have been developed to perform gait analysis, improving quality of data and testing proof of concepts in fNIRS acquisitions involving locomotion and head motion via speech. Superposition of cadence recordings on raw fNIRS data and unfiltered [HbO] and [HbR] data permitted thorough analysis of motion artifacts and trial selection that suggested more representative responses during ST and DT conditions. Another benefit of this study is the preparation of a bilateral personalized montage that targets the left and right sides of the prefrontal cortex. Until now, the optimal montage algorithm has been used to calculate ideal position of optodes in a very localized regions of the brain, often spanning a small region of the motor cortex (Cai, et al., 2021). It appears that the bilateral montage has been used in a similar

fashion using optodes holders across the left and right hemisphere in task-switching paradigms (Vasta, et al. 2018), but has been done using the NIROT workflow and collodion installation for the first time at the MultifunkIm Lab.

In addition to quality assurance of data, our protocol sought to study differences in brain activity during ST and DT conditions in older adults. Although the number of younger versus older adult participants were uneven and very small, therefore group analysis could not be performed, it is evident in our results that both older subjects adjusted their gait to perform the DT condition. This falls in line with current evidence of older adults decreasing their cadence while increase stride time to compensate for dual-tasking (Li et al, 2011; Holtzer, et al., 2011). On this basis, we are compelled to investigate our third hypothesis further (in chapter 1), such that brain activity appears to produce increased [HbO] responses in DT relative to ST, suggesting that our results may be indicating that there is an increase in cognitive involvement during DT in older adults for postural control and gait. Such trends in gait and aging population creates an interest platform for further investigation, and gives portable fNIRS, such as the newly acquired Artinis System, an optimal position in this study and continued investigating of PFC regions involved in dual-tasking (Li, et al, 2018).

The fNIRS and gait analysis study is set to recommence during Summer 2021 and will be optimized according to the description in the discussion section. In this project, I have acquired knowledge in neuroimaging, cognitive aging imaging and fundamentals of biomechanics. I have also developed several applied skills, such programming, data and statistical analysis and use of multiple data recording hardware. I have learned that I enjoy research in this field and look forward to begin acquisitions on this study as a part time research assistant in the weeks to come.

Chapter 8

References

Al-Hakim, R., Fallon, J., et al. (2006). A Dorsolateral Prefrontal Cortex Semi-Automatic Segmenter. *Proceedings of SPIE - The International Society for Optical Engineering*. 6144. 10.1117/12.653643.

Arridge, S. R. (2011) 'Methods in diffuse optical imaging', *Philosophical Transactions of the Bibliography 255 Royal Society A: Mathematical, Physical and Engineering Sciences*, 369(1955), pp. 4558–4576. doi: 10.1098/rsta.2011.0311

Ben-Gal, O., Benady, A., Zadik, S., Doniger, G. M., Schnaide-Beeri, M., & Plotnik, M. (2020). *Using the loading response peak for defining gait cycle timing: A novel solution for the double-belt problem. Journal of Biomechanics*, 109963. doi:10.1016/j.jbiomech.2020.10996

Beurskens R, Helmich I, Rein R, Bock O. Age-related changes in prefrontal activity during walking in dual-task situations: a fNIRS study. *Int J Psychophysiol*. (2014) 92:122–8. doi: 10.1016/j.ijpsycho.2014.03.005

Brigadoi, S., Ceccherini, L., Cutini, S., Scarpa, F., Scatturin, P., Selb, J., Cooper, R. J. (2014). Motion artifacts in functional near-infrared spectroscopy: a comparison of motion correction techniques applied to real cognitive data. *NeuroImage*. (2014), 85, 181–191. doi:10.1016/j.neuroimage.2013.04.082

Buxton, R. B., Uludağ, K., Dubowitz, D. J., & Liu, T. T. (2004). Modeling the hemodynamic response to brain activation. *NeuroImage*, 23 Suppl 1, S220–S233. <https://doi.org/10.1016/j.neuroimage.2004.07.013>

Currie S, Hoggard N, Craven IJ, et al. (2013). Understanding MRI: basic MR physics for physicians. *Postgraduate Medical Journal*; 89: 209-223. doi: <https://doi.org/10.1136/postgradmedj.2012.13142>

Doi, T., Blumen, H. M., Verghese, J., Shimada, H., Makizako, H., Tsutsumimoto, K., Hotta, R., Nakakubo, S., & Suzuki, T. (2017). Gray matter volume and dual-task gait performance in mild cognitive impairment. *Brain imaging and behavior*, 11(3), 887–898. <https://doi.org/10.1007/s11682-016-9562-1>

Faulkner, J. A., Larkin, L. M., Claflin, D. R., & Brooks, S. V. Age-related Changes in the Structure and Function of Skeletal Muscles. *Clinical and Experimental Pharmacology and Physiology*. (2007) 34(11), 1091–1096. doi:10.1111/j.1440-1681.2007.04752.x

Fraser, S.A, Li, K., DeMont, R.G., Penhune, V. (2007). Effects of balance status and age on muscle activation while walking under divided attention. *J Gerontology B Psychol Sci Soc Sci.*;62(3):P171-8. doi: 10.1093/geronb/62.3.p171.

Herman, T., Giladi, N., & Hausdorff, J. M. (2011). Properties of the 'timed up and go' test: more than meets the eye. *Gerontology*, 57(3), 203–210. Doi:[10.1159/000314963](https://doi.org/10.1159/000314963)

Herold, F., Wiegel, P., Scholkmann, F., & Müller, N. G. Applications of Functional Near-Infrared Spectroscopy (fNIRS) Neuroimaging in Exercise-Cognition Science: A Systematic, Methodology-Focused Review. *Journal of clinical medicine*, 2018, 7(12), 466. <https://doi.org/10.3390/jcm7120466>

Holtzer R, Mahoney JR, Izzetoglu M, Izzetoglu K, Onaral B, Verghese J. fNIRS study of walking and walking while talking in young and old individuals. *J Gerontol A Biol Sci Med Sci.* (2011) August; 66(8): 879-87. doi: 10.1093/gerona/qlr068.

Huneau, C., Benali, H., & Chabriat, H. (2015). Investigating Human Neurovascular Coupling Using Functional Neuroimaging: A Critical Review of Dynamic Models. *Frontiers in neuroscience*, 9, 467. <https://doi.org/10.3389/fnins.2015.00467>

Jin, H., Li, C., & Xu, J. Pilot Study on Gait Classification Using fNIRS Signals. *Computational intelligence and neuroscience*, (2018). doi:10.1155/2018/7403471

Korotkevich, Y., Trewartha, K. M., Penhune, V. B., & Li, K. Z. H. (2014). *Effects of age and cognitive load on response reprogramming. Experimental Brain Research*, 233(3), 937–946. doi:10.1007/s00221-014-4169-5

Li, K. Abbud, G., Fraser, S., DeMont, R. Successful adaptation of gait in healthy older adults during dual-task treadmill walking. *Aging, Neuropsychology, and Cognition*, (2012), 19:1-2, 150-167, DOI: 10.1080/13825585.2011.628375

Li, K., Bherer, L., Mirelman, A., Maidan, I., & Hausdorff, J. M. Cognitive Involvement in Balance, Gait and Dual-Tasking in Aging: A Focused Review From a Neuroscience of Aging Perspective. *Frontiers in neurology*, (2018) 9, 913. <https://doi.org/10.3389/fneur.2018.00913>

Lucas, M., Wagshul, M. E., Izzetoglu, M., & Holtzer, R. Moderating effect of white matter integrity on brain activation during dual-task walking in older adults. *The Journals of Gerontology: Series A: Biological Sciences and Medical Sciences.* (2019) 74(4), 435–441. <https://doi.org/10.1093/gerona/gly131>

Machado A, Cai Z, Pellegrino G, Marcotte O, Vincent T, Lina JM, Kobayashi E, Grova C. Optimal positioning of optodes on the scalp for personalized functional near-infrared spectroscopy investigations. *J Neurosci Methods.* (2018) Nov 1;309:91-108. doi: 10.1016/j.jneumeth.2018.08.006.

Machado, A., Cai, Z., Vincent, T. *et al.* Deconvolution of hemodynamic responses along the cortical surface using personalized functional near infrared spectroscopy. *Sci Rep* **11**, 5964 (2021). <https://doi.org/10.1038/s41598-021-85386-0>

Moratal, D., Vallés-Luch, A., Martí-Bonmatí, L., & Brummer, M. (2008). k-Space tutorial: an MRI educational tool for a better understanding of k-space. *Biomedical imaging and intervention journal*, *4*(1), e15. <https://doi.org/10.2349/bij.4.1.e15>

Mulert, C., Lemieux, L. 2010. *EEG - fMRI - Physiological Basis, Technique, and applications*. Springer. [//www.springer.com/us/book/9783540879183](http://www.springer.com/us/book/9783540879183).

Nasreddine, Z. S., Chertkow, H., Phillips, N. A., Bergman, H., Whitehead, V., & Collin, I. (2003). Sensitivity and specificity of the Montreal Cognitive Assessment (MOCA) as a cognitive tool for detection of mild cognitive deficits. Paper presented at the 38th meeting of the Canadian Congress of Neurological Sciences, Quebec, Canada.

Pichora-Fuller, M. K., Mick, P., & Reed, M. (2015). Hearing, Cognition, and Healthy Aging: Social and Public Health Implications of the Links between Age-Related Declines in Hearing and Cognition. *Seminars in hearing*, *36*(3), 122–139. <https://doi.org/10.1055/s-0035-1555116>

Pellegrino, G., Machado, A., et al. (2016) ‘Hemodynamic response to interictal epileptiform discharges addressed by personalized EEG-fNIRS recordings’, *Frontiers in Neuroscience*, *10*(MAR), p. 102. doi: 10.3389/fnins.2016.00102

Pooley, R. A. (2005). *Fundamental Physics of MR Imaging*. *RadioGraphics*, *25*(4), 1087–1099. doi:10.1148/rg.254055027

Pham, T., Tgavalekos, K., Sassaroli, A., Blaney, G., & Fantini, S. (2019). Quantitative measurements of cerebral blood flow with near-infrared spectroscopy. *Biomedical optics express*, *10*(4), 2117–2134. <https://doi.org/10.1364/BOE.10.002117>

Raez, M. B., Hussain, M. S., & Mohd-Yasin, F. (2006). Techniques of EMG signal analysis: detection, processing, classification and applications. *Biological procedures online*, *8*, 11–35. <https://doi.org/10.1251/bpo115>

Santosa, H., Zhai, X., Fishburn, F., Sparto, P. J., & Huppert, T. J. (2020). Quantitative comparison of correction techniques for removing systemic physiological signal in functional near-infrared spectroscopy studies. *Neurophotonics*, *7*(3), 035009. <https://doi.org/10.1117/1.NPh.7.3.035009>

Seidler, R. D., Bernard, J. A., Burutolu, T. B., Fling, B. W., Gordon, M. T., Gwin, J. T., Kwak, Y., & Lipps, D. B. Motor control and aging: links to age-related brain structural, functional, and

biochemical effects. *Neuroscience and biobehavioral reviews*, (2010). 34(5), 721–733. doi: <https://doi.org/10.1016/j.neubiorev.2009.10.005>

Statistics Canada. Validation of cognitive functioning in the Canadian Community Health Survey – Healthy Aging. Vol 82-033-X. (2015) Retrieved from <https://www150.statcan.gc.ca/n1/pub/82-003-x/2010004/article/11391/findings-resultats-eng.htm>

Stute, K., Hudl, N., Stojan, R., & Voelcker-Rehage, C. (2020). *Shedding Light on the Effects of Moderate Acute Exercise on Working Memory Performance in Healthy Older Adults: An fNIRS Study*. *Brain Sciences*, 10(11), 813. doi:10.3390/brainsci10110813

Terentjeviene, A., Maciuleviciene, E., Vadopalas, K., Mickeviciene, D., Karanauskiene, D., Valanciene, D, Skurvydas, A. (2018). *Prefrontal Cortex Activity Predicts Mental Fatigue in Young and Elderly Men During a 2 h “Go/NoGo” Task*. *Frontiers in Neuroscience*, 12. doi:10.3389/fnins.2018.00620

Vasta, R., Cutini, S., Cerasa, A., Gramigna, V., Olivadese, G., Arabia, G., & Quattrone, A. Physiological Aging Influence on Brain Hemodynamic Activity during Task-Switching: A fNIRS Study. *Frontiers in aging neuroscience*, (2018). 9, 433. <https://doi.org/10.3389/fnagi.2017.00433>

Virtanen J, Noponen T, Kotilahti K, Virtanen J, Ilmoniemi RJ. Accelerometer-based method for correcting signal baseline changes caused by motion artifacts in medical near-infrared spectroscopy. *J Biomed Opt*. (2011) Aug;16(8):087005. doi: 10.1117/1.3606576.

Yücel, M. A., Selb, J., Boas, D. A., Cash, S. S., & Cooper, R. J. (2014). Reducing motion artifacts for long-term clinical NIRS monitoring using collodion-fixed prism-based optical fibers. *NeuroImage*, 85 Pt 1(0 1), 192–201. <https://doi.org/10.1016/j.neuroimage.2013.06.054>

Yücel, M., Selb, J., Huppert, T., Franceschini, M., Boas, A. Functional Near Infrared Spectroscopy: Enabling routine functional brain imaging. *Current Opinion in Biomedical Engineering*, (2017). 4 (78-86). doi: 10.1016/j.cobme.2017.09.011.

Yücel, M. A., Lüthmann, A. V., Scholkmann, F., Gervain, J., Dan, I., Ayaz, H., Boas, D., Cooper, R. J., Culver, J., Elwell, C. E., Eggebrecht, A., Franceschini, M. A., Grova, C., Homae, F., Lesage, F., Obrig, H., Tachtsidis, I., Tak, S., Tong, Y., Torricelli, A., Wolf, M. (2021). Best practices for fNIRS publications. *Neurophotonics*, 8(1), 012101. <https://doi.org/10.1117/1.NPh.8.1.012101>

Yücel MA, Selb J, Aasted CM, Lin PY, Borsook D, Becerra L, Boas DA. Mayer waves reduce the accuracy of estimated hemodynamic response functions in functional near-infrared spectroscopy. *Biomed Opt Express*. 2016 Jul 22;7(8):3078-88. doi: 10.1364/BOE.7.003078. PMID: 27570699; PMCID: PMC4986815.

Appendix

Appendix 1 – Montreal Cognitive Assessment (MoCA)

MONTREAL COGNITIVE ASSESSMENT (MOCA)
Version 7.1 Original Version

NAME: _____
Education: _____ Date of birth: _____
Sex: _____ DATE: _____

VISUOSPATIAL / EXECUTIVE		Copy cube	Draw CLOCK (Ten past eleven) (3 points)	POINTS																		
		[]	[] [] []	___/5																		
NAMING					___/3																	
MEMORY Read list of words, subject must repeat them. Do 2 trials, even if 1st trial is successful. Do a recall after 5 minutes.	<table border="1"> <tr> <td></td> <td>FACE</td> <td>VELVET</td> <td>CHURCH</td> <td>DAISY</td> <td>RED</td> </tr> <tr> <td>1st trial</td> <td></td> <td></td> <td></td> <td></td> <td></td> </tr> <tr> <td>2nd trial</td> <td></td> <td></td> <td></td> <td></td> <td></td> </tr> </table>		FACE	VELVET	CHURCH	DAISY	RED	1st trial						2nd trial						No points		
	FACE	VELVET	CHURCH	DAISY	RED																	
1st trial																						
2nd trial																						
ATTENTION Read list of digits (1 digit/ sec.). Subject has to repeat them in the forward order [] 2 1 8 5 4 Subject has to repeat them in the backward order [] 7 4 2				___/2																		
Read list of letters. The subject must tap with his hand at each letter A. No points if ≥ 2 errors [] FBACMNAAJKLBAFAKDEAAAJAMOF AAB				___/1																		
Serial 7 subtraction starting at 100 [] 93 [] 86 [] 79 [] 72 [] 65 4 or 5 correct subtractions: 3 pts , 2 or 3 correct: 2 pts , 1 correct: 1 pt , 0 correct: 0 pt				___/3																		
LANGUAGE Repeat: I only know that John is the one to help today. [] The cat always hid under the couch when dogs were in the room. []				___/2																		
Fluency / Name maximum number of words in one minute that begin with the letter F [] ____ (N ≥ 11 words)				___/1																		
ABSTRACTION Similarity between e.g. banana - orange = fruit [] train - bicycle [] watch - ruler				___/2																		
DELAYED RECALL Has to recall words WITH NO CUE FACE [] VELVET [] CHURCH [] DAISY [] RED [] Points for UNCUEDE recall only				___/5																		
Optional Category cue Multiple choice cue																						

Appendix 2 – Time Up and Go (TUG)

Timed “Up and Go”*

Directions

The timed “Up and Go” test measures, in seconds, the time taken by an individual to stand up from a standard arm chair (approximate seat height of 46 cm [18in], arm height 65 cm [25.6 in]), walk a distance of 3 meters (118 inches, approximately 10 feet), turn, walk back to the chair, and sit down. The subject wears their regular footwear and uses their customary walking aid (none, cane, walker). No physical assistance is given. They start with their back against the chair, their arms resting on the armrests, and their walking aid at hand. They are instructed that, on the word “go” they are to get up and walk at a comfortable and safe pace to a line on the floor 3 meters away, turn, return to the chair and sit down again. The subject walks through the test once before being timed in order to become familiar with the test. Either a stopwatch or a wristwatch with a second hand can be used to time the trial.

Instructions to the patient

“When I say ‘go’ I want you to stand up and walk to the line, turn and then walk back to the chair and sit down again. Walk at your normal pace.”

Variations

You may have the patient walk at a fast pace to see how quickly they can ambulate. Also you could have them turn to the left and to the right to test any differences.

*Podsiadlo D, Richardson S. The timed “up and go”: a test of basic functional mobility for frail elderly persons. *JAGS* 1991; 39: 142-148.

Scoring

Time for ‘Up and Go’ test _____ sec.

Unstable on turning?

Walking aid used? Type of aid: _____

Appendix 3: Evaluating Effectiveness of Accelerometer with Controlled Head Motion Test

Figure 33: Run 01: Rotations Left

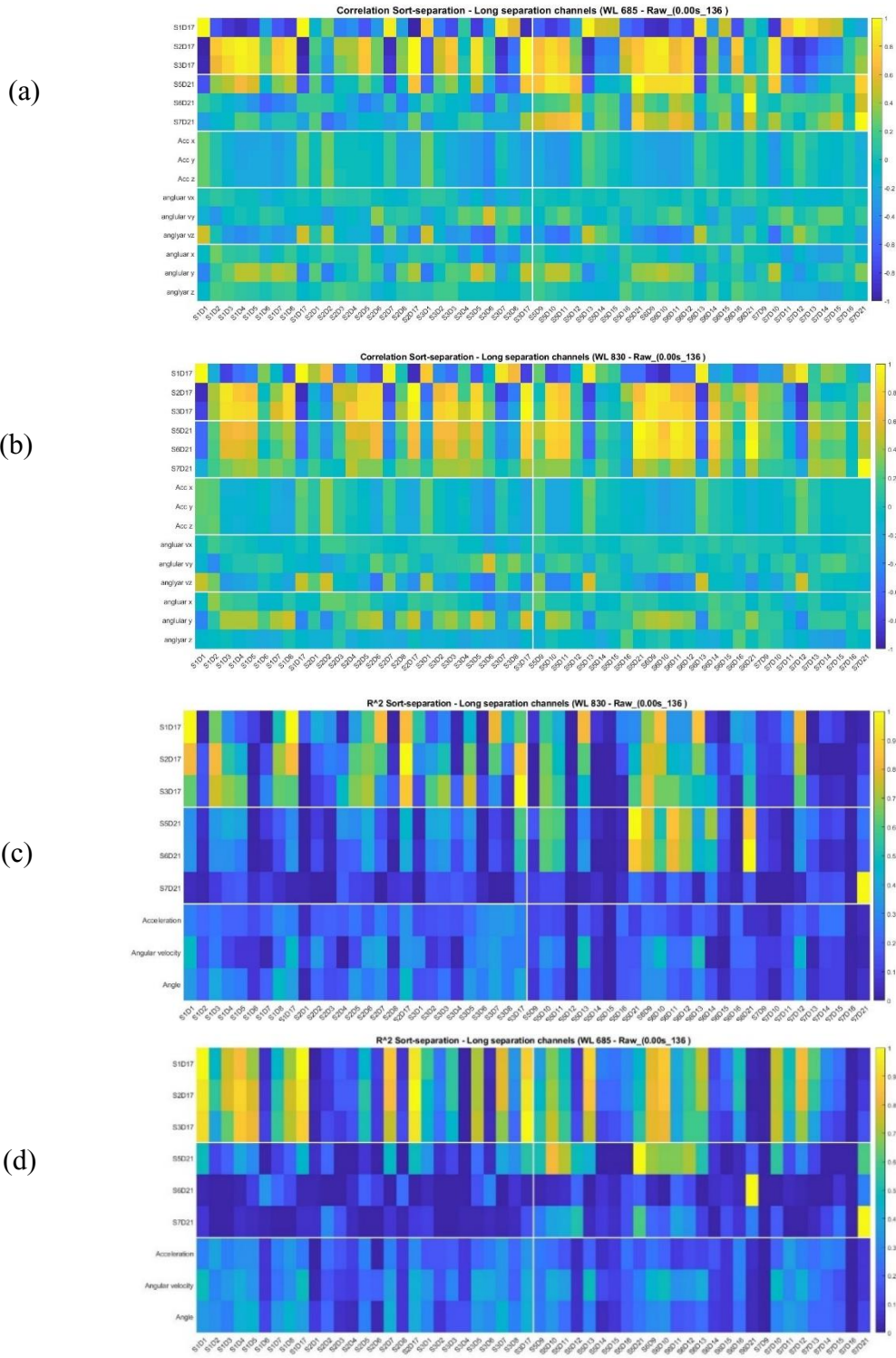


Figure 34: Run 02: Rotations Right

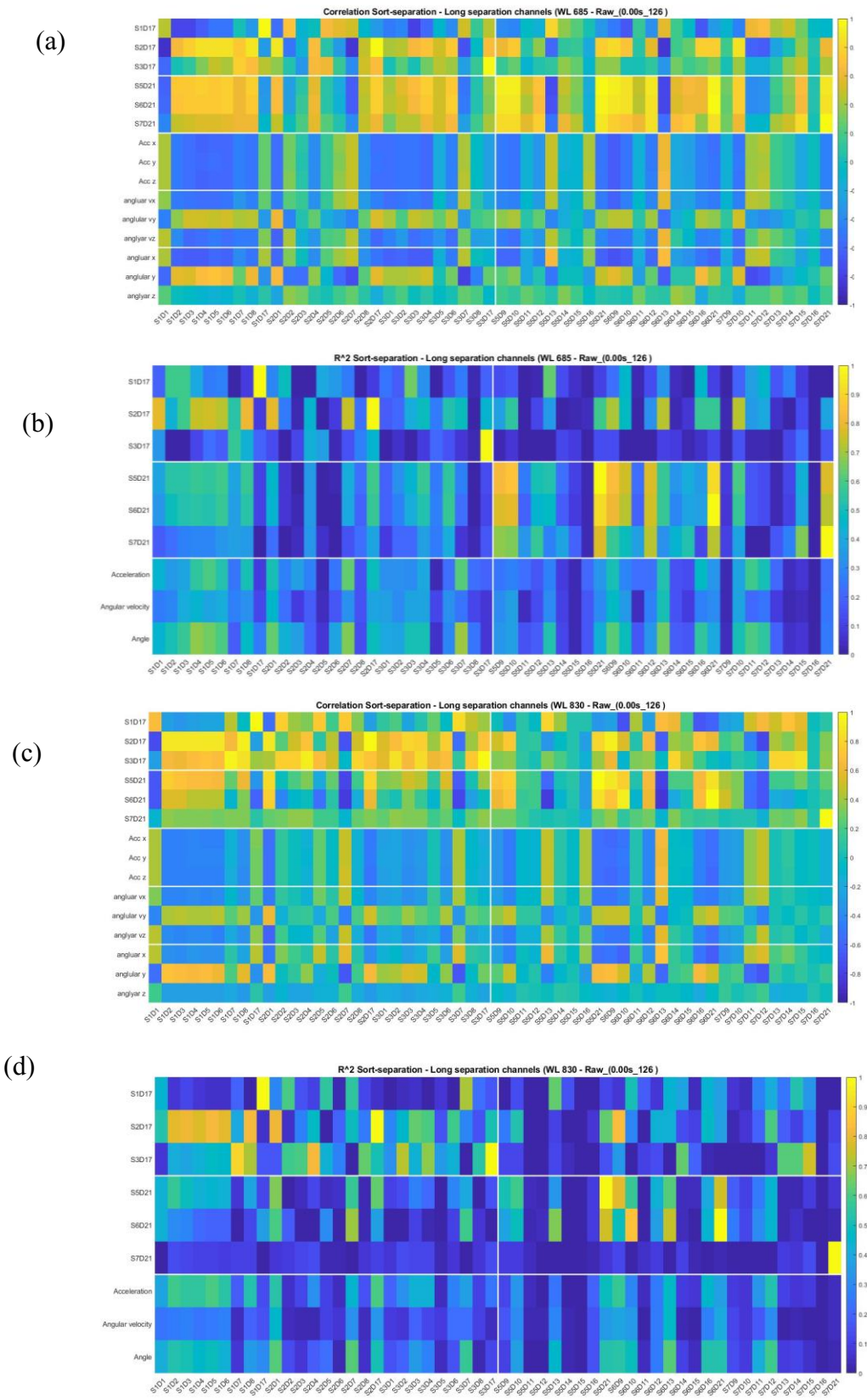


Figure 35: Run 03: Rotations Upwards

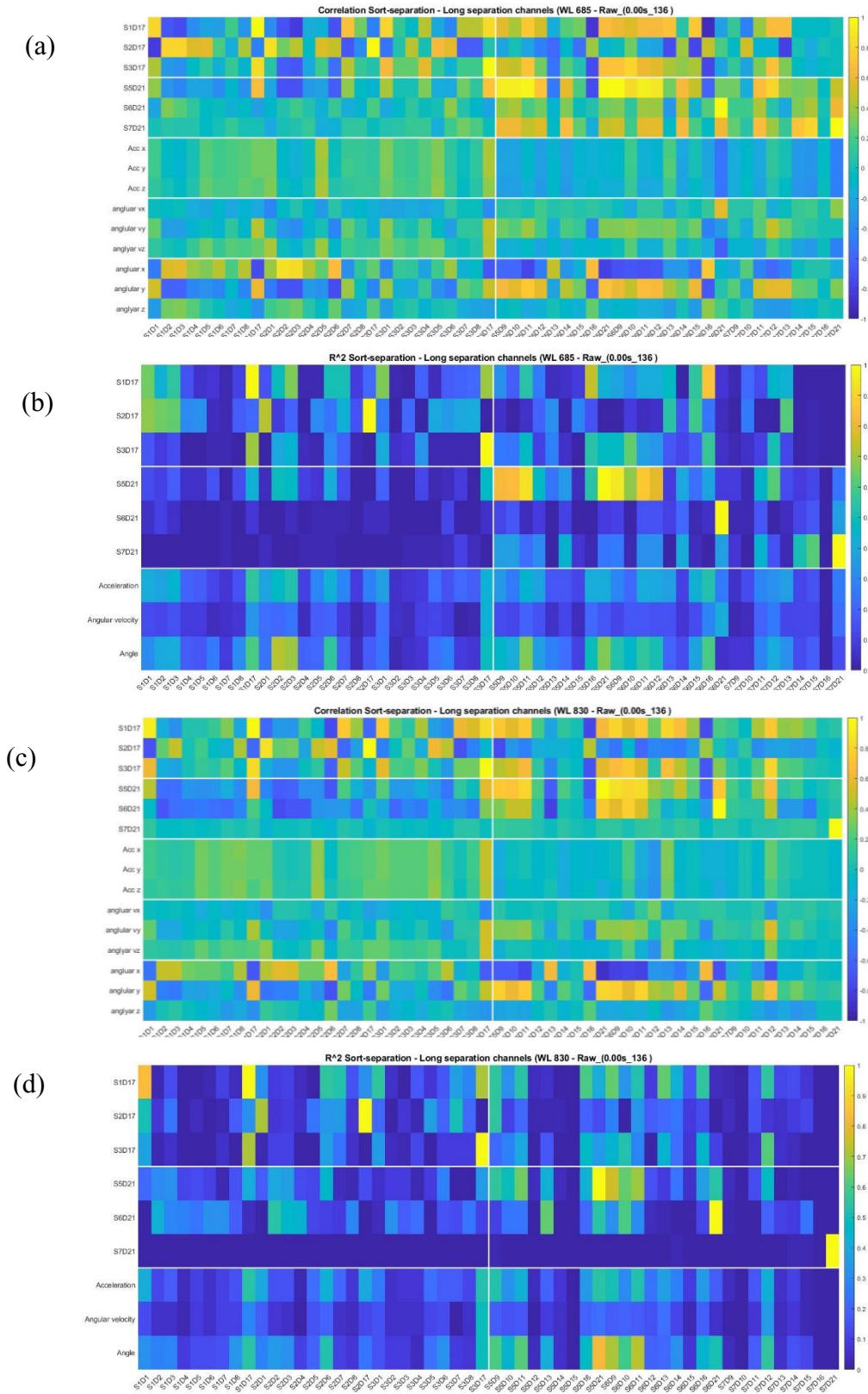


Figure 36: Run 04: Downward Rotation

